Electronic Thesis and Dissertation Repository

8-18-2020 2:00 PM

Implementing a multi-segment foot model in a clinical setting to measure inter-segmental joint motions

Tahereh Amiri, *The University of Western Ontario*

Supervisor: Jenkyn, Thomas R., *The University of Western Ontario*
A thesis submitted in partial fulfillment of the requirements for the Master of Science degree in Biomedical Engineering
© Tahereh Amiri 2020

Follow this and additional works at: https://ir.lib.uwo.ca/etd

Part of the Musculoskeletal System Commons

Recommended Citation

ABSTRACT

It has been illustrated that measuring inter-segmental joint motions of the foot using a dynamic method is required to evaluate the function and level of impairment of the foot joints. Optical motion tracking using the multi-segment foot model (MSFM) developed by Jenkyn and Nicole (2007), has been demonstrated to be a valid tool for measuring the motion of the joints within the foot. However, in current practice, inter-segmental joint motions of this model are measured using a custom-written software (MATLAB) and it limits the clinical usefulness of this model. Hence, this study implemented the MSFM introduced by Jenkyn and Nicole in a clinical user-friendly software, Vicon ProCalc, to measure the joint motions within the foot. Ankle Joint dorsi/plantarflexion, subtalar joint inversion/eversion, hindfoot supination/pronation and internal/external rotation with respect to the midfoot, forefoot supination/pronation with respect to the midfoot, hallux dorsiflexion, the rise and fall of the medial longitudinal arch, and relative motion of the medial and lateral forefoot segments were measured using Jenkyn and Nicole's MSFM and the Vicon ProCalc software for eleven participants in this study. The test was repeated using Oxford foot model (OFM) and the joint motions measured using Vicon ProCalc were compared with the results of the Oxford foot model as well as the results of the previous study on the Jenkyn and Nicole model. Compared data were matching and there was not any significant difference between the results ($p<0.03$) and it demonstrated the validity of using Vicon ProCalc for measuring inter-segmental joint motions of the foot.

Key words: optical motion tracking, inter-segmental joint motions, multi-segment foot model, Vicon ProCalc, Oxford foot model, validation

SUMMARY FOR LAY AUDIENCE

The human foot contains several segments and they move with respect to each other. Every two segments are attached to each other through a joint. Any dysfunction that occurs in the foot joints can cause pain and affect our daily activities. Thus, measuring the functionality of the foot joints is important to clinicians. Optical motion tracking allows us to track the motion of the joints using reflective markers and cameras. In order to use the optical motion tracking for measuring the motion of the foot joints, we need to use models that divide the foot into several segments. However, measuring joint motions using these models is time taking and requires extensive mathematical calculations which is not clinical user-friendly. This study implemented the multi-segment foot model (MSFM) developed by Jenkyn and Nicole (2007) into a clinical setting in order to provide clinicians with functional information of the patients' foot joints.

CO-AUTHORSHIP STATEMENT

I acknowledge Megan Balsdon who helped me in designing the study and data collection process and all the steps written in **chapter 2**.

ACKNOWLEDGMENTS

little bit in my thesis. Throughout our friendship, I found her very supportive, kind, caring, and

knowledgeable and I hope she's in a safe good place with her always beautiful smile on her face.

TABLE OF CONTENTS

LIST OF FIGURES

LITST OF TABLES

1. CHAPTER 1- INTRODUCTION

1.1 Foot anatomy

1.1.1 Bones and joints of the foot

The primary task of the foot and ankle is to directly interact with the ground and provide a flexible and stable articulation between the body and the ground during walking and running. Early in stance, the foot and ankle are required to be compliant, allowing flexibility of motion and enabling the absorption and transfer of forces. Later in stance, the foot achieves rigidity to propel the body forward and apply propulsive forces to the ground through the rigid lever of the longitudinal arch (Nordin & Frankel, 2012).

The ankle is made up of the articulation of the tibia, fibula, and the talus while the foot contains 28 bones distal to the ankle joint plus two sesamoid bones. The talus is the common bone of the foot and ankle. The foot consists of three functional parts: the hindfoot, midfoot, and forefoot. The talus and calcaneus build up the hindfoot, and the midfoot is composed of the navicular, three cuneiforms, and the cuboid (tarsal bones). Lastly, the forefoot comprises the metatarsals and phalanges (Nordin & Frankel, 2012). Figure 1-1.A and 1-1.B represent the bones of the foot, ankle and the lower leg. The first and fifth metatarsals have ranges of motion that allow the foot to conform to varying surface terrain. Whereas the other metatarsals are rigid and fixed at their bases (Chan & Rudins, 1994).

The subtalar joint is part of the hindfoot, between the talus and calcaneus. The midfoot consists of transverse tarsal joint (talonavicular and calcaneocuboid) and intertarsal joints. The forefoot comprises tarsometatarsal joints and metatarsophalangeal joints. The first metatarsophalangeal

joint (MTP) is the articulation of the hallux with the rest of the foot which plays an important roll in lower extremity biomechanics (Nordin & Frankel, 2012).
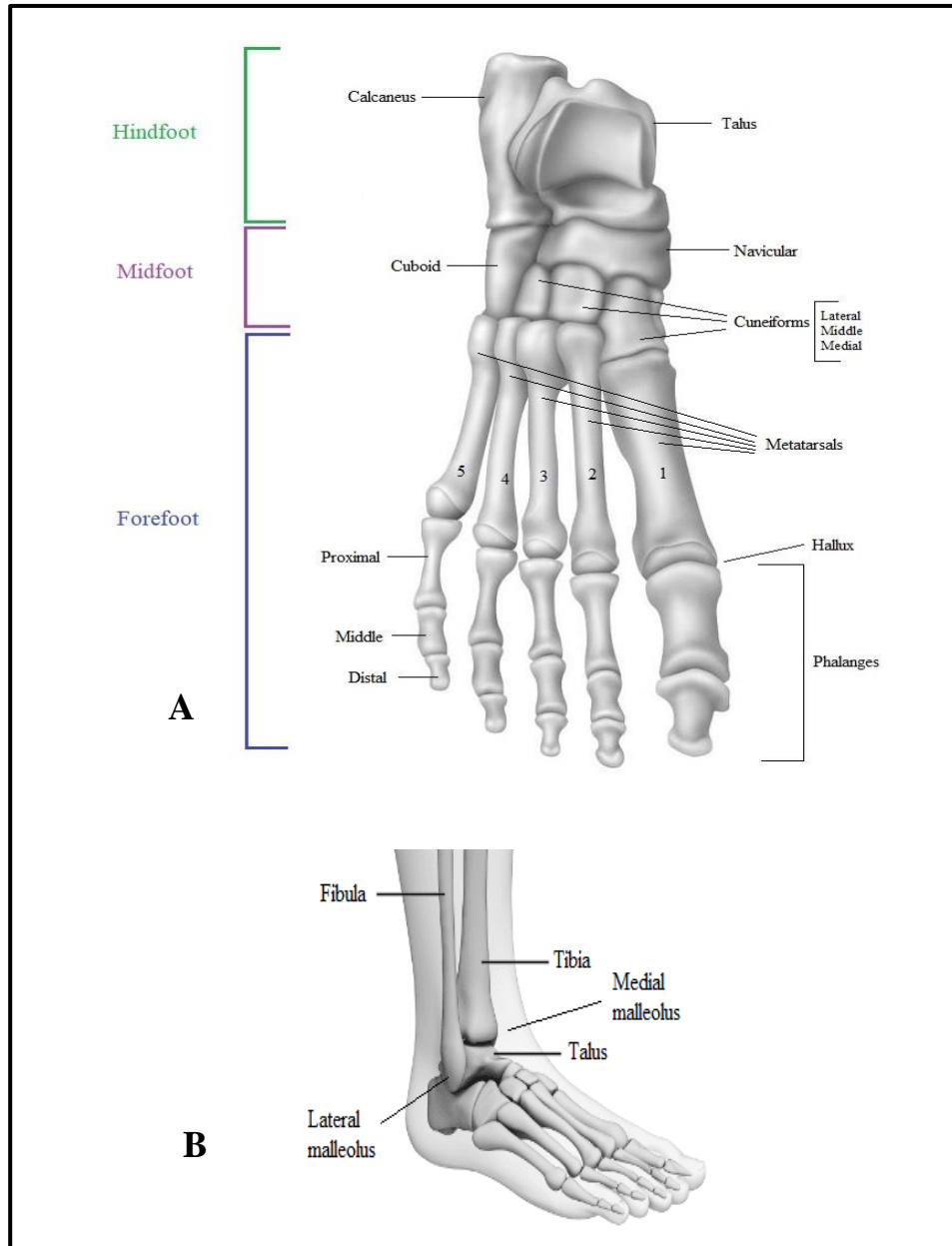
Fig. 1-1: Foot Anatomy. A) bones of the foot and B) bones articulating with the lower leg and the ankle joint. Adapted from (Nordin & Frankel, 2012).

1.1.2 Medial longitudinal arch (MLA)

The arches of the foot connect the forefoot and the hindfoot segments and dissipate the forces incurred during weight-bearing before reaching the bones of the leg and the thigh (Franco, 1987). There are three arches within the foot: the transverse arch, medial longitudinal arch and lateral longitudinal arch (Kapandji, 1975). The transverse arch is located behind the metatarsal heads and across the tarsometatarsal joints. The role of the transverse arch is to assistant in propulsion during locomotion (Kudo et al., 2018). The medial and lateral longitudinal arches are supported by the plantar ligaments originating from the calcaneus and extending forward to meet the metatarsals near the heads (O'Donoghue, 1984).

The medial longitudinal arch buffers the forces during weight-bearing and the lateral longitudinal arch maintains body stability and supports the lower limb during locomotion (Kudo et al., 2018). Figure 1-2 shows the three types of the arch within the foot. Although all three arches play an important role in maintaining body stability and supporting the lower limb, the medial longitudinal arch has been found to be the arch of greatest clinical importance. Malalignments derived from the MLA eventually impact the functioning of the muscles and joints of the lower limb. Two significant abnormalities of the MLA can be described as high arch and flat arch. the high arch is clinically known as pes cavus and the flat is known as pes planus. Pes cavus and pes planus can cause muscular imbalances, structural malalignments of joints, compensatory pronation of the foot, and gait abnormalities. Hence, understanding the biomechanics of the arches of the foot, especially MLA, is significant for physical therapists (Franco, 1987). Figure 1-3 shows the medial view of the medial longitudinal arch.
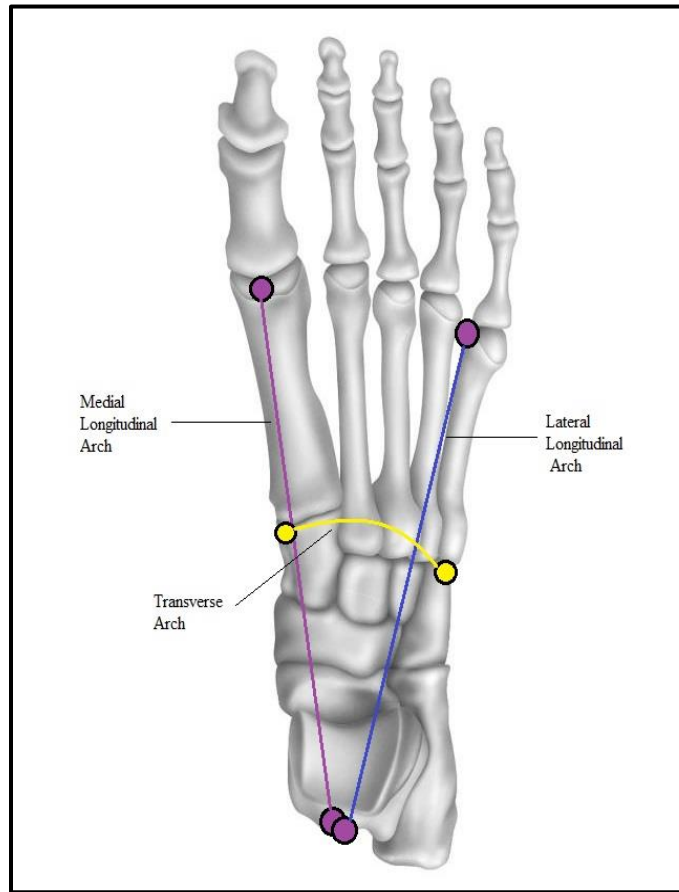
Fig. 1-2: Arches of the foot. Top view of the transverse, medial Longitudinal and lateral Longitudinal arches within the foot. Adapted from (Franco,1987).
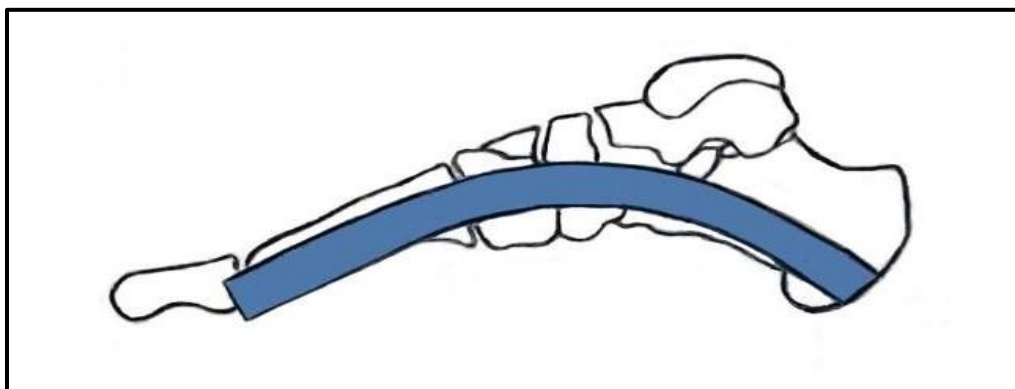
Fig. 1-3: The medial longitudinal arch. The medial view of medial longitudinal arch. Adapted from (Nordin & Frankel, 2012).

1.2 Anatomical planes and terms of movement

The three spatial dimensions of the body are defined by three anatomical planes: sagittal, frontal, and transverse. The plane that splits the body into the right and left parts is the sagittal plane. The frontal plane splits the body into anterior (front) and posterior (back) parts. And the transverse plane divides the body into superior (top) and inferior (bottom) parts (Knudson, 2003). Figure 1-4 represents three anatomical planes and three anatomical axes of the body.
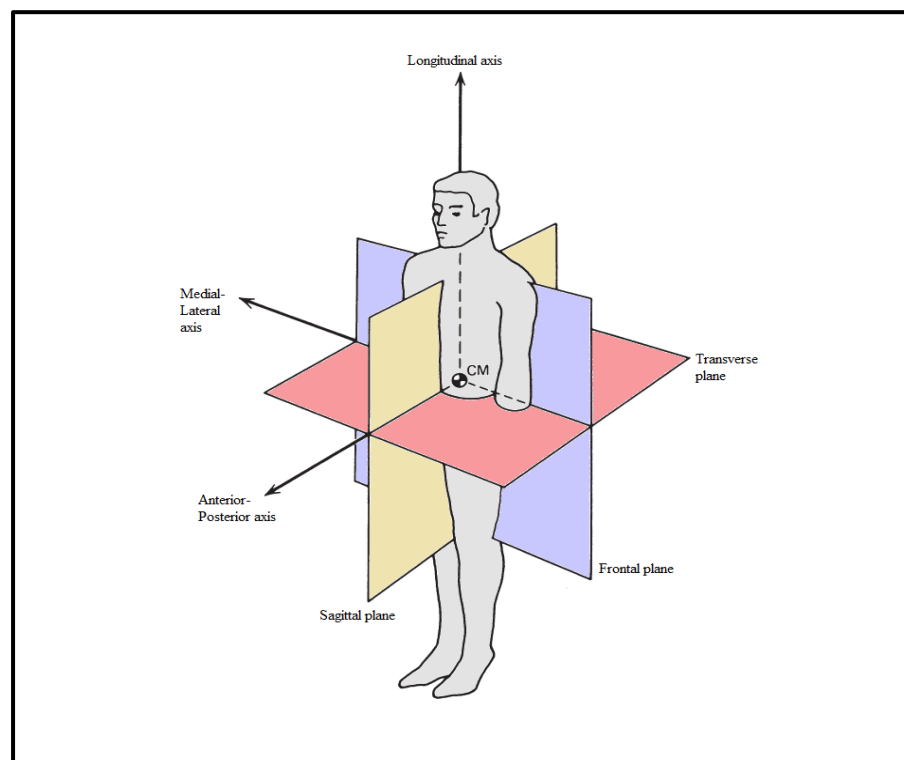
Fig. 1-4: Anatomical planes and axes. The yellow plane represents the sagittal plane, the purple plane indicates the frontal plane, and the red plane shows the transverse plane. Adopted from: Adapted from (Winter, 2009).

There are specific terms to describe the main bone motions at the joints. "Flexion" alludes to a decrease in the joint angle in sagittal plane, whereas "extension" means increasing the joint angle in the sagittal plane. The flexion and extension of the foot and ankle are called "Dorsiflexion" and "Plantarflexion". "Abduction" is moving a body part away from the midline in the frontal plane,

while moving back the body part towards the midline is "Adduction". Joint motions in transverse plane are called "Internal Rotation" and "External Rotation". Internal rotation means the rotation towards the center of the body, while the external rotation is the rotation away from the center of the body (Knudson, 2003). Figure 1-5 shows the relative motions (6 degrees of freedom) of two bones. There are some special joint motions such as "Supination" and "Pronation" which mean the inward and outward roll of the foot during walking or running. Other examples of special joint motions are "Inversion" and "Eversion". Inversion of the subtalar joint refers to leaning the sole towards the midline and eversion of the subtalar joint leans the sole away from the midline (Swartz, 2009). Figure 1-6.A shows the inversion and eversion motions of the foot and figure 1-6.B represents the supination and pronation motions of the hand.
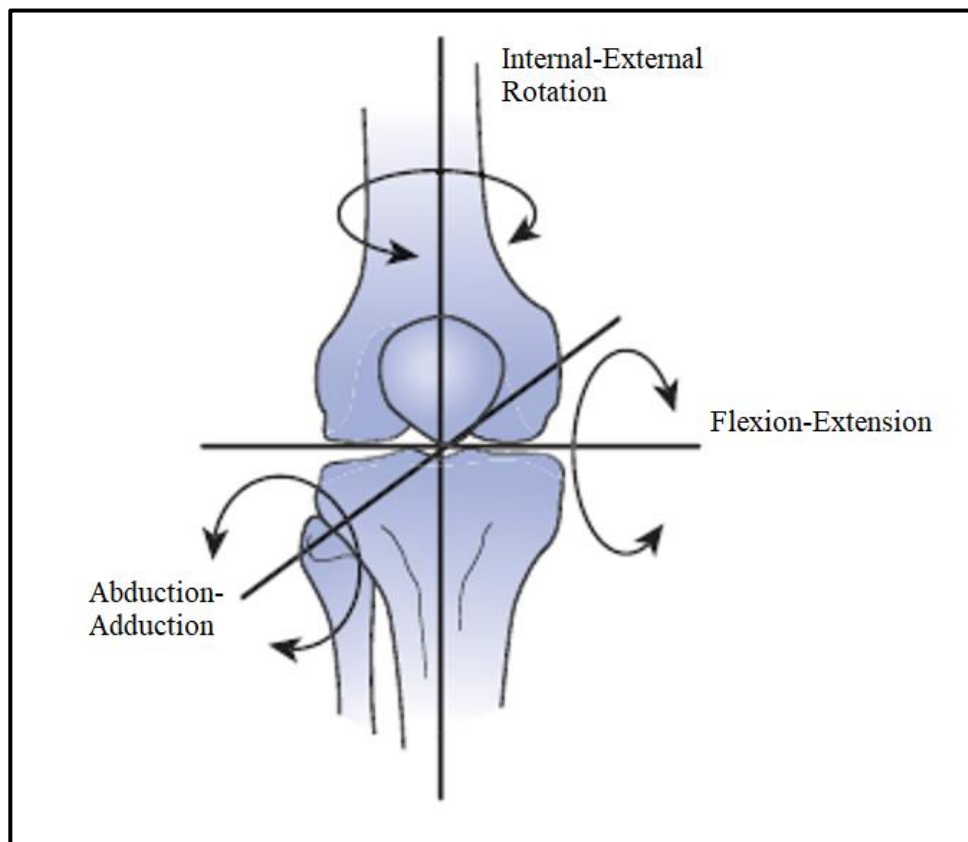
Fig. 1-5: The six degrees of freedom of two bones. Internal/external rotation, flexion/extension, and abduction/adduction of two bones. Adapted from (Nordin & Frankel, 2012).
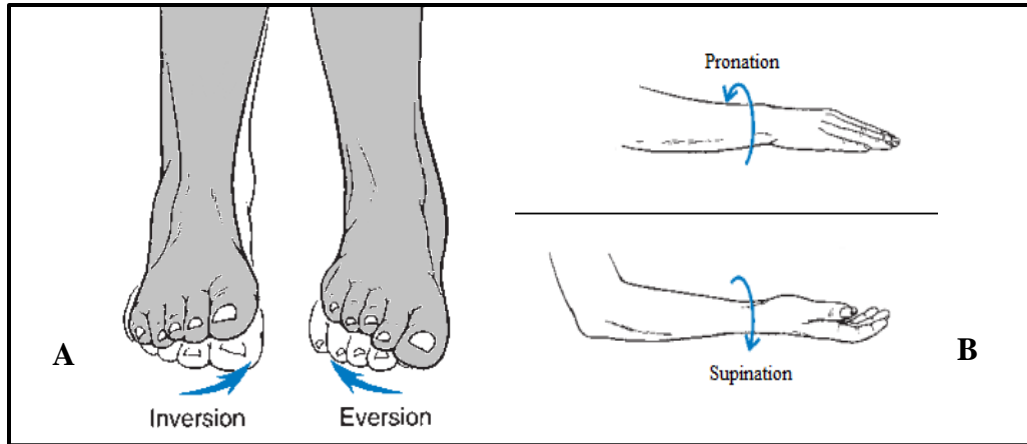
Fig. 1-6: Special joint motions. A) Inversion/Eversion of the foot and B) Supination/Pronation of the hand. Adapted from (Joseph Hamill, 2013).

1.2.1   Walking gait cycle

Normal walking is defined as a cyclic activity with two main phases for each limb: stance phase and swing phase (Crenshaw & Richards, 2006). The stance phase composes 60% of the whole gait cycle and the swing phase occupies the rest of the full gait cycle. A gait cycle starts with an event, typically heel-strike or toe-off, and ends with the occurrence of the same event on the same limb. The heel-strike is the moment when the heel touches the ground and the toe-off is the moment when the toe leaves the ground (Nordin & Frankel, 2012).

There are two other phases during the gait cycle which are called mid-stance and mid swing phase. During the mid-stance phase, the foot is in a stability mode, only one leg has the support role for the body, and ready to change toward propulsion. During the mid-swing phase, the leg swings forward and commences a transfer to the stance phase (Shultz et al., 2016). Figure 1-7 shows the phases and events of a gait cycle.
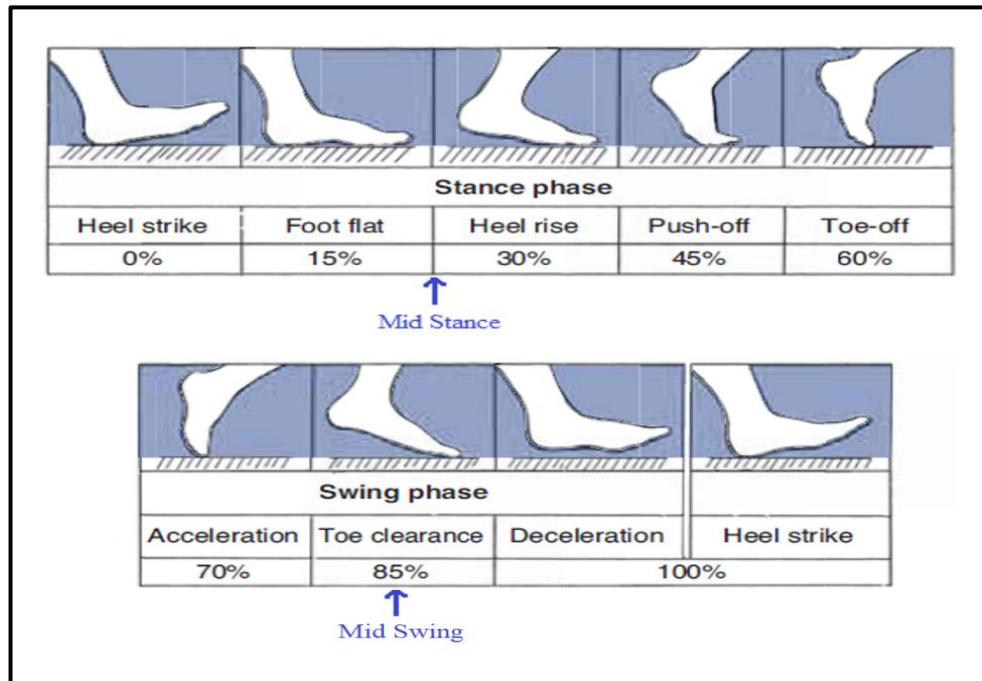
Fig 1-7: The walking gait cycle. Stance phase, swing phase, and the events of the walking gait cycle. Adapted from (Nordin & Frankel, 2012).

1.2.2   Foot joint motions during a gait cycle

During the first 15% of the gait cycle (from heel-strike till foot-flatness), foot segments internally rotate and the heel everts. The ankle joint plantarflexes at heel-strike and plantarflexion increases until 15% of the gait cycle. From the mid-stance until the toe-off event, the foot segments begin to rotate externally, the heel reverse to inversion, and the ankle joint turns to dorsiflexion. Also, the stability of the medial longitudinal arch increases. At toe-off, foot segments obtain maximum external rotation, heel achieves maximum inversion and the stabilization of the medial longitudinal arch is maximized. The ankle joint returns to plantarflexion at toe-off event. All these motions then reverse, except for the ankle joint motion, from the toe-off until foot-flatness is achieved at 15% of the new walking cycle. The ankle joint begins to dorsiflex from the mid-swing phase and changes to the slight plantarflexion at heel-strike (Nordin & Frankel, 2012).

In this study, we focused on the major movements within the foot during a gait cycle which can be described as follow:

- Subtalar joint inversion/eversion
- Ankle joint dorsi/plantarflexion
- Hindfoot Supination/pronation with respect to the midfoot
- Hindfoot Internal/external rotation with respect to the midfoot
- Forefoot supination/pronation with respect to the midfoot
- Hallux dorsi/plantarflexion
- Rise and fall of the medial longitudinal arch
- Relative motion of the medial and lateral forefoot segments

1.3 Gait analysis using motion capture techniques

Motion capture (mocap) systems use sensors to obtain the gait data of human motions and process the acquired data using a mathematical model. In general, there are two motion capture techniques: marker-based techniques and marker-less techniques (Salah & Gevers, 2011).

1.3.1 Marker based motion capture technique

Marker based motion capture technique is performed by tracking retro-reflective markers placed on the skin of the subject and reconstructing their 3D positions in the space using video-based optoelectronic systems. Tracking of retro-reflective markers is performed using cameras with light-emitting diodes (LEDs) placed around the lens of each. The infrared stroboscopic illumination produced by the LEDs tracks the markers. Cameras can be adjusted so that only bright reflective markers are recognized and captured using image-based techniques. A marker must be visible from at least two calibrated cameras to be reconstructed in the reference frame of the

laboratory (Salah & Gevers, 2011). In this study, we used Vicon system Bonita cameras for capturing motion and Vicon Nexus application for post-processing data. Vicon system and its corresponded applications will be more explained in section 1.10.

1.3.2 Triad cluster markers vs single markers

There are two types of retro-reflective markers being used in biomechanical models: Single markers and triad cluster markers. Conventional gait models (such as Helen Hays) use single retro-reflective markers and limits tracking of the foot and ankle complex in 2 degrees of freedom (Baker, 2006). These limitations are due to the fact that data acquisition techniques were initially developed for low resolution motion capture systems with a minimized number of cameras and few spaced markers (Della Croce et al., 2005). Current optical motion tracking systems have the ability to track markers with high frequency and they do not limit the biomechanical models (Baker, 2006). As a result, triad cluster markers were introduced. A triad cluster marker is a group of three nonlinear markers attached to the base of the marker allowing to track anatomical bony landmarks on each segment of the body (Fig. 1-8) (Cappozzo et al., 1997). Using triad cluster markers, each segment can be tracked independently in 6 degrees of freedom (6 DOF). In addition, using cluster markers in a biomechanical model can reduce soft tissue artefacts. In a conventional gait model, every single marker is susceptible to the errors of the motion of underlying soft tissue. In biomechanical models with cluster markers, these errors can be reduced by appropriate marker positioning on each segment (Zuk & Pezowicz, 2015).

Furthermore, using cluster markers can reduce the number of required holes on the shoe and enhance the accuracy in data collection with shoes on. Gait analyzing with shoes on requires cutting holes on the shoe allowing to place markers on the foot. Using cluster markers will reduce the number of required holes to be cut on the shoe. On the other hand, data obtained from the heel

of the shoe with single markers is not as accurate as collecting data with cluster markers due to the thick heel counter of the shoe. A triad cluster marker is shown in figure 1-8.
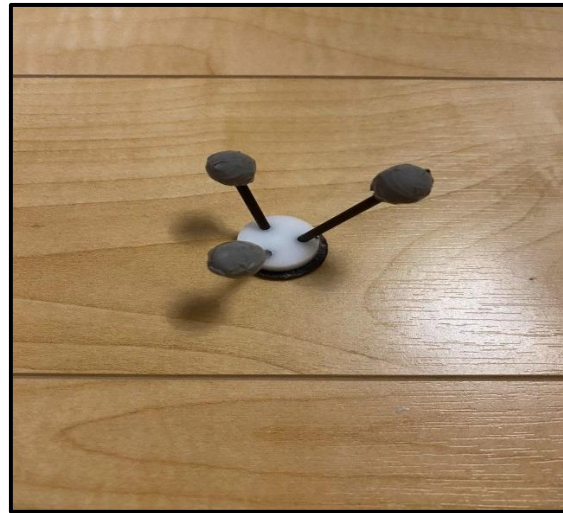
Figure 1-8: A triad cluster marker. A triad cluster marker contains a base and three reflective markers attached to the base.

1.4   Conventional gait models

The conventional gait analysis considers the foot as a rigid segment, not allowing the measurement of joint motions within the foot (Kadaba et al., 1989). Joints of the foot are exposed to injury during weight-bearing movement. Several clinical studies have evaluated the function of the foot joints in the static phase (Hunter & Prentice, 2001). However, there is a weak relation between the foot function in the static phase and weight-bearing movement (Cavanagh et al., 1997). As a result, a clinical evaluation is needed to measure inter-segmental joint motions within the foot. Several studies have presented multi-segment foot models (MSFM) addressing this problem. (Carson et al., 2001; Hunt et al., 2001; Rattanaprasert et al., 1999)

1.5   Multi-segment foot models (MSFM)

A multi-segment foot model divides the foot into several segments to be able to measure intersegmental joint motions. The configuration of foot segments is of great importance and has

been controversial in the literature. An arrangement with too many segments will be clinically impractical. On the other hand, modeling the foot with too few segments will reduce the clinical usefulness of the model. Several studies have presented multi-segment foot models in the literature (Kidder et al., 1996; Moseley et al., 1996; Liu et al., 1997; Leardini et al., 1999; Jenkyn & Nicol, 2007). These studies mostly divide the foot into the hindfoot and forefoot segments. Only one study considered the midfoot as an individual segment and divided the foot into hindfoot, midfoot, medial forefoot, and hallux segments (Leardini et al., 1999). In order to measure hindfoot supination-pronation, forefoot supination-pronation, and subtalar inversion-eversion, a midfoot segment is required. In 2007, Jenkyn and Nicol presented a multi-segment foot model with hindfoot, midfoot, medial and lateral forefoot segments. The lower-leg and thigh were also defined as segments. This model is superior in several aspects:

- First, this model considers the midfoot as an individual segment allowing the measurement of following motions with respect to the midfoot: Hindfoot supination-pronation, hindfoot internal-external rotation, and forefoot supination pronation. Ankle and subtalar joint motions are defined as the motion of the midfoot with respect to the lower leg. Hence, the ankle joint dorsiflexion and subtalar joint inversion-eversion can be measured as well.

- In addition, this model divides the forefoot into medial and lateral segments. As a result, the relative motion of metatarsal bones can be measured.

- Finally, this model uses triad cluster markers and a wand for digitizing landmarks that allow having fewer holes in the shoe in sampling data with shoes on. Also, data collected from the heel segment will be more accurate.

The multi-segment foot model used for this study was adopted from the model presented by Jenkyn and Nicol. Since hallux dorsiflexion is a clinically important motion to be measured, the hallux segment was added to this model.

1.5.1   MSFM used for this study

The foot was subdivided into five segments: the hindfoot (calcaneus), midfoot (tarsals: cuneiforms I–III, navicular, and cuboid), medial forefoot (metatarsals I and II), lateral forefoot (metatarsals III–V), and hallux (first metatarsophalangeal joint).

The lower leg was also defined as a segment. The talus was not tracked directly, but the motions of the ankle and subtalar joints could be entirely determined by tracking lower leg and midfoot segments. Figure 1-9 shows the configuration and placement of markers on the foot and lower leg.
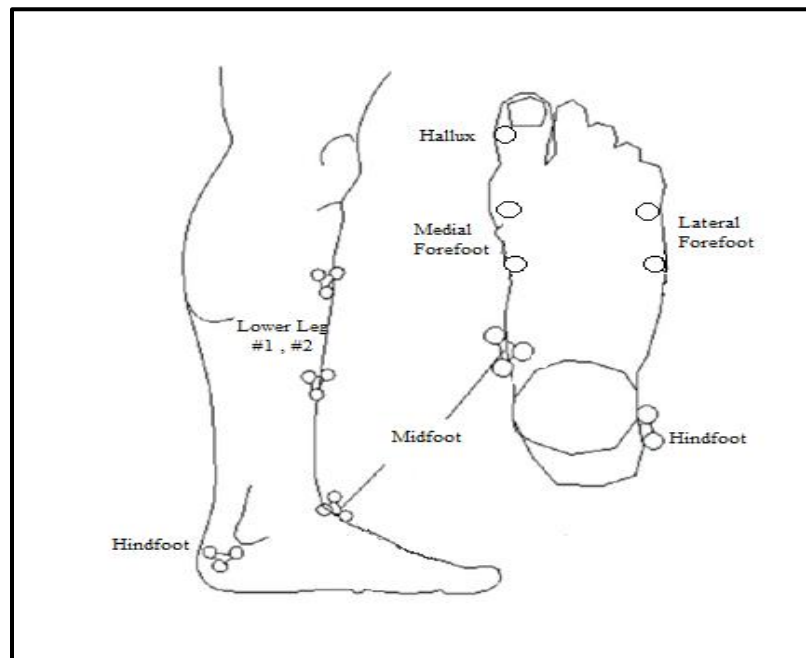
Fig. 1-9: The marker set for Jenkyn and Nicole's model. Configuration and placement of markers on the foot and lower leg. Adapted from (Jenkyn & Anas, 2008).

1.6   Method of Grood and Suntay (Grood & Suntay, 1983)

Anatomical joint motions include three dimensional movements described by 6 degrees of freedom (6 DOF). Three movements are rotations and three are translations (Routh, 2015). For measuring the relative motions of foot segments only angular positions and the corresponding rotational motions are needed. In 1983, Grood and Suntay presented a method for quantifying the relative motions of two rigid bodies. The superiority of using this method over measuring Euler angles is that joint motions are independent of the order in which the rigid bodies translations and rotations occur. Hence, specifying the order of the rotation is not required (Grood & Suntay, 1983).

In this method, the first step is to apply a coordinate system to each rigid body. For defining a coordinate system for the segment, we need to identify at least three points on the segment. Then the coordinate system can be created by the following steps:

1. Creating two vectors and their affiliated unit vectors using three points defined on the segment. In this study, we call these two vectors $\vec{v}_1$ and $\vec{v}_2$.

2. Creating a perpendicular unit vector to the first two vectors by taking the cross product of them. In this study, we call this vector $\vec{v}_x$.

3. Taking a cross product of $\vec{v}_x$ and $\vec{v}_2$ and create another unit vector which is called $\vec{v}_z$ in this study. Now, an orthogonal coordinate system can be created using $\vec{v}_x$, $\vec{v}_y$ ($\vec{v}_2$) and $\vec{v}_z$.

After creating an anatomical coordinate system for each segment, rotational motions of the segments can be calculated. Rotational movements in three dimensions can be described by three independent angles (α, β, and γ) (Whittaker & McCrae, 1988). Hence, three nonorthogonal rotational axes should be identified about which correlated rotational motions occur. The unit vectors of these three axes are called $\vec{e}_1$, $\vec{e}_2$, and $\vec{e}_3$. Two of the axes ($\vec{e}_1$ in segment A and $\vec{e}_3$ in segment B) are body fixed axes placed in the two segments whose relative motion is to be

14

measured. Then, a floating axis must be created by crossing two fixed body axes. The third axis,

F, is the common perpendicular to the $\vec{e}_1$ and $\vec{e}_3$. Two of the rotational motions (α and γ) can be

described by the spin of each body about its body-fixed axis while the other body remains

immobilized. These rotations can be calculated by measuring the angle between the floating axis

and a reference line placed in each segment. The third rotational motion (β) is described as the

rotation about the floating axis and can be calculated by measuring the angle between the two

segment-fixed axes (Grood & Suntay, 1983).

Figure 1-10 represents two segments and their body fixed axes. The floating axis created by taking

cross product of the segment fixed axes.
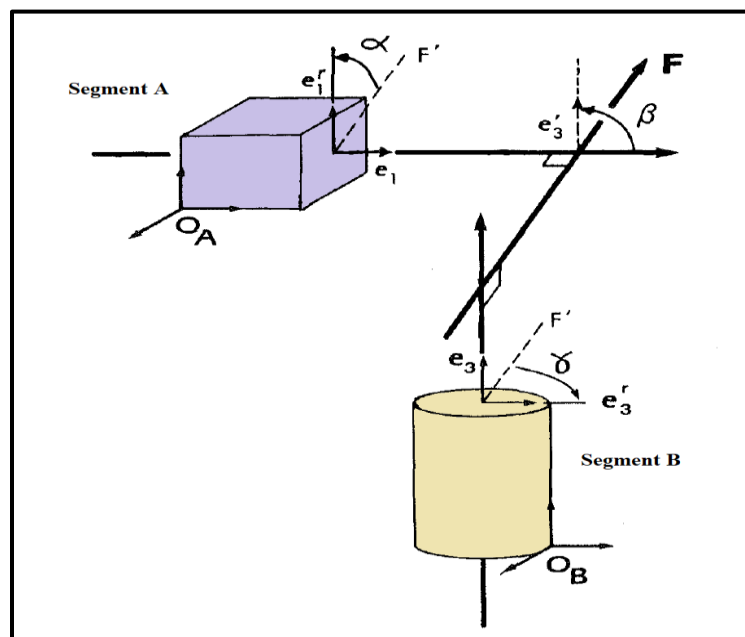
Fig. 1-10: Two segments and their body fixed axes. Segment A and segment B with their body fixed unit axes
($\vec{e}1$ and $\vec{e}3$). F is the common perpendicular axis to $\vec{e}1$ and $\vec{e}3$. α and γ are the spin of each body about its body
fixed axis while the other body remains stationary and β is the rotation about the floating axis. Adapted from (Grood
and Suntay, 1983).

1.7 Rational: limitation of previous studies

The rationale of this study was based on the study that has been accomplished in the Wolf

Orthopedic and Biomechanics Laboratory. A multi-segment kinematic model of the foot and ankle

complex was developed by Jenkyn and Nicole in 2007, for use in a gait analysis during normal walking. This model is proposed to measure gait kinematics using an optical motion-capture system with digital cameras. This method has many benefits, such as being able to measure subtalar joint motion and hindfoot and forefoot supination-pronation with respect to midfoot. Also, this model allows us to measure the relative motion of metatarsal bones. This method is non-invasive and uses triad cluster markers and a wand for digitizing landmarks on the segments. Using triad cluster markers allows us to use fewer reflective markers for the data collection and as a result, having fewer holes on the shoe for collecting data with shoes on. On the downside, in the study of Jenkyn and Nicole, intersegmental joint motions were measured using a custom-written software (MATLAB, The Mathworks, Natick, MA). As explained in section 1.6, measuring intersegmental joint motions requires extensive mathematical calculations and using MATLAB for these calculations limits the clinical usefulness of the multi-segment foot model. Therefore, Implementation of Jenkyn and Nicole's model into a clinically user-friendly software is required. Hence, in the current study we decided to use Vicon ProCalc (Vicon, Oxford Metrics Ltd., Oxford, UK) software. ProCalc is a software that makes it easy to develop, implement, and run biomechanical models. Furthermore, variables, events, and parameters can easily be created in this software as well. Before running data through Vicon ProCalc software, post-processing data such as reconstruction and labeling marker trajectories as well as filling gaps and filtering data was done in Vicon Nexus software. In the next part, Vicon Nexus and Vicon ProCalc will be explained.

1.8 Anatomical and technical coordinate systems

There are two types of the coordinate systems for a body segment: the anatomical coordinate system and technical coordinate system. An anatomical coordinate system is determined during the static calibration with digitizing three bony landmarks on the segment. A technical coordinate

system is determined during a dynamic motion tracking (the motion tracking test in which walking was performed) with technical markers located at optimal sites (Saraswat et al., 2014). Using anatomical and technical coordinate systems, a virtual marker can be created in a static calibration trial using digitized landmarks and can be reconstructed in a dynamic trial. Using anatomical and technical coordinate systems for reconstructing bony landmarks will be more explained in chapter 2.

1.9 Vicon systems

1.9.1 Vicon Nexus

The Vicon Nexus application makes it easy to connect to the Vicon 3D motion capture systems and control, collect and process data from video cameras. Video cameras collect data as movement trials using Vicon Nexus application, and then trials can be processed through this application as well. Vicon Nexus allows us to reconstruct and label marker trajectories and create a labeling skeleton and marker-set for each subject. This is the first step of processing data. In a trial, there may be frames with gaps in trajectories due to some markers that could not be reconstructed (Fig. 1-11) (Vicon Nexus user guide, 2010). Vicon Nexus enables to fill the gaps as well as filter noises in a movement trial. After processing, data transferred to the Vicon ProCalc application for measuring intersegmental joint motions.
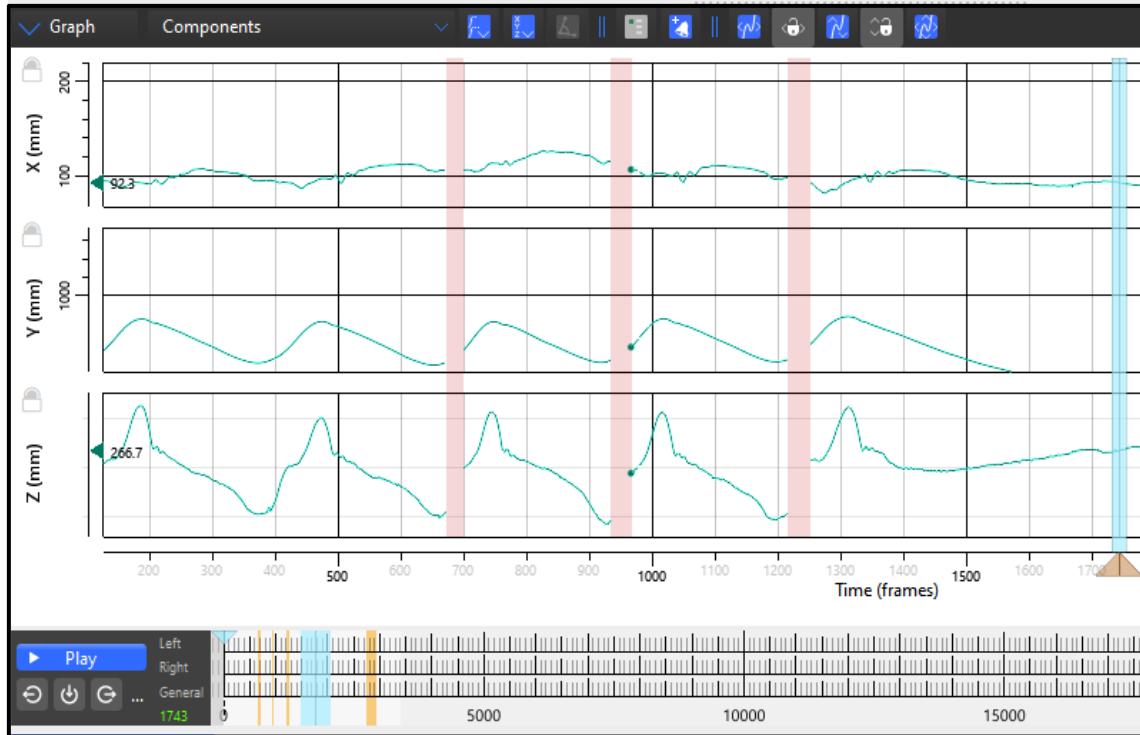
Fig. 1-11: The gaps of a trial. Red lines show the gaps in trajectories of a marker in a trial in Vicon Nexus software.

1.9.2   Vicon ProCalc

ProCalc is a software application that makes it easy to develop, implement, test, and run biomechanical models. In this application, we can create vectors based on digitized landmarks and then create coordinate systems for the segments. ProCalc allows calculating kinematics such as the relative motion of segments by measuring the angle between vectors or Euler angles. In addition, variables, parameters, and events can be created in this application (Vicon ProCalc user guide, 2018). In chapter 2, all steps for creating the multi-segment foot model that we used in this study will be explained.

1.9.3   Oxford foot model (OFM)

In presenting a method to measure inter-segmental joint motions, it is important to validate the method with a gold-standard. The most used multi-segment foot model in literature for validation

is the Oxford foot model (OFM). The oxford foot model divides the foot and ankle complex into hindfoot, forefoot, and hallux to measure inter-segmental joint motions (Carson et al., 2001). This model has been used to measure kinematics for the normal and pathological gait of children (Alonso-Vázquez et al., 2009; Mindler et al., 2014; Hösl et al., 2014) and adults. The markers for the Oxford foot model are attached in addition to the standard lower-body markers (Helen Hayes lower body marker-set). The Oxford foot model marker-set for the right foot and leg and the description and position of the markers will be explained in chapter 2.

1.10 Objective and hypothesis

The main objective of this study was to implement the MSFM presented by Jenkyn and Nicole (2007), in Vicon Procalc software which is a clinical setting to be able to measure inter-segmental joint motions. In order to reach the main objective, the following steps were done during research study:

1. Comparing the results of this study which were intersegmental joint motions of the foot and ankle measured by the Vicon ProCalc software with the previous study on this model (Jenkyn & Nicole, 2007) which used MATLAB for measuring relative motions of the segments within the foot.

2. Validating this method with the output motions measured using Oxford foot model. Since OFM does not consider midfoot as an individual segment, we compared the motion of the forefoot with respect to the midfoot in our study with the forefoot motion with respect to the hindfoot measured by the Oxford foot model. Also, the subtalar joint motion in our study was compared with the motion of the hindfoot with respect to the lower leg measured by OFM (hindfoot-tibia motion).

It was hypothesized that:

1. The use of Vicon ProCalc software would be faster, easier, and more clinical user-friendly than using MATLAB for measuring inter-segmental joint motions.

2. The multi-segment foot model used for this study can be built in Vicon ProCalc application. Gait cycle events will be defined accurately using Vicon ProCal application and the results for the inter-segmental joint motions will be accurate.

3. Comparing results to the previous study on this model, and to the Oxford foot model, graph trends will be similar and the difference between angles will be less than $5°$.

1.11 Thesis overview

Chapter 2 describes the methodology of this study, subjects' demographic, data collection, and data processing procedures. Chapter 3 validates the use of Vicon ProCalc software for measuring inter-segmental joint motions by comparing the results of Vicon ProCalc output angles with the results of the Jenkyn and Anas (2008) study and with the Oxford foot model output angles. Chapter 4 summarizes the conclusions obtained from this study and discusses its significance for future research.

2. CHAPTER 2- METHODOLOGY

2.1 Experimental equipment

All kinematic data collection was done at the SoleSience Clinic in London, Ontario, Canada. Prior to each subject participating in this study, subjects filled a demographic form and then their Arch Hight Index (AHI) was measured in weight-bearing. For measuring the AHI, we measured the length of the heel to toe (HT), heel to the ball of the foot or first metatarsal head (HB), and dorsum height (DH) which was taken at ½ the HT measurement for each subject with an arch height index measurement device (AHIMS). The AHI was calculated for each subject by dividing the DH measurement by the HB measurement. This method was first developed by Williams and McClay in 2000 (Fig. 2-1). The AHI measurement was done for both dominant and non-dominant feet for each subject. Table 2-1 shows patient demographics and the AHI for both dominant and non-dominant feet measured in 90% weight bearing for each subject.

Eleven participants took part in this study in three groups of high arch, normal arch and, flat foot. Participants were eight females (with an average age of 31 years old and an average weight of 63 kg) and three males (with an average age of 27 years old and an average weight of 81 kg). Participants were recruited from SoleScience clinic staff and friends. Participants did not have any musculoskeletal abnormalities.
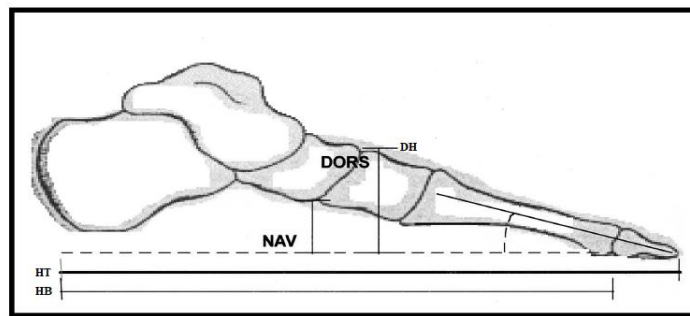
Fig. 2-1. The arch height index measurement. Schematic of the anatomical landmarks used to measure the arch height index. Adapted from (Williams & McClay, 2000).

Patient	Age	Gender	Weight	Height	Dominant foot	AHI Classification (WB)	
						L	R
1	25	M	73	180	R	Pes-Planus	Neutral
2	28	F	50	157	R	Pes-Planus	Pes-Planus
3	37	F	54.5	157	R	Pes-Cavus	Pes-Cavus
4	28	F	75	173	R	Pes-Planus	Pes-Planus
5	26	F	58	170	L	Neutral	Neutral
6	40	F	67	153	R	Neutral	Neutral
7	28	M	90	177	R	Neutral	Pes-Cavus
8	28	M	81	172	R	Neutral	Neutral
9	34	F	57	164	R	Pes-Planus	Pes-Planus
10	26	F	73	176	R	Neutral	Neutral
11	30	F	70	170	R	Neutral	Pes-Planus

Table 2-1: Patient demographics table. Patient demographics and AHI index measured for the left and right feet with 90% weight bearing for each subject.

2.2 Motion analysis equipment

The data collection room at SoleScience clinic was equipped with 8 real-time 3D optical motion capture cameras (Vicon, Oxford Metrics, UK) at a sampling rate of 50 Hz and a motorized treadmill that allows participants to perform walking tests. The origin of the reference frame was established as the center of the treadmill belt during the calibration process using a wand.

2.3 Calibration

Before starting the data collection process, Vicon motion capture cameras have to be connected to a Vicon Nexus application and then, Vicon motion capture system needs to be calibrated. Before calibration, all markers and the source of any unwanted reflections should be removed from the data collection room.

The first step for calibrating the system is to mask cameras. Masking enables cameras to ignore the reflection of the reflective objects other than markers that cannot be removed. Masking cameras enhances reconstruction quality and calibration robustness.

The second step is to calibrate the digital video cameras. Calibrating cameras means specifying capturing volume to the Nexus system and enables it to produce more accurate 3D data. This process needs an active wand to be waved throughout the area that we want to capture 3D data. By clicking start, system starts to capture wand wave data and the stop button appears while the camera registers valid frames where the whole wand is visible.

The last step of calibration is to set the volume origin. By setting the volume origin (global coordinate system), the center of the capture volume and the orientation (x, y, and z axes) can be specified. This process can be done by placing a calibration wand flat on the floor at the center of the treadmill belt and clicking set origin button.

2.4 Data collection

2.4.1 Data collection sections

This study includes a two-part data collection. In the first part, data were collected using the MSFM presented by Jenkyn and Nicole marker set. In the second part, we collected data using Oxford foot model marker set from the same subject in order to be able to validate our study with the Oxford foot model.

2.4.2 Data collection using our model

2.4.2.1 Preparing participants for collecting data

The first step for preparing participants for data collection is to place cluster markers and single markers on the skin of the subjects using the MSFM marker set that we used for our study. In this market set, two cluster markers were placed on the lower leg and on each of the hindfoot and midfoot, one cluster marker was placed. Two single markers were placed on the medial forefoot on the first metatarsal head and base. Likewise, two single markers were placed on the base and head of the fifth metatarsal on the lateral forefoot (fig 2-2.A and 2-2.B). Data were only captured from right foot and leg. Table 2-2 shows the cluster and the single markers configuration and their locations on each segment.

Fig. 2-2: Jenkyn and Nicole's model marker set. A) Frontal view and B) lateral view of the MSFM marker-set configuration used for this study.

2.4.2.2 Digitizing landmarks

Based on the method of Grood and Suntay which was explained in chapter 1, in order to create an anatomical coordinate system on each segment, three bony landmarks are needed on each segment. In this study, we digitized three bony landmarks on each segment using a wand with three reflective markers on it and three vectors on each segment were created using the corresponded landmarks on each segment. (Fig. 2-3). Table 2-2 shows the location and specification of the bony landmarks and vectors on each segment . For digitizing each bony landmark, the wand was held against the position of each bony landmark in quiet standing and a static trial was captured for each digitized landmark for a duration of few seconds (Fig. 2-4). In the data processing section, the process of creating a virtual marker in the location of each bony landmark using Vicon ProCalc is explained.
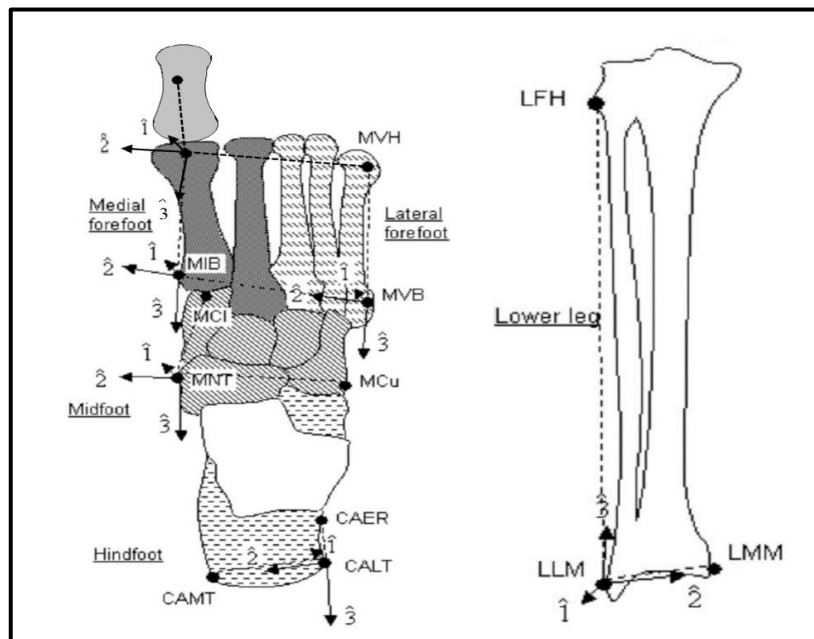
Fig. 2-3: Segments of the right lower leg and foot. Three bony landmarks defined on each segment for constructing the segment-fixed axis systems. Adapted from (Jenkyn et al., 2009).

Fig. 2-4: Digitizing landmarks. Holding a wand against the position of a bony landmark for digitizing a landmark.

Segment	Cluster locations	Tracked landmarks	Defining vectors
Lower leg	Anterior tibial crest	**LLM:** lateral malleolus (most lateral point) **LFH:** fibular head (most lateral point) **LMM:** medial malleolus (most medial point)	$\vec{v}_1$ = LLM-LFH $\vec{v}_2$ = LMM-LLM O = LLM
Hindfoot	Lateral to achilles tendon	**CAER:** eminentia retrotrochlearis (greatest lateral elevation) **CALT:** lateral tuberosity (lateral to achilles tendon attachment) **CAMT:** medial tuberosity (medial to achilles tendon attachment)	$\vec{v}_1$ = CAER-CALT $\vec{v}_2$ = CAMT-CALT O = CALT
Midfoot	Dorsal to navicular tuberosity	**MCI:** first cuneiform (distal dorsal crest) **MNT:** navicular tuberosity (most medial point) **MCU:** cuboid (lateral dorsal edge at joint with calcaneus) **STH:** talar head (most dorsal point at joint with navicular)	$\vec{v}_1$ = MCI-MNT $\vec{v}_2$ = MNT-MCu O = MNT

Medial forefoot	Single markers attached to the position of the landmarks	**MIH:** first metatarsal head (most dorsal point) **MIB:** first metatarsal base (most dorsal point)	$\vec{v}_1$ = MIH-MIB $\vec{v}_2$ = MIB-MVB $\underline{O}$ = MIB
Lateral forefoot	Single markers attached to the position of the landmarks	**MVH:** fifth metatarsal head (most dorsal point) **MVB:** fifth metatarsal base (most dorsal point)	$\vec{v}_1$ = MVH-MVB $\vec{v}_2$ = MIB-MVB $\underline{O}$ = MVB
Ankle JCS		**LMM:** defined on the lower leg segment **LLM:** defined on the lower leg segment **STH:** defined on the midfoot segment	$\vec{v}_1$ = STH-LMM $\vec{v}_2$ = LMM-LLM $\underline{O}$ = 1/2 (LMM-LLM)
Subtalar JCS		**LMM:** defined on the lower leg segment **LLM:** defined on the lower leg segment **STH:** defined on the midfoot segment **CALT:** defined on the hindfoot segment	$\vec{v}_1$ = LLM-LMM $\vec{v}_2$ = STH-CALT $\underline{O}$ = STH
Hallux JCS	A single marker attached to the position of the landmark	**HX:** hallux **MIH:** defined on the medial forefoot segment **MVH:** defined on the lateral forefoot segment	$\vec{v}_1$ = HX-MIH $\vec{v}_2$ = MIH-MVH $\underline{O}$ = HX

Table 2-2: The landmarks and axes of each segment. The location and specification of reflective markers, bony landmarks, and defining vectors for each segment.

2.4.2.3 Capturing dynamic trials

After digitizing landmarks, participants walked on the treadmill at their self-selected speed and performed a normal walking gait and three dynamic trials that each had a duration of one minute, were captured from each participant's walking. After capturing dynamic trials, cluster and single markers were removed from the skin of the participants to start the next part of the data collection.

2.4.3 Data collection using Oxford foot model

2.4.3.1 Preparing participant for collection data

For this part, we used only single reflective markers for data collection. We used the OxforFootModel_Right marker-set and the attached markers to the participants. After placing all markers, three static trials were captured in quiet standing. Since Vicon Nexus needs some measurements from subjects for calculating kinematics of motion with the Oxford foot model, we asked participants their weight and height and measured their left and right leg length, knee width, and ankle width and imported the measurements to the Vicon Nexus application. Figure 2-5 shows the Oxford foot model marker-set for the right foot and leg and table 2-3 shows the description and the position of the markers.
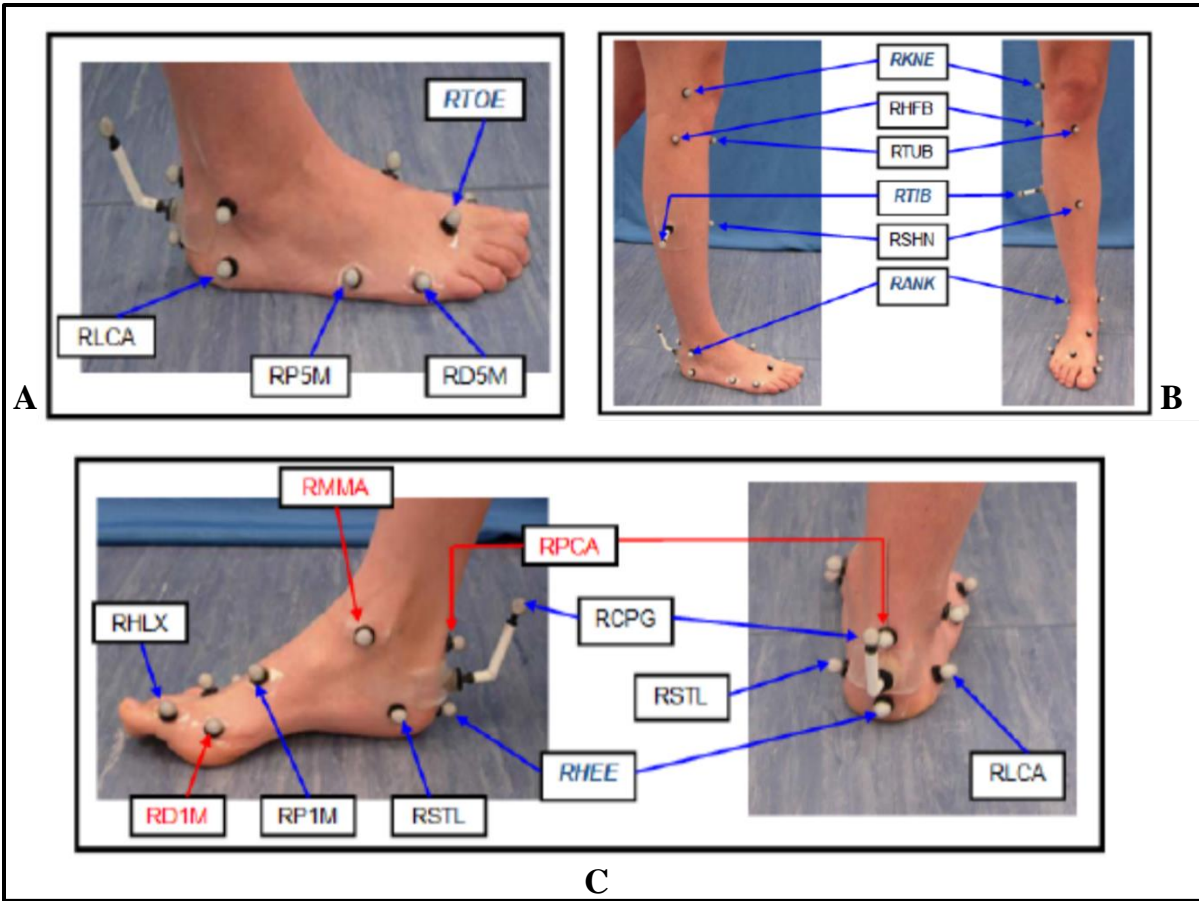
Fig. 2-5: The Oxford foot model marker set. A) Lateral view of the foot markers. B) Lateral and frontal view of the lower leg and ankle markers. C) Lateral and dorsal view of the foot markers. Markers pointed on with the red arrows are only for static trials and the markers with blue arrows are for both static and dynamic trials. Adapted from (Vicon Motion Systems, 2012).

Marker	Description-Position
RKNE	Standard lateral knee
RHFB	Lateral head of fibula
RTUB	Tibial tuberosity
RTIB	Tibial marker
RSHNK	Anterior aspect of the shin
RANK	Ankle
RMMA	Medial Malleoli
RSTL	Sustaniculum Tali
RPCA	Posterior calcaneus proximal
RHEE	Heel
RCPG	Posterior end of the calcaneus
RLCA	Lateral calcaneus
RP5M	5th metatarsal, proximal lateral
RD5M	5th metatarsal, distal lateral
RTOE	Toe
RD1M	1st metatarsal, distal medial
RP1M	1st metatarsal, proximal dorsal
RHLX	Hallux

Table 2-3: The Oxford foot model marker set. Description and the position of the markers on the right lower leg and foot for the Oxford foot model. Markers prefixed with R indicates right side. Adapted from (Vicon Motion Systems, 2012).

2.4.3.2   Capturing dynamic trials

After capturing static trials, participants walked on the treadmill with the same speed that they walked in the previous part and three dynamic trials were captured in a total period of three minutes walking.

2.5   Data processing

2.5.1   Processing data using Vicon Nexus application

The first step for processing data is to reconstruct and label marker trajectories. For labeling markers, a labeling skeleton need to be created by specifying the name of each marker. Figure 2-6 shows the labeling skeleton for the MSFM used for this study.
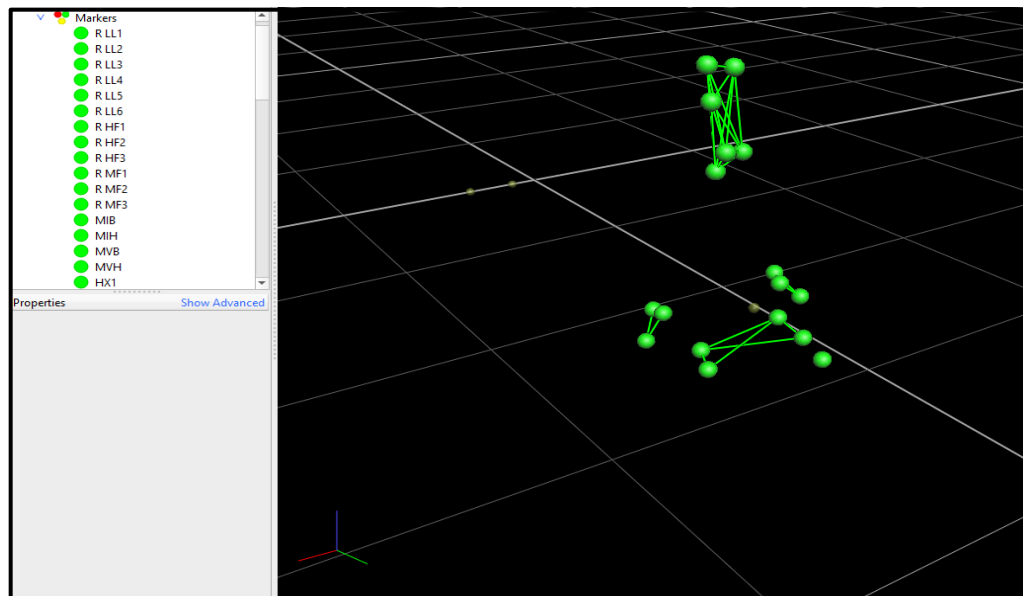
Fig. 2-6: Labeling skeleton. Labeling all markers and creating the marker-set for the MSFM used for this study.

After creating the labeling skeleton, the static and dynamic trials for each subject are needed to be uploaded and each trial was processed individually. After uploading the trials, all markers were labeled using the labelling skeleton we created before. In a trial, there might be some missing

information caused by occlusion or detachment of markers. Vicon Nexus facilitates filling these gaps using different methods such as spline fill, pattern fill, rigid body fill, kinematic fill, and cyclic fill. In this study, for filling gaps for marker trajectories with less than10 gaps in the whole trial and less than 100 frames in a gap, we used cyclic fill and for trajectories with more than 10 gaps in the trial, we used kinematic fill. Also, we used fourth order Butterworth smoothing zero-lag filter with a 6 HZ cut off frequency for removing noises from marker trajectories.

After processing static and dynamic trials for each subject, trials were uploaded into the Vicon ProCalc application for further analyzing and measuring motions.

2.5.2 Processing data using Vicon ProCalc application

The first step for analyzing data in Vicon ProCalc application is to create virtual markers based on the static digitization trials. In each trial, three markers of the calibration wand can be seen in addition to the MSFM marker-set. For each bony landmark, a virtual marker can be created by going through the corresponded static trial and using the wand orientation and dimension. The process of creating a virtual marker for LFH bony landmark is shown in figure 2-7 as an example. Vicon ProCalc allows creating a vector using two points in the space. As a result, a vector can be created using the first and second markers of the wand. We called this vector the "LFH vector". There is an option in Vicon ProCalc to create a point in direction of a selected vector and in a given distance from a chosen point. In this study, we chose the first marker of the wand as a base marker and used the direction of the vector created by the first and second markers of the wand. Based on the dimension of the wand used for this study, the distance from the base of the wand to the first marker is 122 millimeters. Thus, we created a marker in a 122 mm distance from the first marker of the wand, along the LFH vector. A virtual marker was created for each bony landmark using this method.
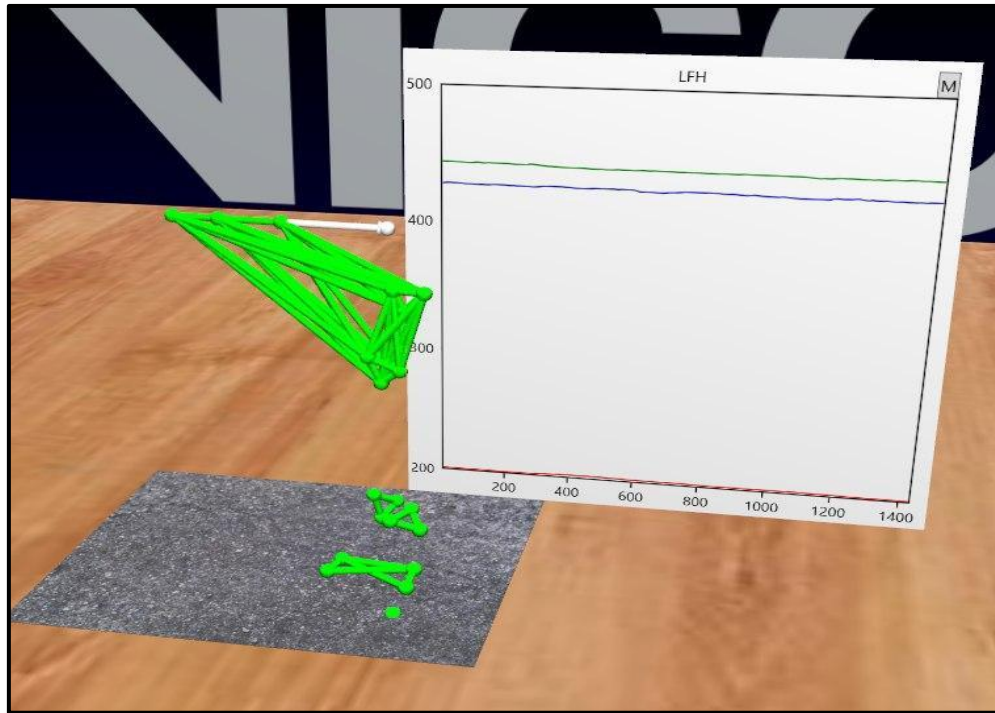
Fig. 2-7: Creating landmarks. The LFH bony landmark created virtually in Vicon ProCalc.

On the other hand, creating a virtual marker for each of the bony landmarks is particular for the corresponded static trial and the virtual marker can not be seen in other static or dynamic trials. To overcome this limitation, we need to find the transformation matrix between the virtual marker and the technical coordinate system of the segment. Using this method, the virtual marker can be reconstructed in other static and dynamic trials by having the technical coordinate system of the segment and transformation matrix. ProCalc allows finding the transformation matrix between a landmark and the correlated coordinate system and reconstruct the virtual marker in other trials by having the technical coordinate system of the segment. Hence, the next step is to create a technical coordinate system for each segment.

ProCalc allows the creation of a coordinate system using 3 markers on each segment. A technical coordinate system was created using 3 cluster markers on each of the following segments: lower

leg, hindfoot, and midfoot. For the medial and lateral forefoot segments, we used three single markers on each segment for creating a technical coordinate system (Fig. 2-8).
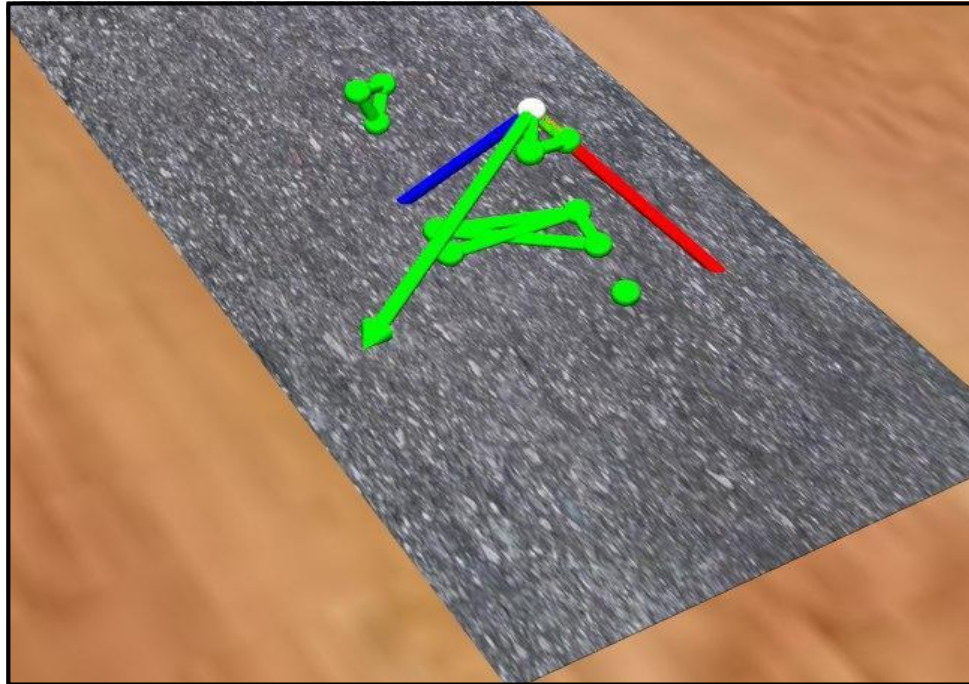
Fig. 2-8: Technical coordinate systems. The midfoot technical coordinate system created in Vicon ProCalc.

After the reconstruction of bony landmarks, an anatomical coordinate system for each segment was created using three bony landmarks on each segment with the axes oriented as follows:

1ˆ or $\vec{v}_1$- anterior or dorsal, 2ˆ or $\vec{v}_y$- medial on the right limb, and 3ˆ or $\vec{v}_z$- proximal along segment long axis. To do so, two defining vectors were created using bony landmarks, $\vec{v}_1$ and $\vec{v}_2$. Then, the third vector was created by crossing the first vectors as follow: $\vec{v}_x = \vec{v}_1 \times \vec{v}_2$. The last vector was created by crossing $\vec{v}_x$ and $\vec{v}_2$ ($\vec{v}_y$) and as follow: $\vec{v}_z = \vec{v}_x \times \vec{v}_y$.

Table 2-2 shows three bony landmarks on each segment and the defining vectors used to create an anatomical coordinate system on each segment.

2.5.3   Measuring angles

After creating Anatomical coordinate systems, the relative motion of segments was measured using the method of Grood and Suntay. The process of measuring ankle complex dorsi/plantarflexion based on this method is explained in the next section as an example.

2.5.3.1   Ankle complex dorsi/plantarflexion

The motion of the ankle complex is the rotation of the talus with respect to the lower-leg segment about the y-axis of the ankle joint coordinate system (Jenkyn et al., 2009). Based on the Grood and Suntay method, first we need to find a common floating axis between the Ankle complex and the lower-leg segments. The floating axis was created by taking the cross product of the x-axis of the Ankle joint coordinate system and y-axis of the lower-leg segment (Fig. 2-9. A). For measuring the ankle joint dorsi/plantarflexion, the angle between the floating axis of the ankle joint and lower-leg segment and the z-axis of the lower-leg segment should be calculated. ProCalc provides several options to calculate angles and one of them is to measure the angle between two vectors. The angle between the common vector created for the ankle joint and the lower-leg segment and the z-axis of the lower-leg segment was measured in order to define the ankle joint dorsi/plantarflexion (Fig. 2-10).
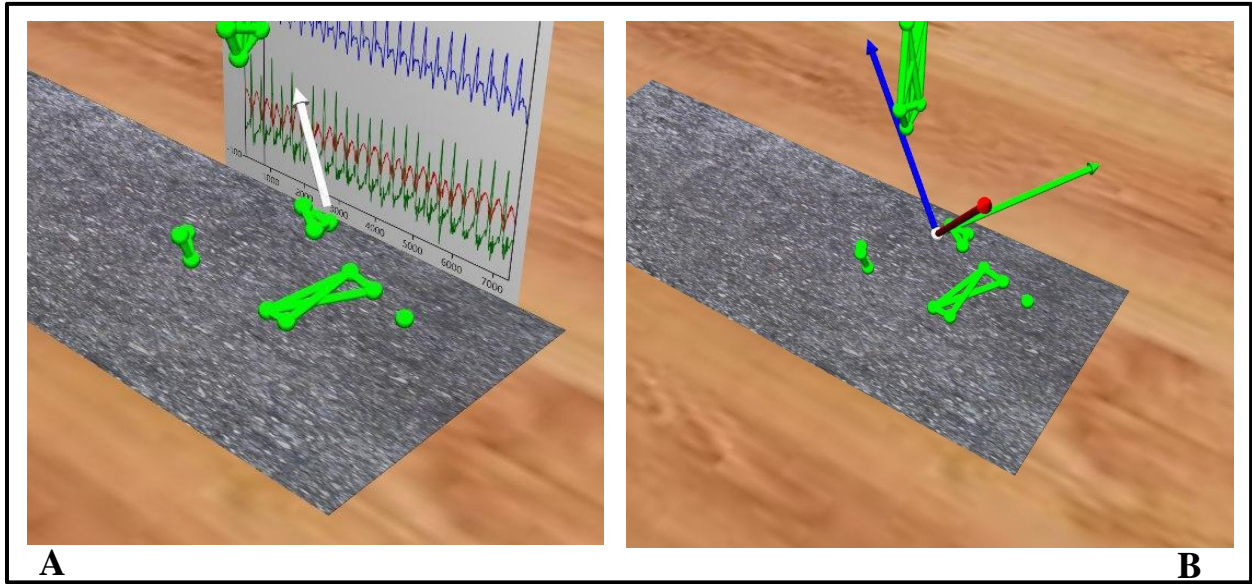
Fig. 2-9: Creating axes and coordinate systems in Vicon ProCalc. A) Ankle JCS and Lower leg common floating axis created in Vicon ProCalc and B) Ankle joint coordinate system.
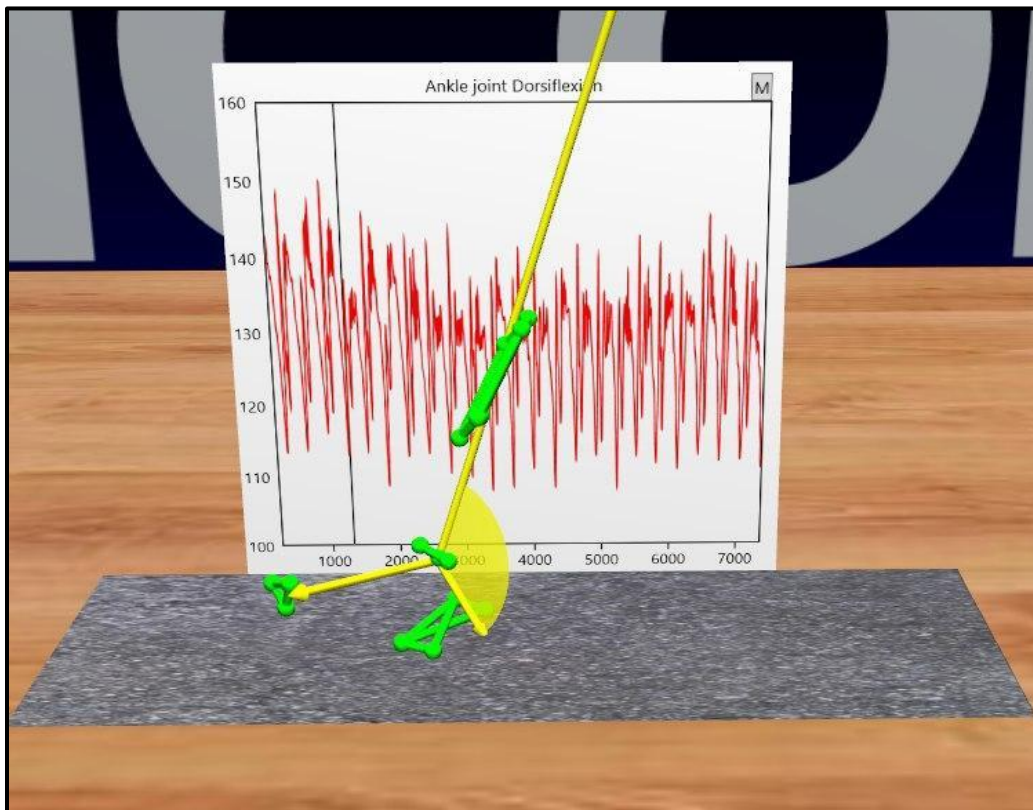
Fig. 2-10: Measuring motion in Vicon ProCalc. Ankle JCS dorsi/plantarflexion calculated in Vicon ProCalc over a dynamic trial.

Table 2-4 shows the process of creating floating axis and measuring angles for other motions within the foot and ankle.

Motion	Angle between	Floating axis
Ankle JCS Dorsi/Plantarflexion	Ankle and Lower leg floating axis- Lower leg v_z	Cross product of: Ankle v_x and Lower leg v_z
Forefoot Supination/Pronation wrt midfoot	A vector from MVH to MIH- Midfoot v_y	–
Hindfoot internal rotation wrt midfoot	Hindfoot and midfoot floating axis- Hindfoot v_y	Cross product of: Hindfoot v_x and Midfoot v_z
Hindfoot supination/pronation wrt midooft	Hindfoot and midfoot floating axis- Midfoot v_y	Cross product of: Hindfoot v_x and Midfoot v_z
Hallux dorsiflexion	Hallux and medial forefoot floating axis- Medial forefoot v_x	Cross product of: Hallux v_x and Medial forefoot v_y
Subtalar JCS inversion/eversion	Midfoot and subtalar JCS floating axis- Subtalar JCS v_x	Cross product of: Midfoot v_x and Subtalar JCS v_y
Relative motion of the medial and lateral forefoot segments	Medial forefoot v_z- lateral forefoot v_z	–

Table 2-4: The relative motions of the foot and ankle segments. For each motion, the process of creating the floating axis between corresponded two segments as well as the vectors articulating with the motion is described.

2.5.4   The rise and fall of the Medial Longitudinal Arch

The rise and fall of the medial longitudinal arch were calculated as the ratio of the arch height to length. The arch length was the magnitude of the vector from the CAMT landmark (medial posterior aspect of the hindfoot) to the MIH landmark (first metatarsal head). Arch height was the magnitude of the vector from MNT landmark (navicular tuberosity) perpendicular to the arch length (Fig. 2-11. A). The arch height and length vectors were created in ProCacl application and the ratio was calculated by dividing the magnitude of the arch height by the length (Fig. 2-11. B).
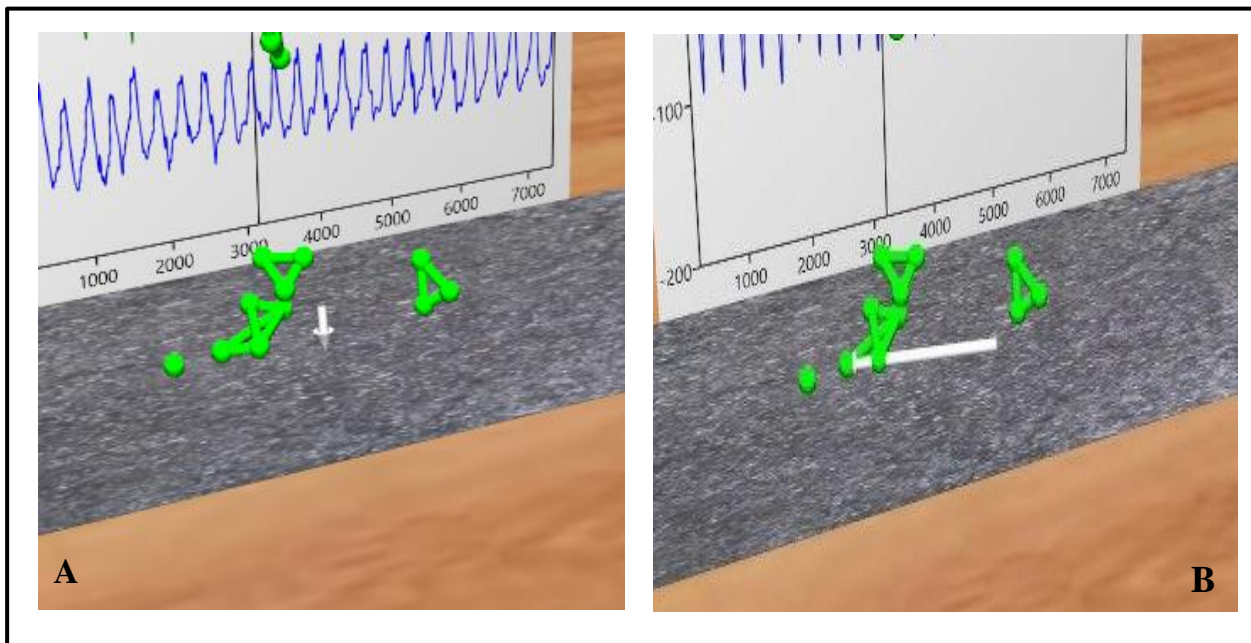
Fig. 2-11: The medial longitudinal arch vectors created in Vicon ProCalc. A) Height and B) Length of the medial longitudinal arch created in Vicon ProCalc.

2.5.5   Defining events

Events identify time points in a trial where something important such as heel-strike or toe-off occurs (Vicon ProCalc user guide, 2018). Vicon Nexus application defines gait events for the

Oxford foot model automatically. Since we used a custom foot model in this study, events were created manually using the Vicon ProCalc application.

In this study, a gait cycle starts with the heel-strike of the right foot and ends with the next heel-strike. Two important gait cycle events were defined using Vicon ProCalc application, heel-strike and toe-off.

For defining heel-strike or toe-off, we need to create a variable that changes its value cyclically during a trial. We can generate the event when the variable attains its maximum or minimum value in each cycle. However, we must find events that can uniquely identify each cycle before defining the heel-strike or toe-off. These events are called "cyclic events".

In this study, in order to define cyclic events, we created a plane parallel to the sagittal plane which passes through the MNT landmark on the midfoot segment of the foot (Fig. 2-12).
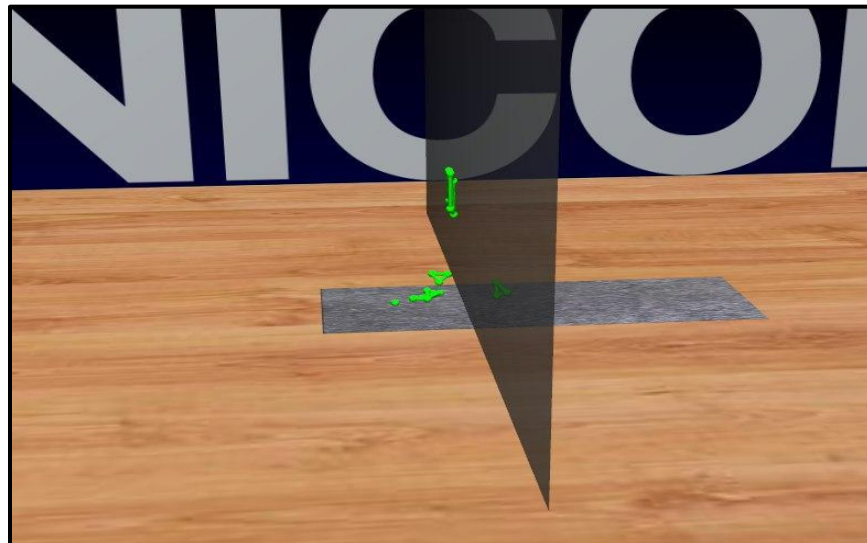
Fig. 2-12: Creating a plane for the cyclic event in Vicon ProCalc. A parallel plane to the sagittal plane which passes through the MNT landmark created in Vicon ProCalc for defining cyclic events.

Afterward, we created a vector that connects the hallux landmark to its projection on the plane (Fig. 2-13). The first cyclic event was defined when the value of the vector is equal to zero and it goes down. Likewise, the second cyclic event was created when the value of the vector is equal to zero and it goes up. Next, the time that foot goes from the first cyclic event to the second cyclic event was identified as a cycle.
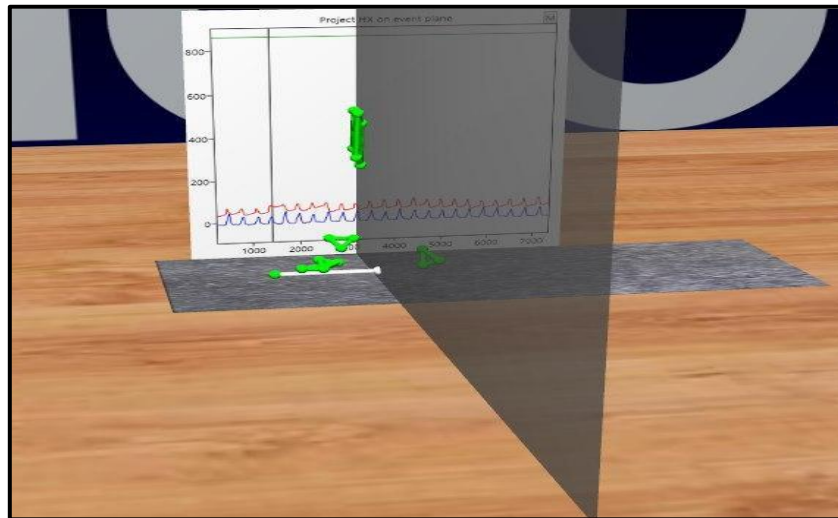
Fig. 2-13: Creating a vector for the cyclic event in Vicon ProCalc. Projection of the hallux on the plane created for defining cyclic events in Vicon ProCalc.

For the heel-strike event, a vector was created that connects the CAMT landmark of the heel to its projection on the floor plane and the vector was called the "heel-strike vector" (Fig. 2-14). The heel-strike event was generated when the heel-strike vector attains its minimum value between the first and second cyclic events.
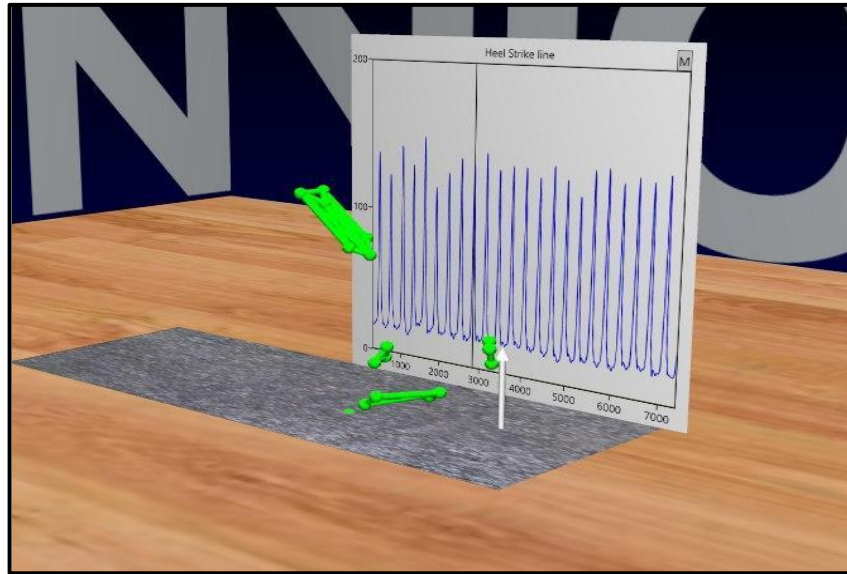
Fig. 2-14: Creating the heel-strike vector. The heel-strike vector created in Vicon ProCalc for defining the heel-strike event.

Similarly, for the toe-off event, a vector was generated that connects the hallux landmark to its projection on the floor plane and it was called "toe-off vector". The toe-off event was defined when the y-axis of the toe-off vector reaches its minimum value in each cycle (fig. 2-15).
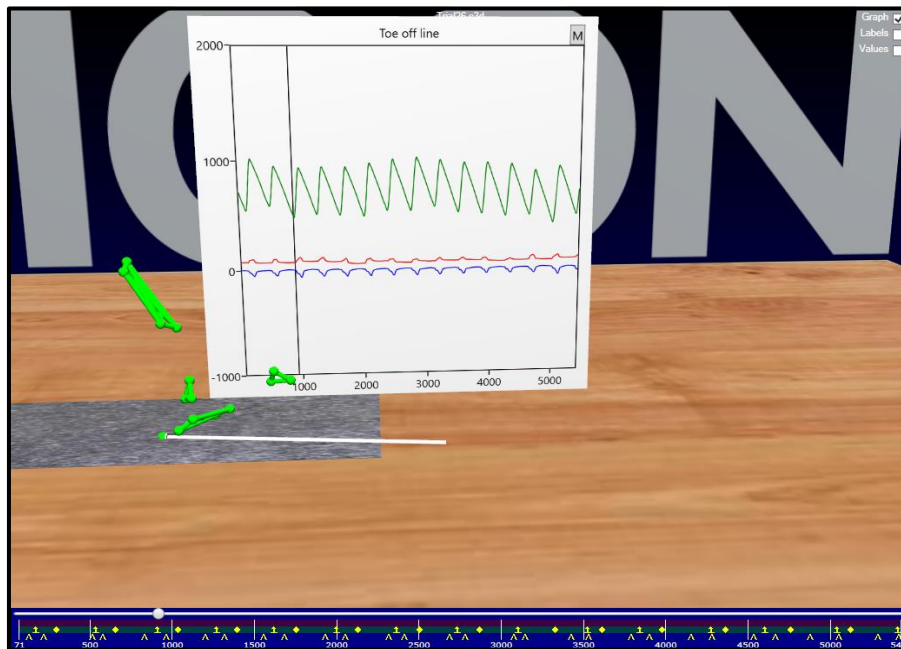
Fig. 2-15: Creating the toe-off vector. The Toe-off vector created in Vicon ProCalc for defining the toe-off event.

2.5.6 Exporting files

After measuring angles and defining events, trials need to be exported for further analysis. First, all trials were exported from Vicon ProClac application to Vicon Nexus application. Then, all angles and events were exported from Vicon Nexus application to excel files. Later, the excel files were used to calculate the average of the cycles and the results of the subjects using MATLAB.

2.5.7 Calculating the average

In order to attain more reliable measurements, we calculated the average of 10 gait cycles for each motion within the foot using custom-written codes in MATLAB. For each participant, three static standing trials were used to calculate the average of motions in quiet standing trials and a dynamic trial with 10 cycles used to measure the motions in the dynamic trial. In order to calculate the final result of each motion in a complete gait cycle, the average of the motion in 3 static trials was measured and reduced from the average of 10 dynamic cycles of the motion. However, for the medial longitudinal arch, the average of the height to length ratio in 10 dynamic cycles was divided by the average of the ratio in 3 static trials.

MATLAB codes for calculating the average of motions are attached to the appendix 7.1.

The average of each motion for 11 participants was calculated. the graphs of averaged overall subjects for each motion with one positive and one negative standard deviation will be presented in the next chapter.

3. CHAPTER 3-RESULTS

3.1 Joint motions measured using Vicon ProCalc

A total of eleven subjects successfully completed the testing session and the seven-segment foot model (lower leg, hindfoot, midfoot, forefoot, hallux, ankle JCS, and subtalar JCS) was successfully tracked for all subjects. Eight motions of the foot and ankle joint structures were reported for all eleven subjects: Ankle joint dorsi/plantarflexion (talus with respect to the lower leg), subtalar joint inversion/eversion (midfoot with respect to the talus), hindfoot segment supination/pronation and internal/external rotation (with respect to the midfoot), forefoot segment supination/pronation (with respect to the midfoot), hallux dorsiflexion (the motion of the first metatarsophalangeal joint), the rise and fall of the medial longitudinal arch, and the relative motion of the medial and lateral forefoot.

In this chapter, the eight joint motions measured with the multi-segment foot model developed by Jenkyn and Nicole are presented. Since the hallux dorsiflexion and the relative motion of the medial and the lateral forefoot were not measured in the study of Jenkyn and Anas (2008), only six of the motions were compared with the motions measured in the Jenkyn and Anas study (Thomas R. Jenkyn et al., 2009). By comparing the results of these two studies, the use of Vicon ProCalc for measuring joint motions will be validated with the use of MATLAB for measuring inter-segmental joint motions. Also, the joint motions measured using Oxford foot model are presented and compared with the Vicon ProCalc output angles.

Each joint motion is presented with two figures: The first figure for each motion shows all the individual curves for eleven subjects and the second graph presents the average over all subjects

(blue line) with one positive (green line) and one negative (red line) standard deviation. Each graph is scaled to 100% of a gait cycle with 0 at heel-strike and 100 at the next cycle heel-strike.

3.1.1 Ankle JCS dorsi/plantarflexion

Figure 3-1 shows the ankle JCS dorsi/plantarflexion normalized to zero for individual subjects and figure 3-2 represents the motion average over all subjects with one positive and one negative standard deviation. The minimum amount, maximum amount, and the range of the averaged over all subjects ankle dorsi/plantarflexion were -7.0, 8.1, and 15.1 degrees respectively (table 3-1). At heel-strike, the figures show a plantarflexed position of the ankle (-6.3±3.4 degrees) and when approaching foot-flat, the position of the ankle approached -4.6±3.7 degrees. Then the ankle underwent gradual dorsiflexion until toe-off at 62% of the gait cycle (1.5±7.2 degrees).
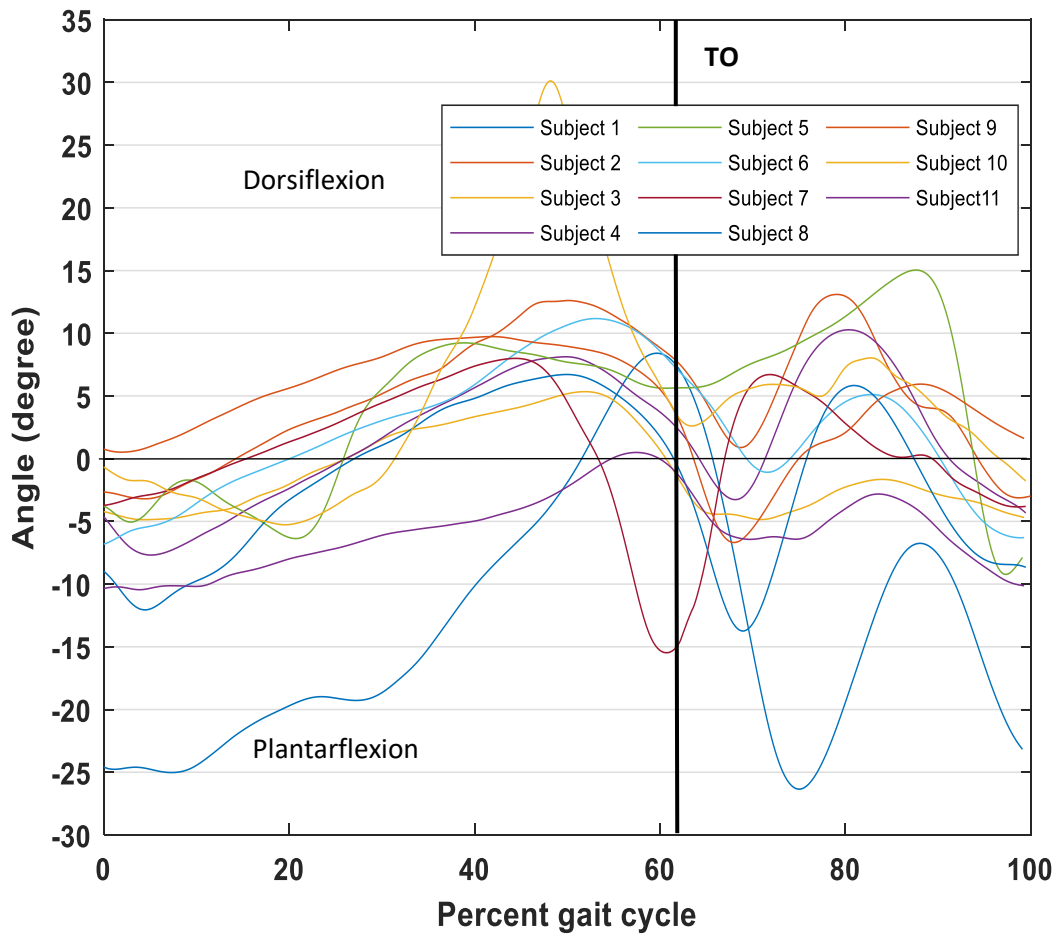
Fig. 3-1: The ankle joint dorsi/plantarflexion for individual subjects. The ankle JCS dorsi/plantarflexion in a walking gait cycle for individual subjects measured using Vicon ProCalc. 0% indicates the heel-strike and 62% indicates the toe-off. Next cycle heel-strike occurs at 100%.
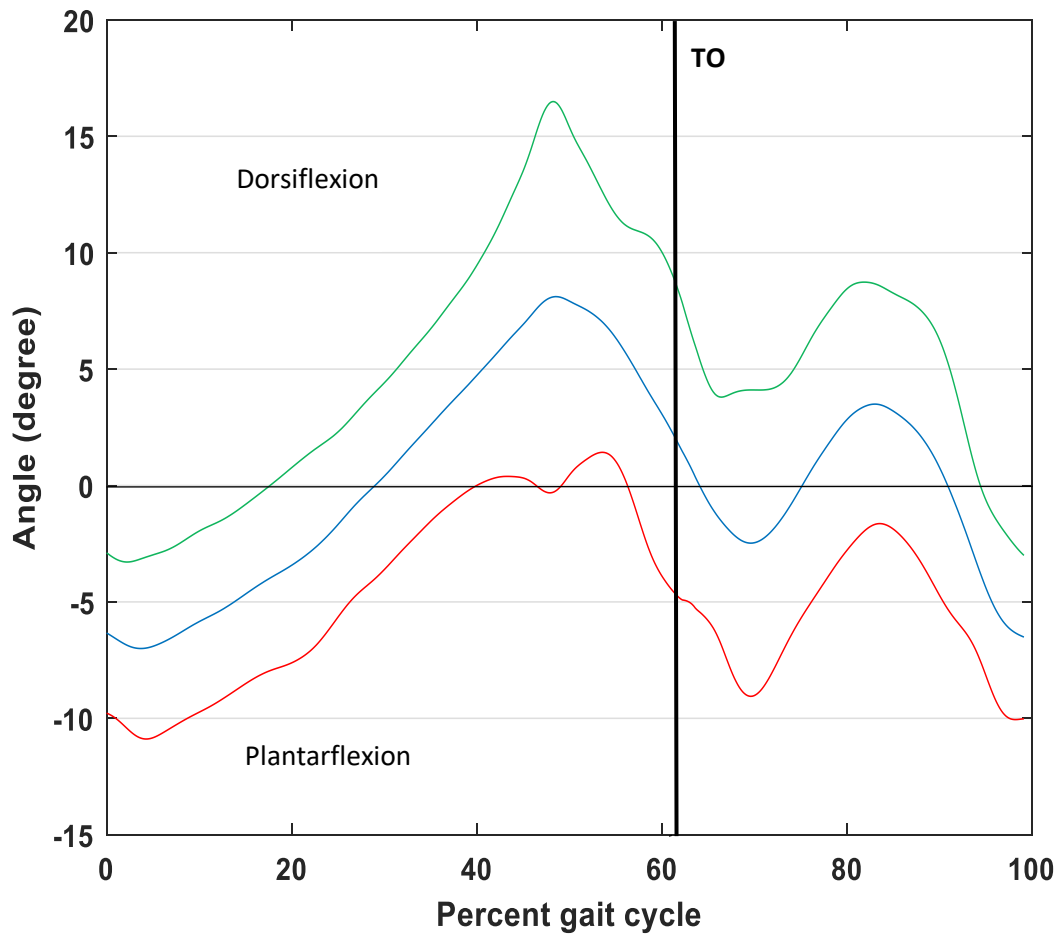
Fig. 3-2: The averaged overall subjects ankle dorsi/plantarflexion. The averaged over all eleven subjects ankle JCS dorsi/plantarflexion (blue) with one positive (green) and one negative (red) standard deviation in a walking gait cycle. Toe-off occurs at 62% of the gait cycle.

3.1.2   Subtalar JCS inversion/eversion

Figure 3-3 shows the subtalar JCS inversion/eversion normalized to zero for all subjects and figure 3-4 indicates the motion averaged over all subjects with one positive and one negative standard deviation. The mean of the motion over all subjects had a maximum amount of 6.6 degrees and a minimum amount of -1.7 degrees with a range of 8.3 degrees (table 3-1). At heel-strike, the subtalar joint began at an inverted position (1.4±3.0 degrees) and moved into eversion until the foot-flat (-1.2±2.5 degrees), then reached the greater eversion at mid-stance (-1.7±3.0 degrees). Next,

gradually inversion occurred at the joint until it reached the maximum amount at toe-off (6.5±4.0 degrees). Finally, from the toe-off, the subtalar joint underwent an eversion until the next gait cycle.
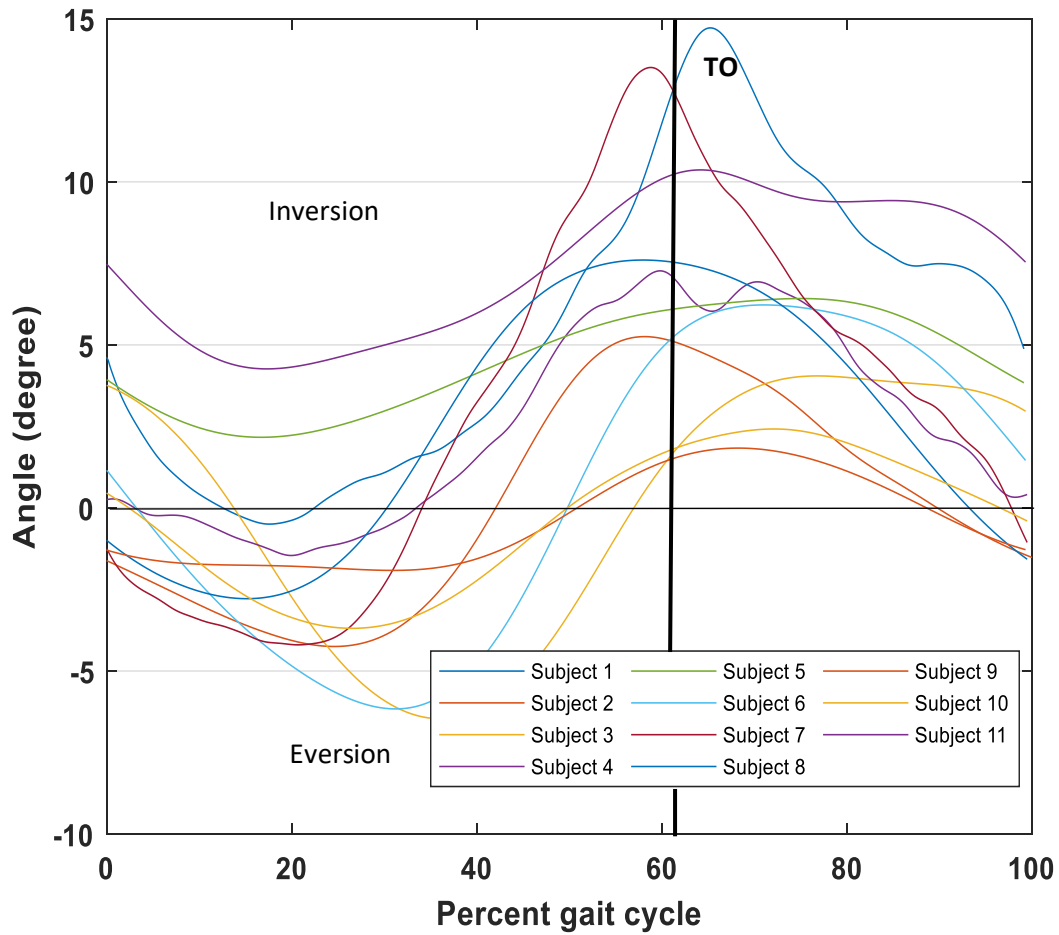
Fig. 3-3: The subtalar joint inversion/eversion for individual subjects. The subtalar joint inversion/eversion motion normalized to zero in a walking gait cycle for all eleven subjects.
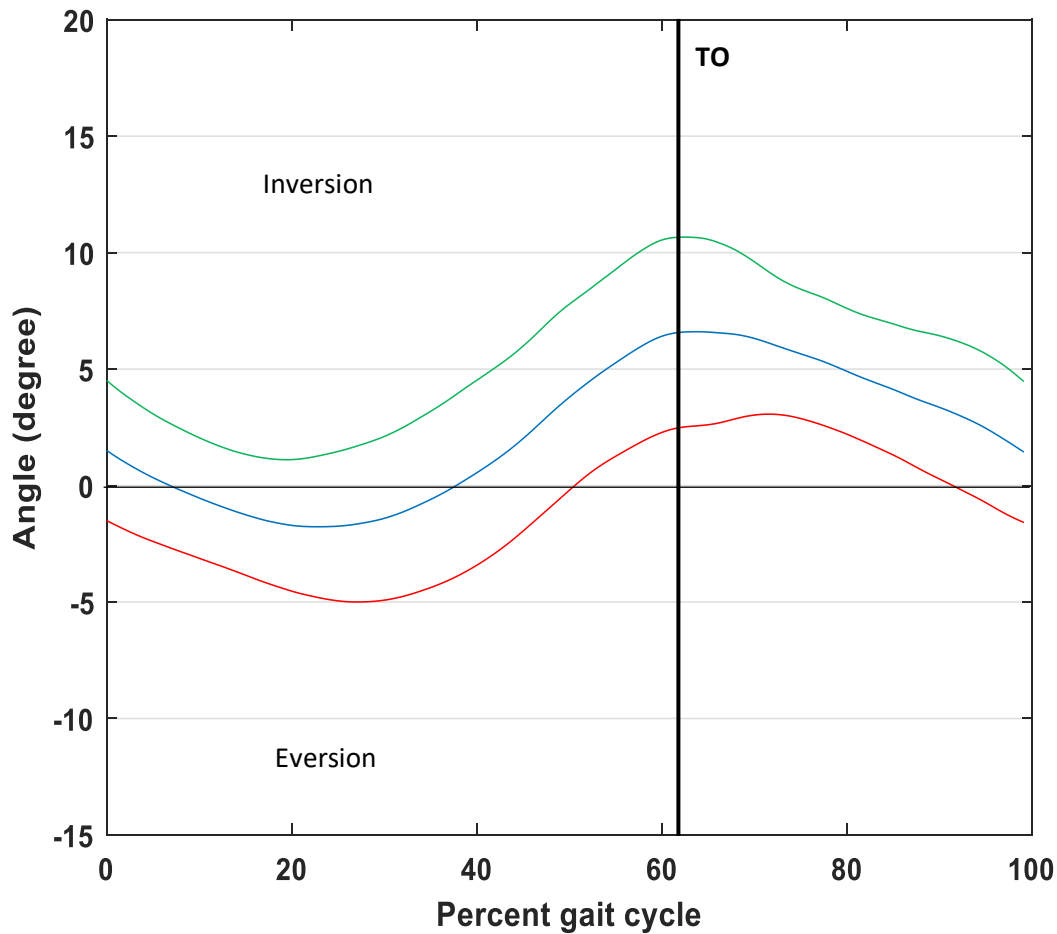
Fig. 3-4: The averaged over all subjects subtalar joint inversion/eversion. The averaged over all subjects (blue) with a positive (green) and negative (red) standard deviation for the subtalar joint inversion/eversion in a complete gait cycle.

3.1.3   Hindfoot supination/pronation with respect to the midfoot

Figure 3-5 shows normalized to zero hindfoot segment supination/pronation with respect to the midfoot for all eleven subjects and figure 3-6 indicates the averaged over all motion in a walking gait cycle with the maximum amount of 2.4 degrees, the minimum amount of -3.5 degrees, and the range of 5.9 degrees (table 3-1). Based on figure 3-6, it can be perceived that the hindfoot began at slight pronation at heel-strike with -1.0±2.3 degrees and reached to -3.4±5.5 degrees at mid-stance. From mid-stance until the toe-off, the hindfoot underwent gradual supination and it

reached 1.6±3.5 degrees at toe-off. Then, from 80% of the gait cycle up to the end, the hindfoot

had slight pronation.
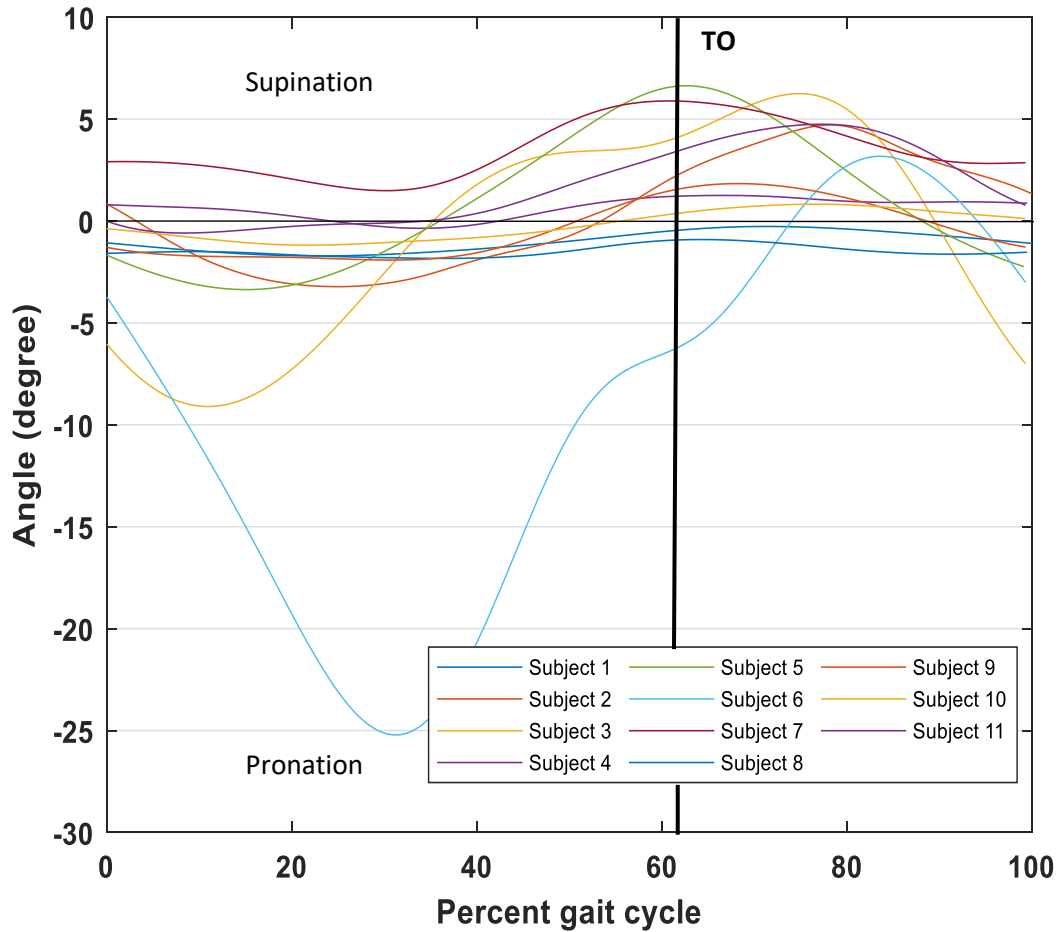
Fig. 3-5: The hindfoot supination/pronation with respect to the midfoot for all subjects. The normalized to zero hindfoot supination/pronation with respect to the midfoot segment in a walking gait cycle for all eleven subjects.
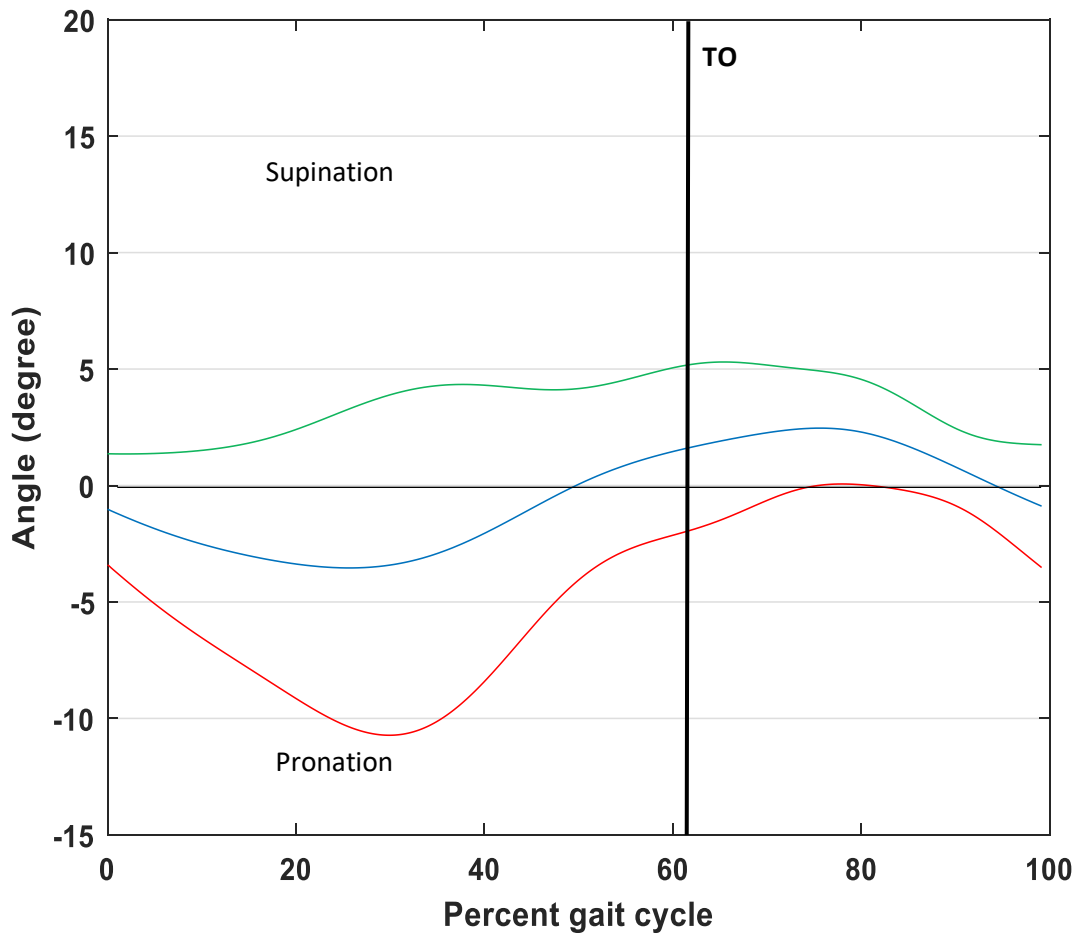
Fig. 3-6: The average supination/pronation of the hindfoot with respect to the midfoot. The averaged over all subjects (blue) hindfoot segment supination/pronation with respect to the midfoot with one positive (green) and one negative (red) standard deviation in a walking gait cycle.

3.1.4 Hindfoot internal/external rotation with respect to the midfoot

Figure 3-7 shows the hindfoot segment motion in the transverse plane with respect to the midfoot for all subjects in a walking gait cycle and figure 3-8 shows the averaged over all subjects motion with the maximum amount of 2.4 degrees and the minimum amount of -1.8 degrees. The range of motion was 4.2 degrees (table 3-1). the hindfoot began at a neutral position (-0.04±4.2 degrees) at the heel-strike, and when approaching the mid-stance, the position of the hindfoot reached 2.3±3.2

degrees. Then, gradually underwent an external rotation until it reached -1.4±2.0 degrees at the toe-off. Finally, the hindfoot had slight internal rotation up to the next gait cycle.
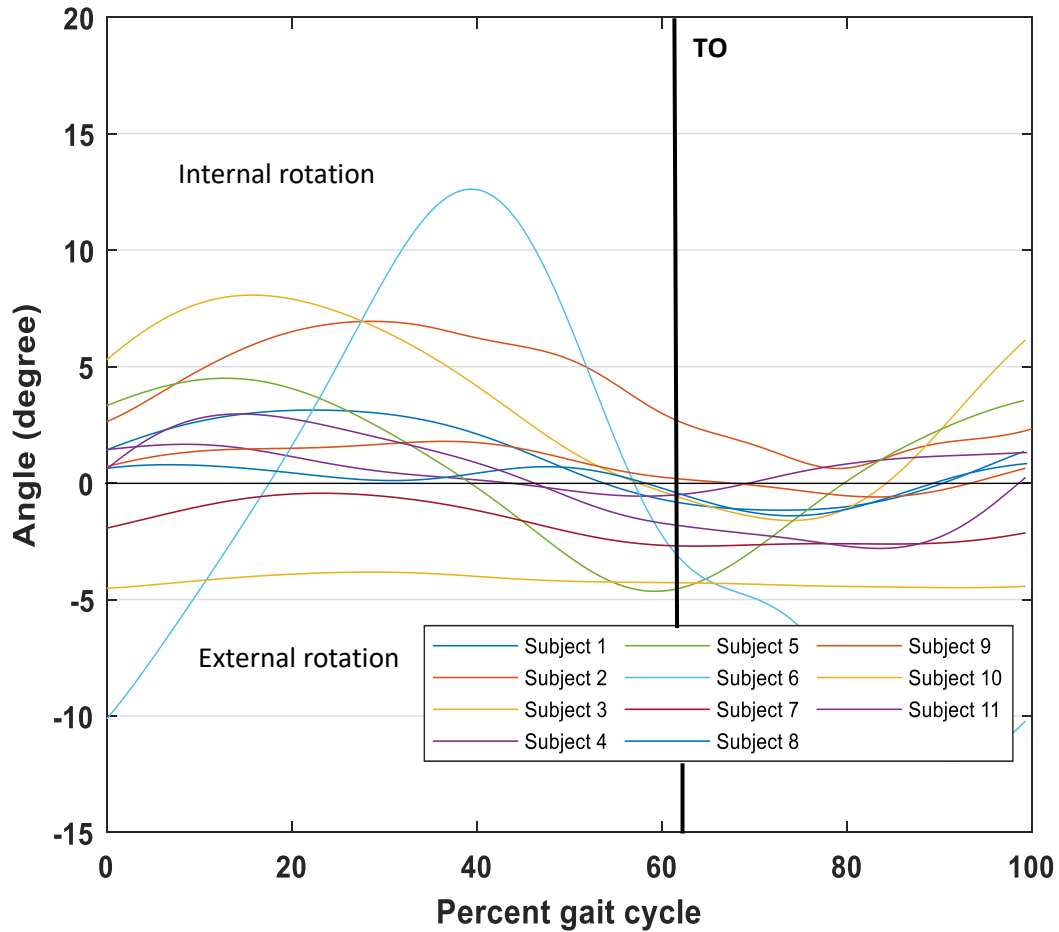
Fig. 3-7: The internal/external rotation of the hindfoot with respect to the midfoot for all subjects. The normalized to zero hindfoot segment internal/external rotation with respect to the midfoot for all subjects participated in the study.
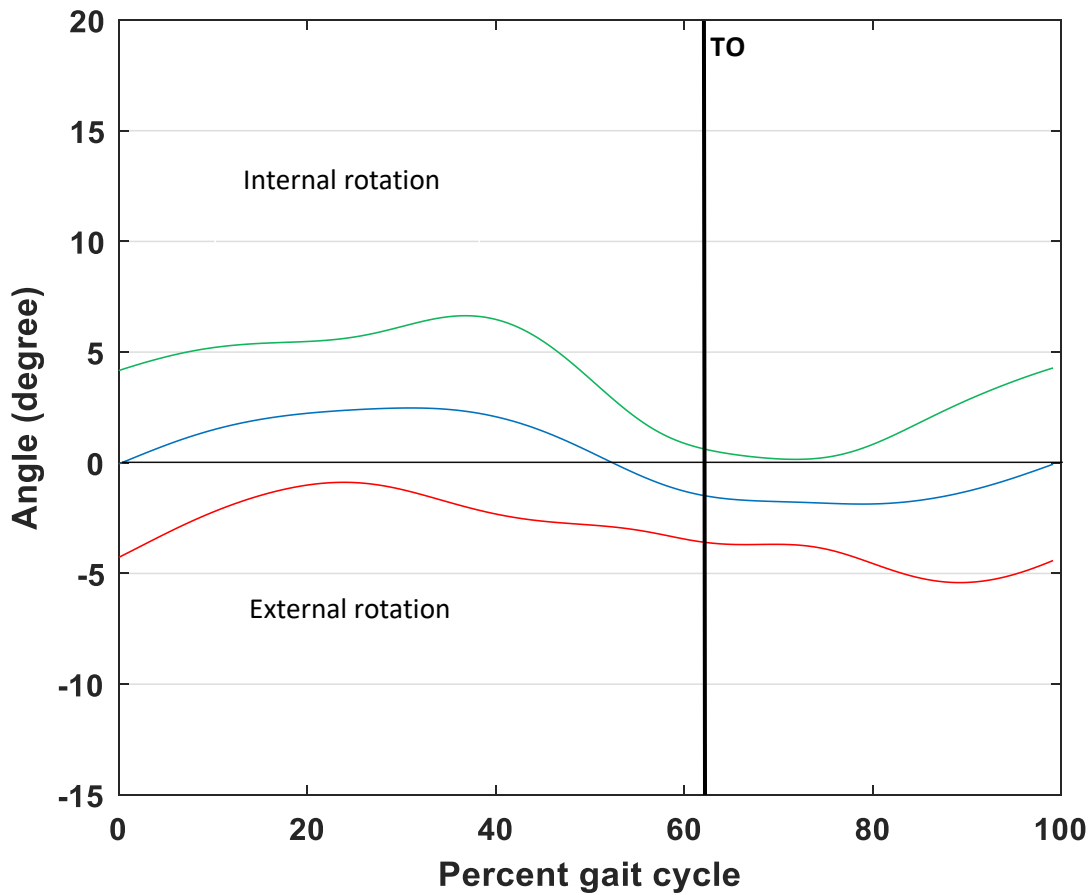
Fig. 3-8: The mean hindfoot internal/external rotation with respect to the midfoot. The averaged over all subjects hindfoot segment motion in the transverse plane with respect to the midfoot (blue) with one positive (green) and one negative (red) standard deviation.

3.1.5 Forefoot supination/pronation with respect to the midfoot

Figures 3-9 and 3-10 show the forefoot segment motion in the frontal plane with respect to the midfoot for all eleven subjects participated, and the averaged over all subjects motion in a complete gait cycle respectively. It can be noticed from the figures that the range of motion for the forefoot supination/pronation was 3.3 degrees with the maximum and minimum amounts of 2.3 degrees and -1.0 degrees respectively (table 3-1). The forefoot began at a neutral position (-0.2±1.4

degrees) at the heel-strike followed by slight pronation until it reached the mid-stance with -1.0±1.8 degrees. From the mid-stance up to the toe-off, the forefoot had supination and it attained its maximum amount (2.3±2.8 degrees) at the toe-off. Finally, from the toe-off until the next gait cycle, the forefoot had slight pronation and it reached the neutral position again at the end of the cycle.
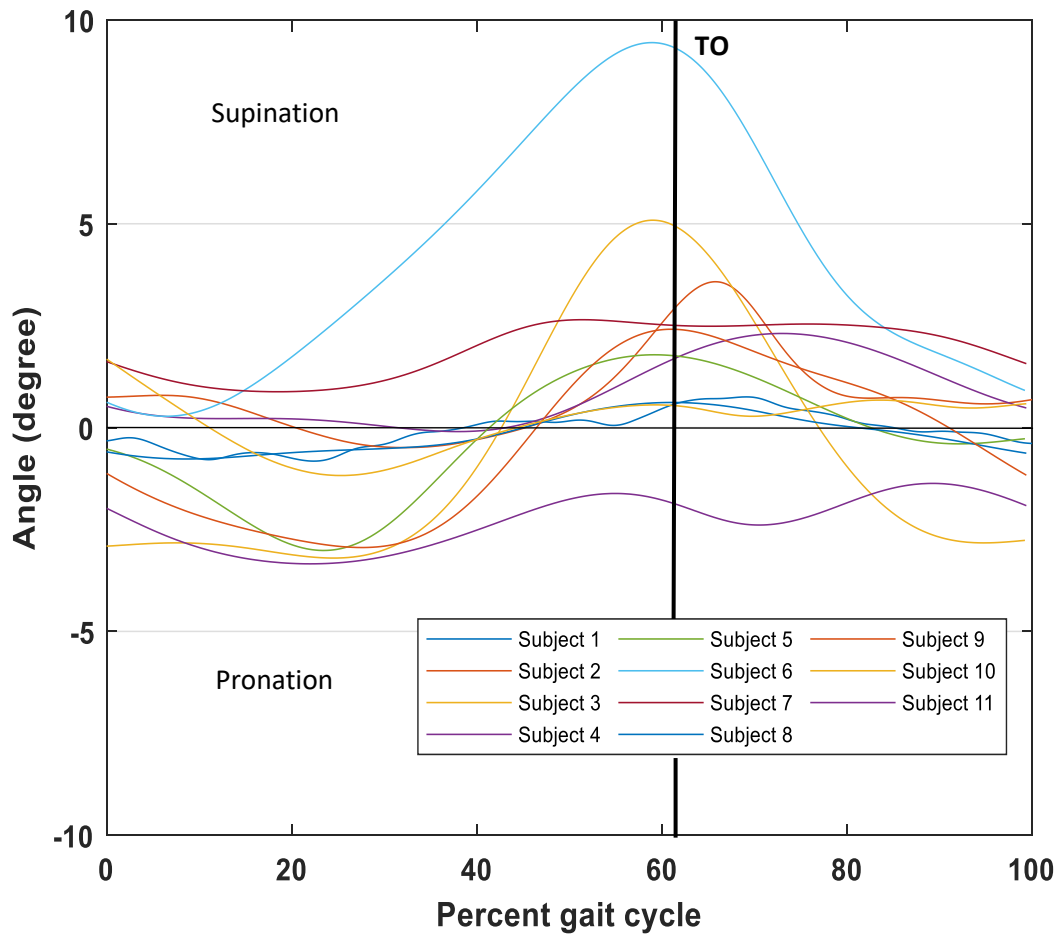
Fig. 3-9. The forefoot supination/pronation for all subjects. Normalized to zero forefoot supination/pronation with respect to the midfoot segment for all eleven subjects participated.
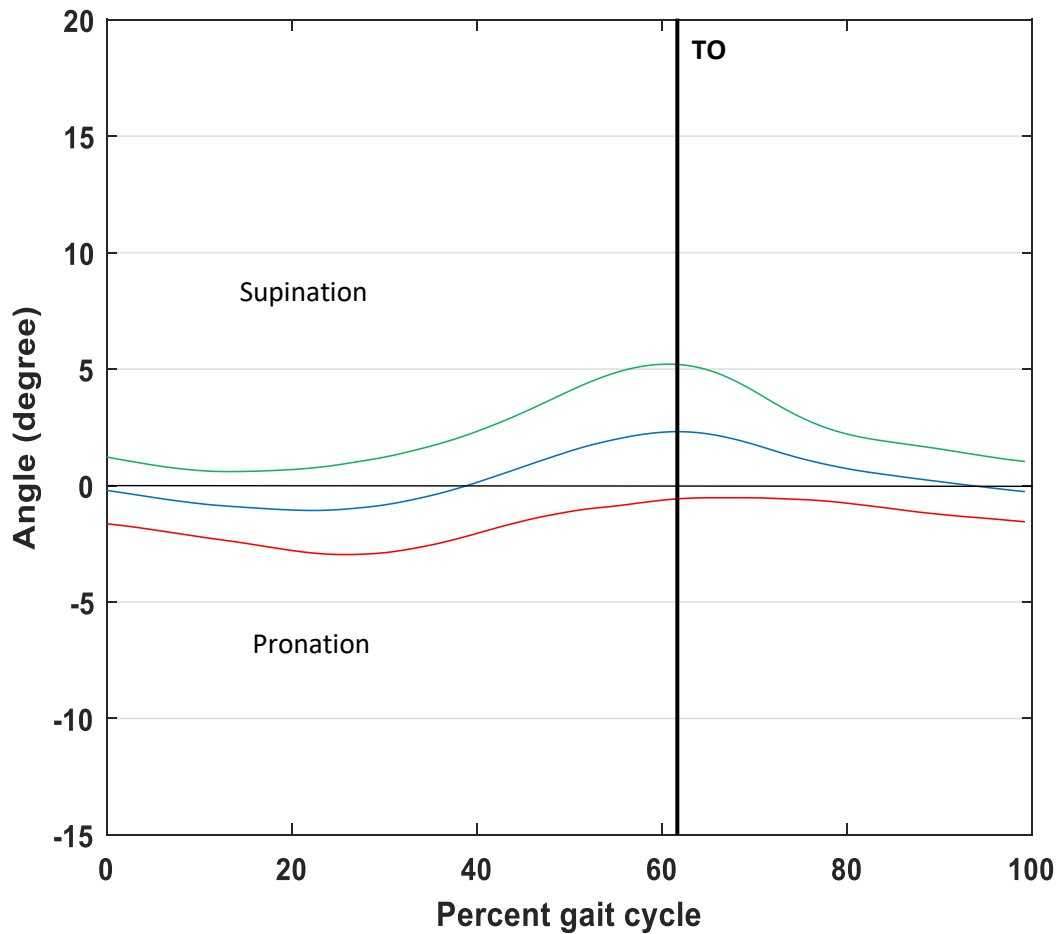
Fig 3-10: The mean forefoot supination/pronation over all subjects. The averaged over all subjects (blue) forefoot segment supination/pronation with respect to the midfoot with one positive (green) and one negative (red) standard deviation.

3.1.6 Hallux dorsiflexion

Figure 3-11 shows the normalized to zero hallux dorsiflexion in a walking gait cycle for all eleven subjects and figure 3-12 represents the averaged over all subjects motion. The maximum amount, the minimum amount, and the range of motion for the hallux dorsiflexion were 16.3, 0.5, and 15.8 degrees respectively (table 3-1). The hallux began at a dorsiflexed position (2.6±6.1 degrees) at the heel-strike and reached to a neutral position (0.9±2.6 degrees) at foot-flat. From the foot-flat until the toe-off, the hallux had a dorsiflexion until it reached close to its maximum amount at toe-

off (16.2±9.1 degrees). Finally, from toe-off up to the next gait cycle, hallux had a plantarflexion and it reached 3.0 ± 6.3 degrees at the end of the cycle.
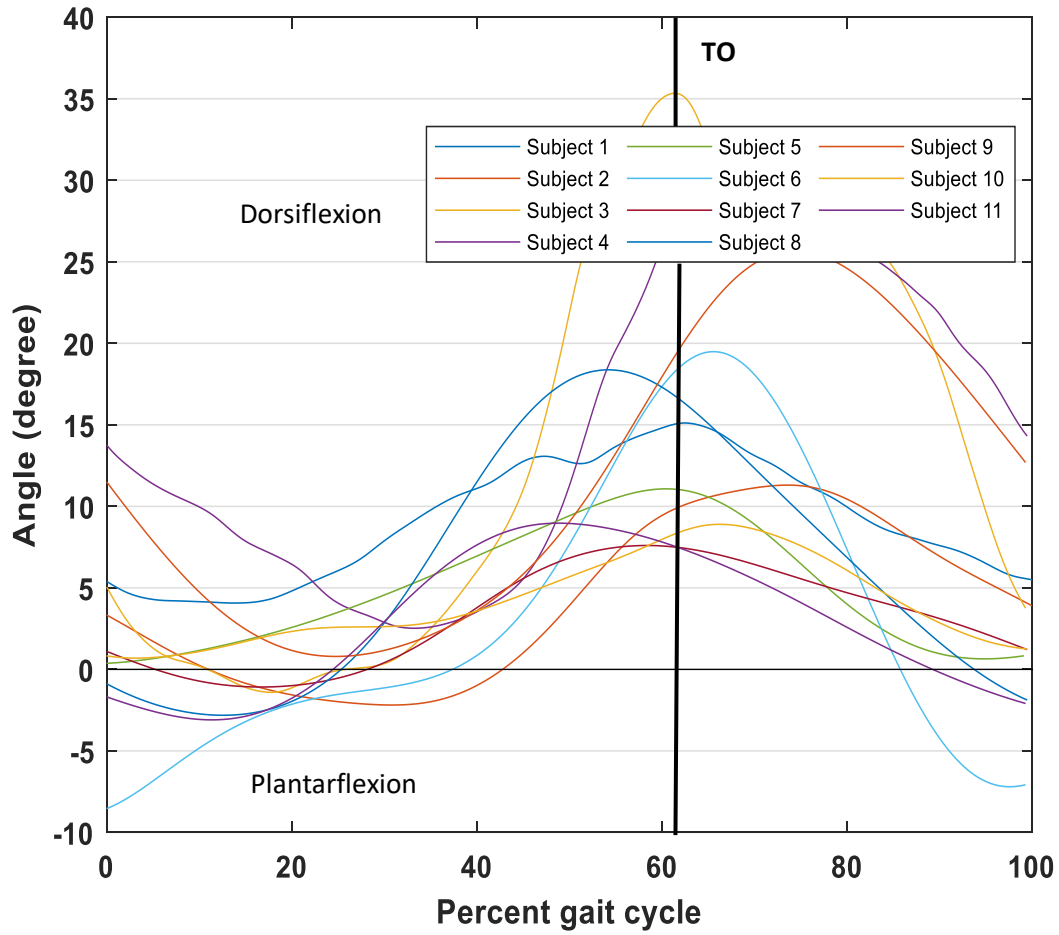
Fig. 3-11: The hallux dorsiflexion for all individual subjects. The normalized to zero hallux dorsiflexion curves plotted for all eleven subjects in a walking gait cycle.
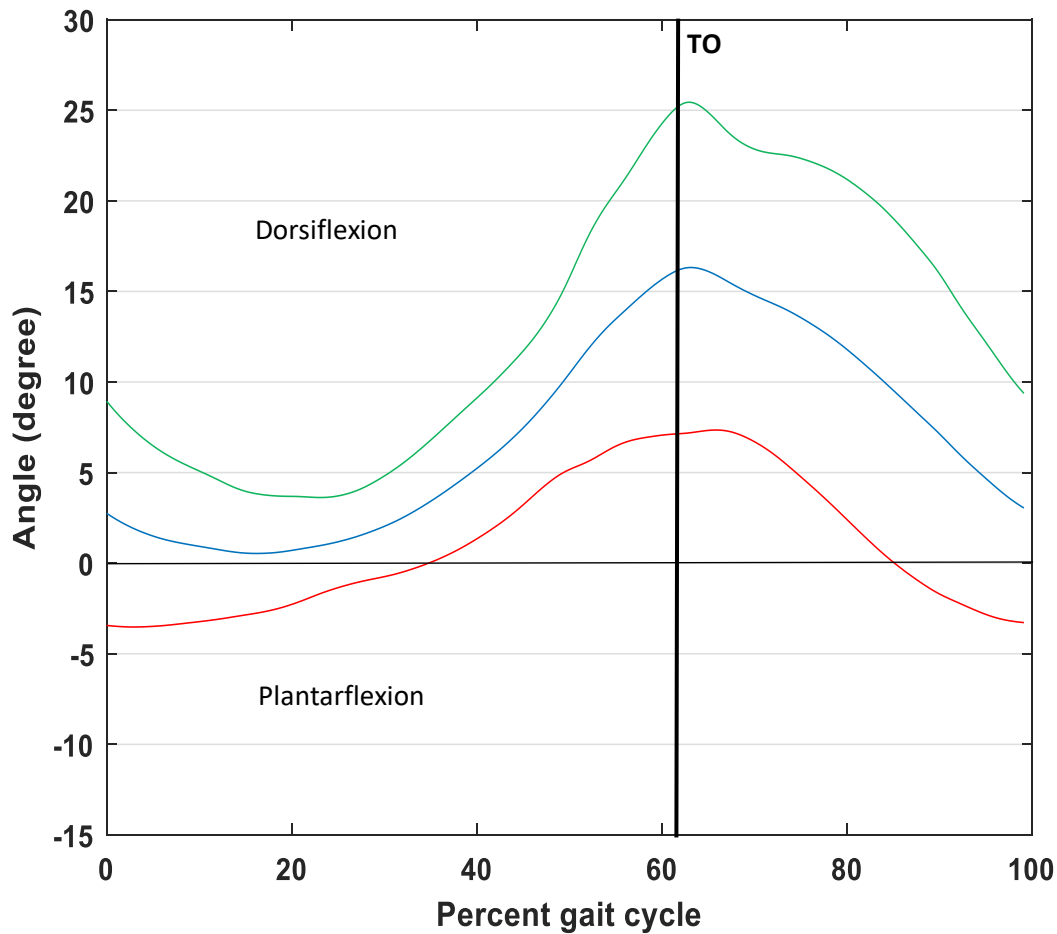
Fig. 3-12: The mean hallux dorsiflexion over all subjects. The averaged over all subjects (blue) hallux dorsiflexion with one positive (green) and one negative (red) standard deviation in a walking gait cycle.

3.1.7 Rise and fall of the medial longitudinal arch

Figure 3-13 indicates the normalized to 1 height to length ratio of the medial longitudinal arch for all eleven subjects and figure 3-14 shows the averaged over all motion with one positive and one negative standard deviation. The range of motion of the medial longitudinal arch was 0.27 with the minimum and maximum amounts of 0.95 and 1.22 respectively (table 3-1). The height to length ration of the MLA is unitless. At the beginning of the gait cycle, the height to length ratio of the arch was 1.0±0.07 and while reaching the mid-stance, the arch dropped until it reached the

minimum amount at mid-stance (0.9±0.05). From the mid-stance until the toe-off, the arch raised

and the ratio reached the 1.2±0.1 at the toe-off. Then from the toe-off, the arch dropped until its

next cycle heel-strike.
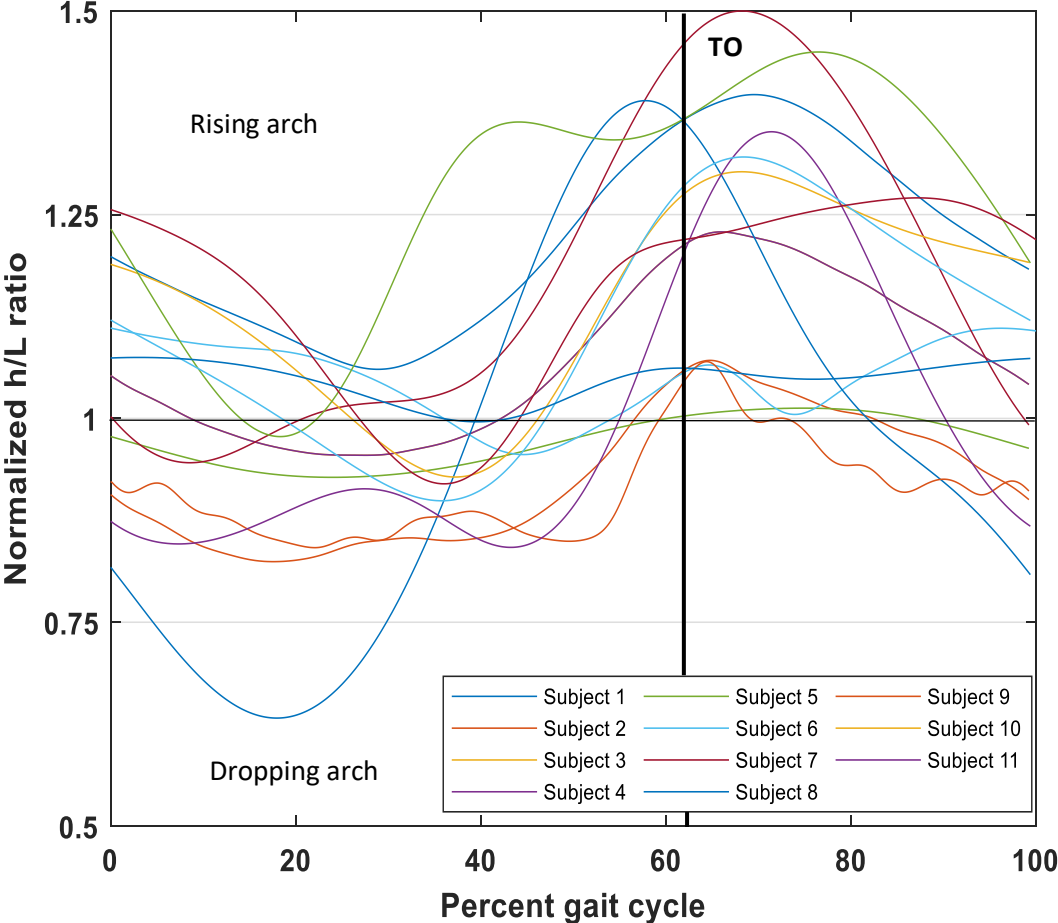
Fig. 3-13: The medial longitudinal arch motion for all subjects. The normalized to 1 height to length ratio of medial longitudinal arch plotted for all eleven subjects in a walking gait cycle.
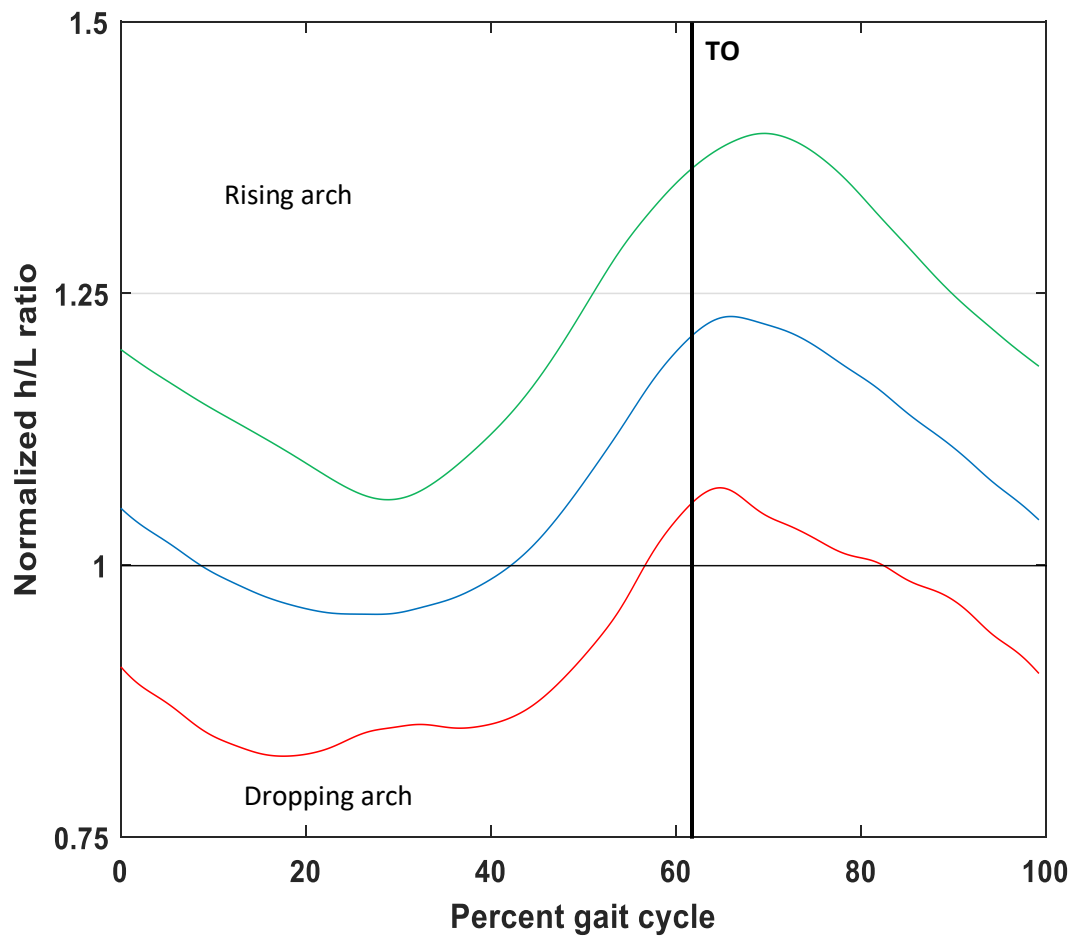
Fig. 3-14: The mean medial longitudinal arch motion over all subjects. The normalized to zero averaged over all subjects height to length ratio of the medial longitudinal arch (blue) with one positive (green) and one negative (red) standard deviation in a walking gait cycle.

3.1.8 Relative motion of the medial and lateral forefoot segments

Figures 3-15 shows the motion of the medial forefoot with respect to the lateral forefoot in the sagittal plane for all subjects individually and figure 3-16 represents the averaged over all subjects motion with one positive and one negative standard deviation. The range of motion for the relative motion of the medial and lateral forefoot was 4.1 degrees with the minimum and the maximum amount of 2.1 and 6.2 degrees respectively (table 3-1). Based on figure 3-16, the medial forefoot started the gait cycle at a dorsiflexed position (2.5±2.7 degrees) with respect to the lateral forefoot. From the heel-strike until the foot-flat, the medial forefoot moved into a plantarflexion and it reached the minimum amount of dorsiflexion (2.1±3.1 degrees) a foot-flat. From the foot-flat, the medial forefoot underwent a dorsiflexion and reached 6.2±5.4 degrees at toe-off. The medial forefoot then moved into a slight plantarflexion and got closed to its initial position at the end of the gait cycle.
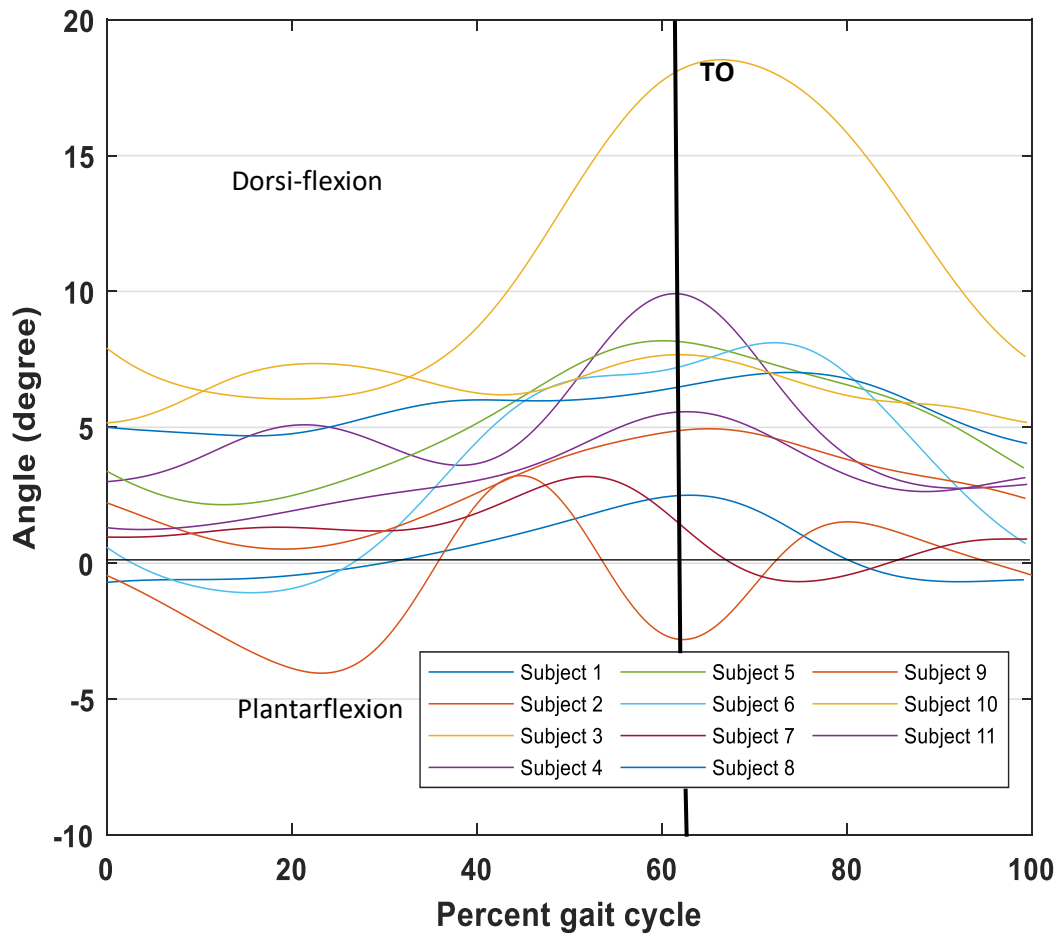
Fig. 3-15: The relative motion of the medial and lateral forefoot. The normalized to zero medial forefoot segment motion with respect to the lateral forefoot in the sagittal plane plotted for all individual subjects in a walking gait cycle.
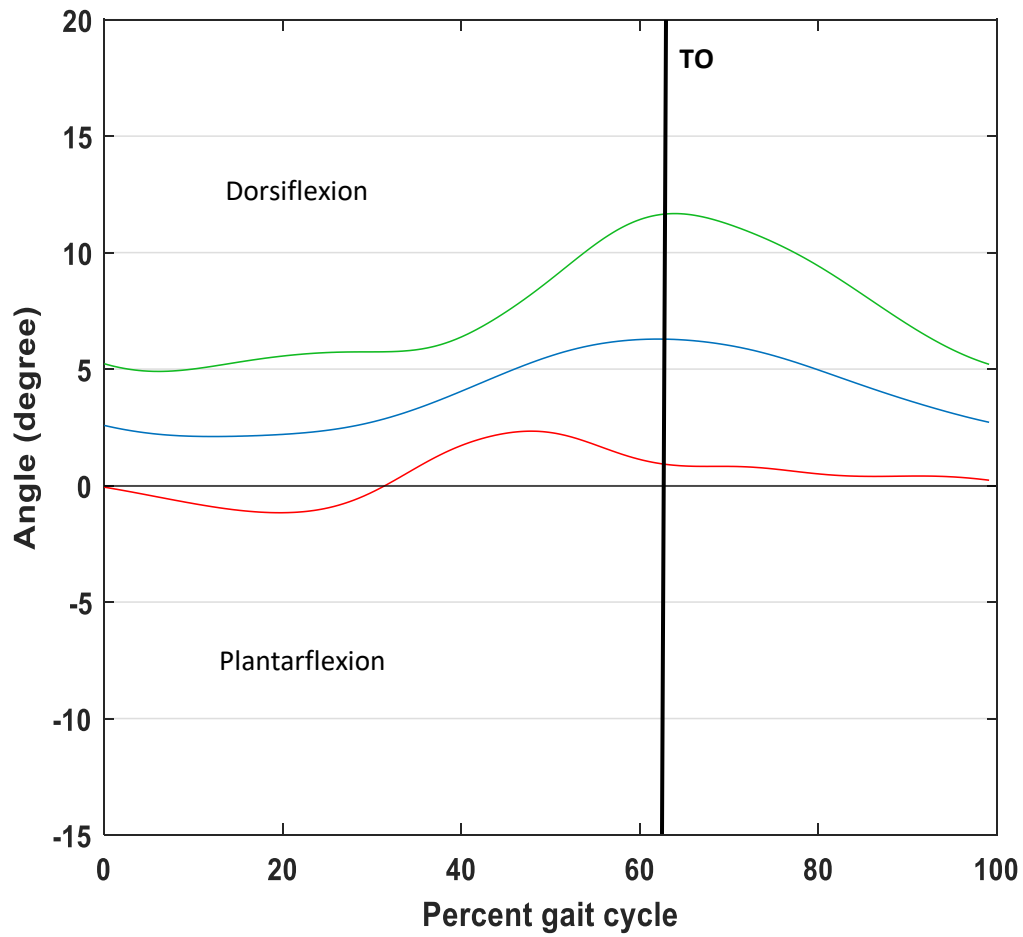
Fig. 3-16: The mean relative motion of the medial and lateral forefoot over all subjects. The normalized to zero averaged over all subjects (blue) medial forefoot dorsi/plantarflexion with respect to the lateral forefoot with one positive (green) and one negative (red) standard deviation.

Joint motion	Range of motion	Maximum	Minimum
Ankle dorsi/plantarflexion	15.1°	8.1°	-7.0°
Subtalar joint inversion/eversion	8.3°	6.6°	-1.7°
Hindfoot segment supination/pronation	5.9°	2.4°	-3.5°
Hindfoot segment internal/external rotation	4.2°	2.4°	-1.8°
Forefoot segment supination/pronation	3.3°	2.3°	-1.0°
Hallux dorsiflexion	15.8°	16.3°	0.5°
Rise and fall of the medial longitudinal arch	0.27	1.22	0.95
Relative motion of the forefoot segments	4.1°	6.2°	2.1°

Table 3-1: The maximum, minimum and the range of motion for the averaged over all subjects intersegmental joint motions measured using Vicon ProCalc. The range of motion and the maximum and minimum amount of the motion for all joint motions, except for the rise and fall of the medial longitudinal arch, are in degree. The height to length ration of the MLA is unitless.

3.1.9 Statistics

The coefficient of multiple correlation (CMC) was measured for all motions between subjects for measuring the repeatable patterns of motions using data analysis in Excel. The CMCs and the mean standard deviation over the gait cycle for all joint motions are listed in table 3-2. The CMC values show the greatest repeatability between subjects for the subtalar joint motion (0.81) and the smallest amount for the rise and fall of the medial longitudinal arch and the relative motion of the forefoot segments (0.52).

Joint motion	CMC	SD (mean)
Ankle JCS dorsi/plantarflexion	0.57	6.97
Subtalar JCS inversion/eversion	0.81	3.30
Hindfoot segment supination/pronation	0.77	4.06
Hindfoot segment internal/external rotation	0.61	3.34
Forefoot segment supination/pronation	0.69	1.94
Hallux dorsiflexion	0.72	6.01
Rise and fall of the medial longitudinal arch	0.52	0.14
Relative motion of the forefoot segments	0.52	3.55

Table 3-2: The Coefficients of multiple correlation (CMC) and the mean standard deviation measured for all joint motions. The CMC assessed the repeatability of joint motion curves between subjects and the mean standard deviation was calculated over the gait cycle for all joint motions.

3.2   Categorizing the arch type using Vicon ProCalc

In this section, the medial longitudinal arch type will be categorized and compared with the results of the arch height index measurement. Figure 3-17 shows the normalized height to length ratio of the medial longitudinal arch during a gait cycle for all eleven subjects and figure 3-18 shows the range of arch motion for each subject and the averaged over all subjects range of motion. Table 3-3 represents the maximum amount, minimum amount, the average of maximum amounts, the average of minimum amounts, and the standard deviation of the maximum amounts and minimum amounts of the height to length ratio for each subject. Based on this table, the foot arches that their minimum amount of height to length ratio was less than the "minimum of average-SD" are

categorized as pes-planus or foot-flat and foot arches that their maximum amount of height to length ratio was more than the "maximum of average+SD" are categorized as pes-cavus or high-arch. The foot arches that their maximum and minimum amounts of the h/L ratio were between the range of "minimum of average-SD" and "maximum of average+SD" are categorized as normal arch. Table 3-3 represents that in comparison to the AHI measurement categorization, the results of the 63% of the subjects were matching.
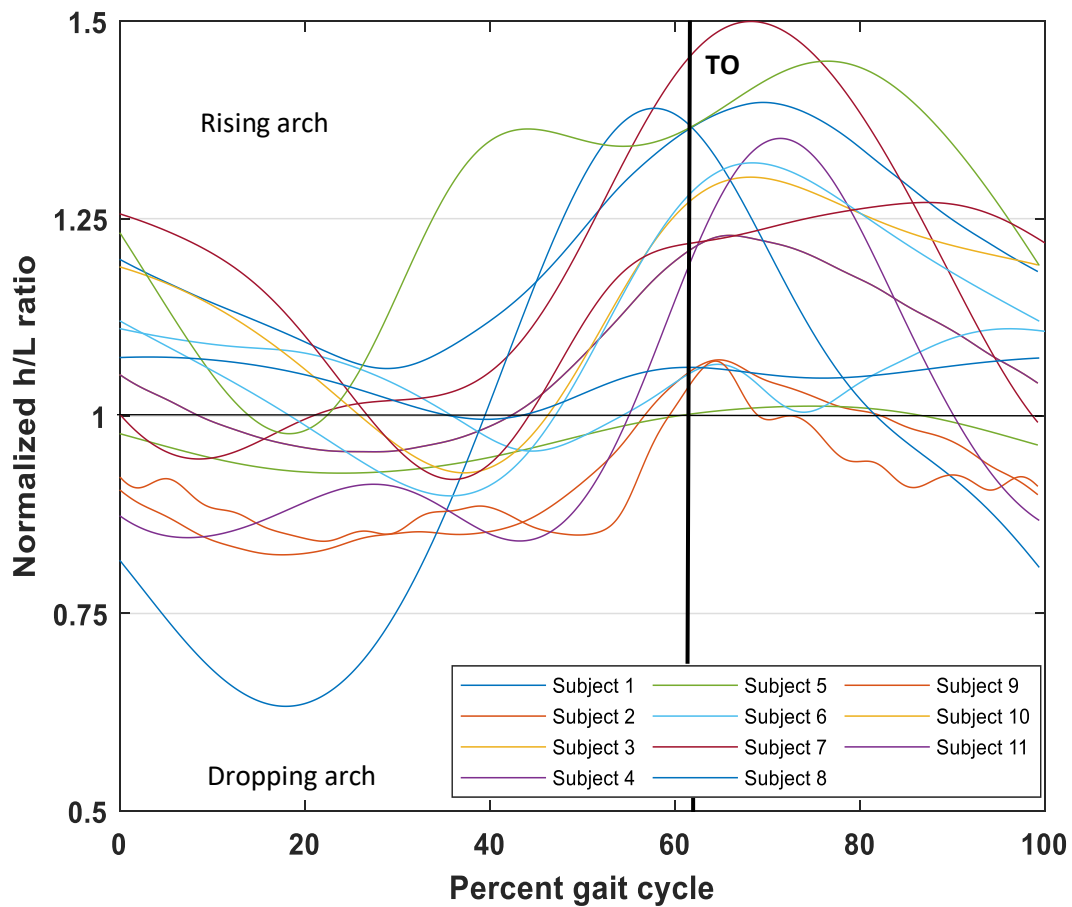
Fig. 3-17: The h/L ratio of the MLA for all subjects. The normalized to one h/L ratio measured using Vicon ProCalc for all individual subjects during the walking gait cycle.
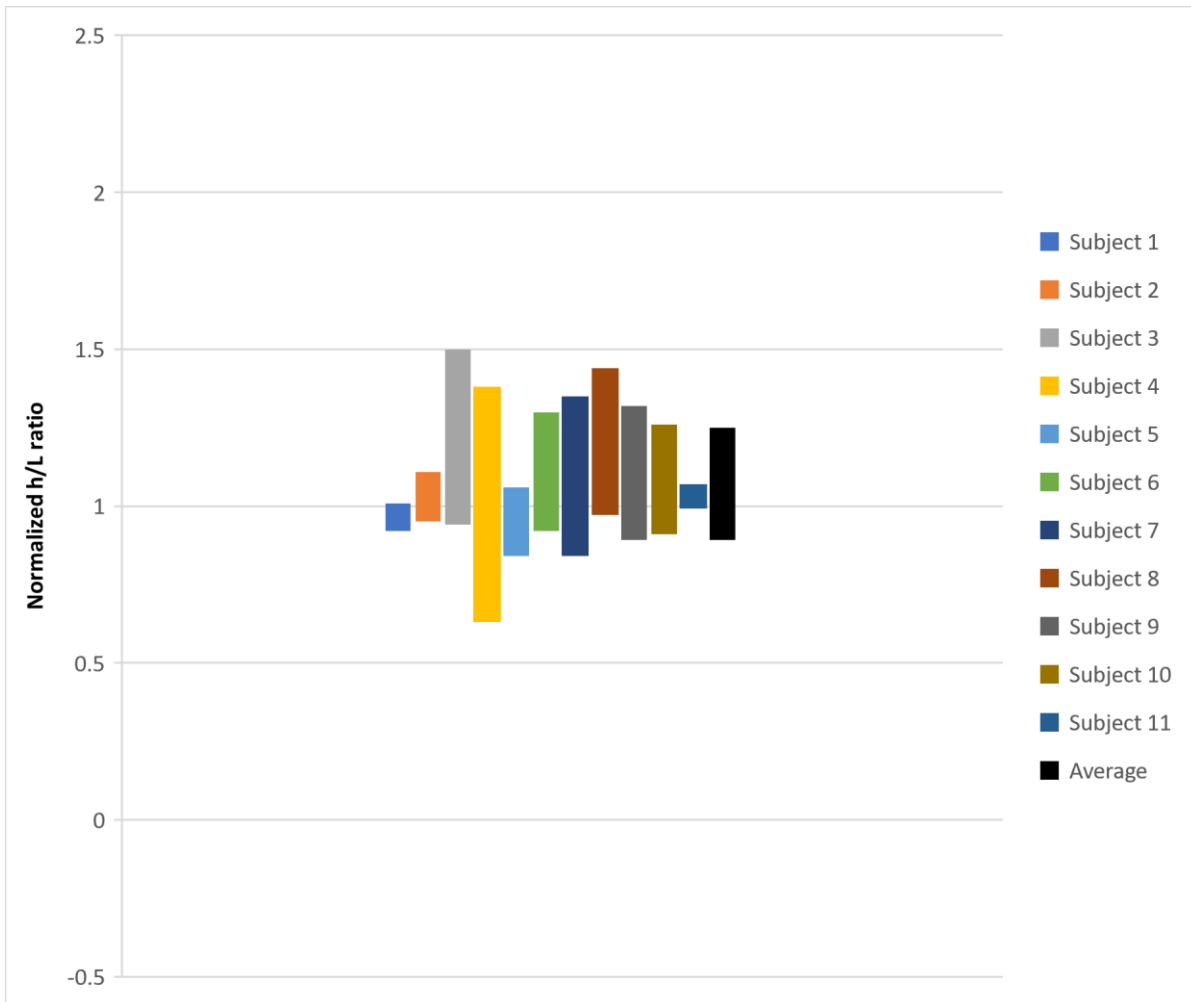
Fig. 3-18: The range of h/L ratio of the MLA measured using Vicon ProCalc for all subjects. The range of normalized to one h/L ratio for the medial longitudinal arch calculated using Vicon ProCalc for each subject during a gait cycle and the averaged over all subjects range of the h/L ratio.

Subject	Maximum h/L ratio	Minimum h/L ratio	Arch type	Arch type based on the AHI measurement
Subject 1	1.01	0.92	Neutral	Neutral
Subject 2	1.11	0.95	Neutral	Neutral
Subject 3	1.50	0.94	Pes-Cavus	Pes-Cavus
Subject 4	1.38	0.63	Pes-Planus	Pes-Planus
Subject 5	1.06	0.84	Neutral	Pes-Planus
Subject 6	1.30	0.92	Neutral	Neutral
Subject 7	1.35	0.84	Neutral	Neutral
Subject 8	1.44	0.97	Pes-Cavus	Pes-Planus
Subject 9	1.32	0.89	Neutral	Neutral
Subject 10	1.26	0.91	Neutral	Pes-Planus
Subject 11	1.07	0.99	Neutral	Pes-Cavus
Mean	1.25	0.89	-	-
SD	0.159	0.094	-	-
Mean max+ SD	1.40	-	-	-
Mean min- SD	-	0.79	-	-

Table 3-3: The arch type categorization for all subjects using results gathered from Vicon ProCalc. The maximum and minimum h/L ratio of the medial longitudinal arch measured using Vicon ProCalc for each subject, the mean and standard deviation of maximum amounts and minimum amounts, and the arch type categorized based on the mean and SD calculated for the h/L ratio and the AHI measurement.

3.3 Validation

In order to compare the use of the Vicon ProCalc application with the use of MATLAB for measuring inter-segmental joint motions, we compared the results of this study with the results of the Jenkyn and Anas study (Thomas R. Jenkyn et al., 2009) in which they used the same multi-segment foot model and a custom-written MATLAB code to calculate the motion of the foot and ankle joints. Only hallux dorsiflexion was not measured in the study of the Jenkyn and Anas (2009). P-value was determined for all motions using T-test (T-Test: Paired Two Sample for Means) in excel to test for statistical differences between the data in this study and the results of the Jenkyn and Anas study. Statistical significance was set at p< 0.03. The T-test output data is printed in appendix 7.3.

3.3.1 Ankle JCS Dorsi/plantarflexion

Figure 3-17 shows the ankle JCS dorsi/plantarflexion averaged over all twelve normal subjects with one positive and one negative standard deviation measured in Jenkyn and Anas (2009) study. The range of motion of the ankle JCS in the Jenkyn and Anas study 15.1 degrees which was as the same range of motion as in our study (15.11 degrees). It can be noticed that the trends of the ankle dorsi/plantarflexion curves in both studies are similar (p < 0.03). In the Jenkyn and Anas study, the ankle began at plantarflexed position at the mid-stance with 2.8±1.0 degrees of plantarflexion which is 3.5 degrees smaller than the degree of the plantar flexion in our study. At foot-flat, the ankle moved to greater plantarflexion with -4.1±1.0 degrees in Jenkyn and Anas study which was close to the degrees of plantarflexion in our study (-4.6 degrees). At the toe-off, the position of ankle in Jenkyn and Anas study was 1 degree of dorsiflexion greater than the position of the ankle at toe-off in our study. In general, the standard deviation for ankle dorsi/plantarflexion in our study

was greater compared with the standard deviation in Jenkyn and Anas study (2.4 and 2.7 degrees greater at heel-strike and foot-flat respectively).
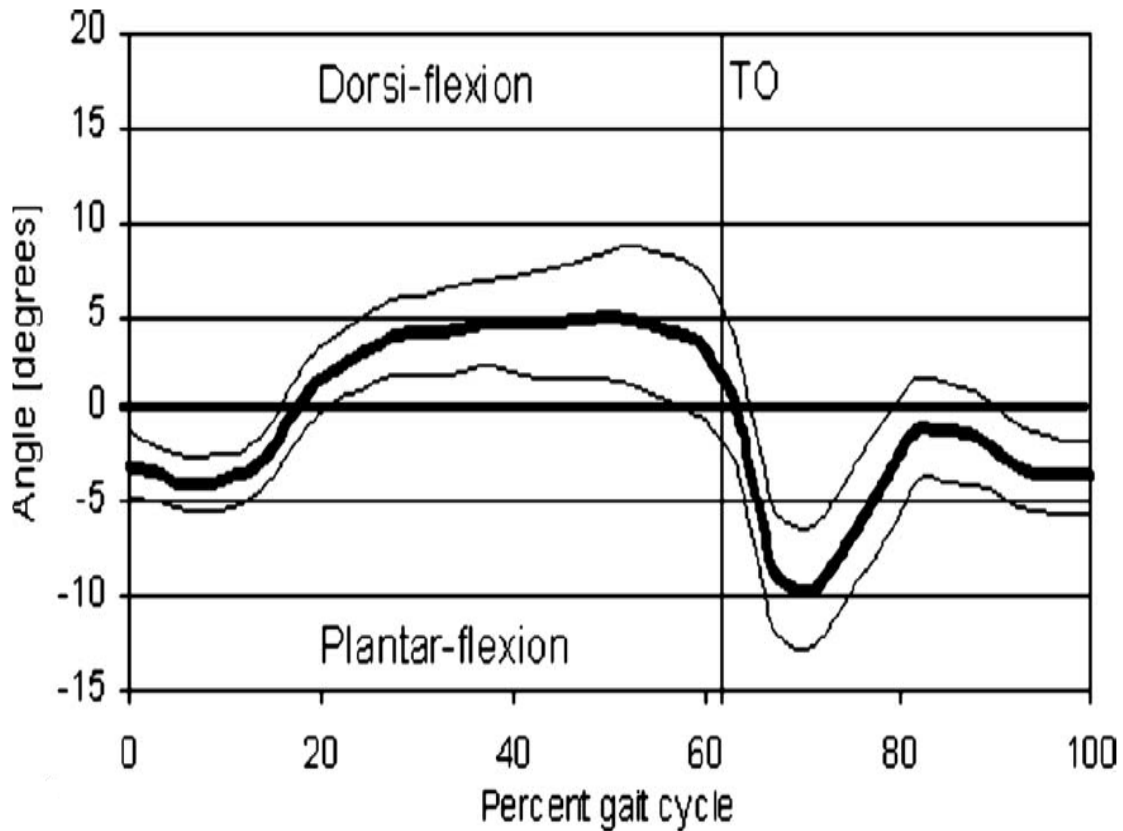
Fig. 3-19: Ankle JCS motion measured in Jenkyn and Anas study (2009). The normalized to zero averaged over all twelve subjects ankle JCS dorsi/plantarflexion with one positive and one negative standard deviation in Jenkyn and Anas study (Jenkyn and Anas, 2009).

3.3.2   Subtalar JCS inversion/eversion

Figure 3-18 represents the subtalar JCS inversion/eversion averaged over all twelve subjects in Jenkyn and Anas study. The range of motion for the subtalar joint was 9.7 degrees in Jenkyn and Anas study which was 1.5 degrees greater than the range of motion in our study. The subtalar joint began at a neutral position (0.7±3.6 degrees), however, it started at 1.4 degrees of inversion in our

study. Then, the subtalar moved to an everted position at foot-flat (-5.1±1.0 degrees) which was 3.9 degrees greater than the degree of eversion at foot-flat in our study. The subtalar joint finally moved to 4.4±1.3 degrees of inversion at toe-off while it was 2.1 degrees smaller than the degrees of inversion in our study at toe-off. It can be observed that the trend of the subtalar inversion/eversion curves in both studies are similar to each other (p < 0.03). The joint in both studies went through an eversion until mid-stance and then gradually moved into inversion until it reached close to its maximum degrees of inversion at toe-off. The standard deviation was 3.6 degrees at the beginning of the cycle in Jenkyn and Anas study which was 0.6 degrees greater than the standard deviation at heel-strike in our study. Then it reached 1.5 and 3 degrees smaller than the standard deviation at foot-flat and toe-off respectively in our study.
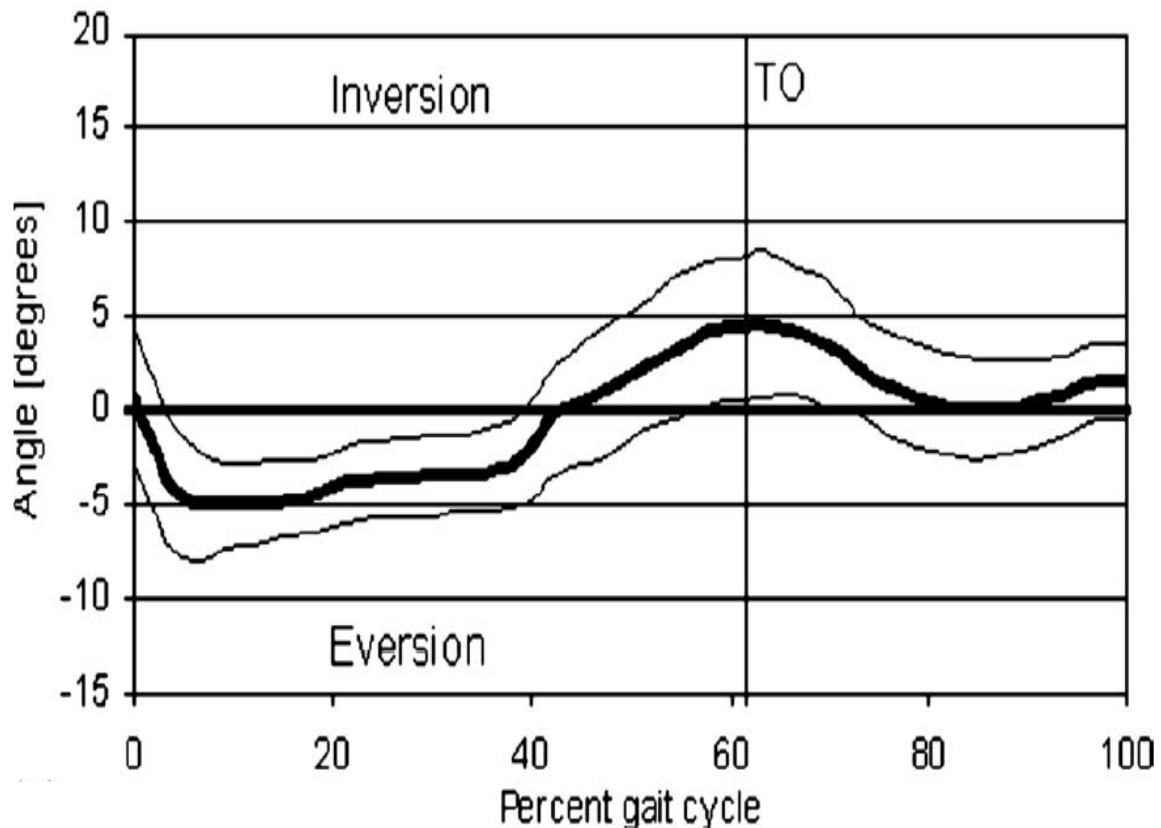
Fig. 3-20: The subtalar joint motion measured in Jenkyn and Anas study (2009). The averaged over all subjects subtalar JCS inversion/eversion in Jenkyn and Anas study (Jenkyn and Anas, 2009) with one positive and one negative standard deviation.

3.3.3   Hindfoot supination/pronation with respect to the midfoot

Figure 3-19 represents the average hindfoot segment supination/pronation with respect to the midfoot over twelve normal subjects with one positive and one negative standard deviation in Jenkyn and Anas study (2009). The figure shows that the range of motion for hindfoot supination/pronation was 11.4 degrees. Also, it indicates that the hindfoot started the gait cycle at a pronated position with 2.5±2.0 degrees of pronation which was 1.5 degrees greater than the pronated position of the hindfoot at heel-strike in our study. The hindfoot then reached a greater

70

pronated position at mid-stance with -8.2±2.0 degrees and it was 4.8 degrees greater than the

pronation degree of hindfoot at mid-stance in our study. Eventually, the hindfoot underwent

gradual supination until it reached 2.9±2.3 degrees of supination at toe-off which was 1.3 degrees

greater in comparison with the supination degrees in our study. The curve trend of hindfoot

supination/pronation in our study is matching with the resulting trend of the Jenkyn and Anas study

$(p < 0.03)$.
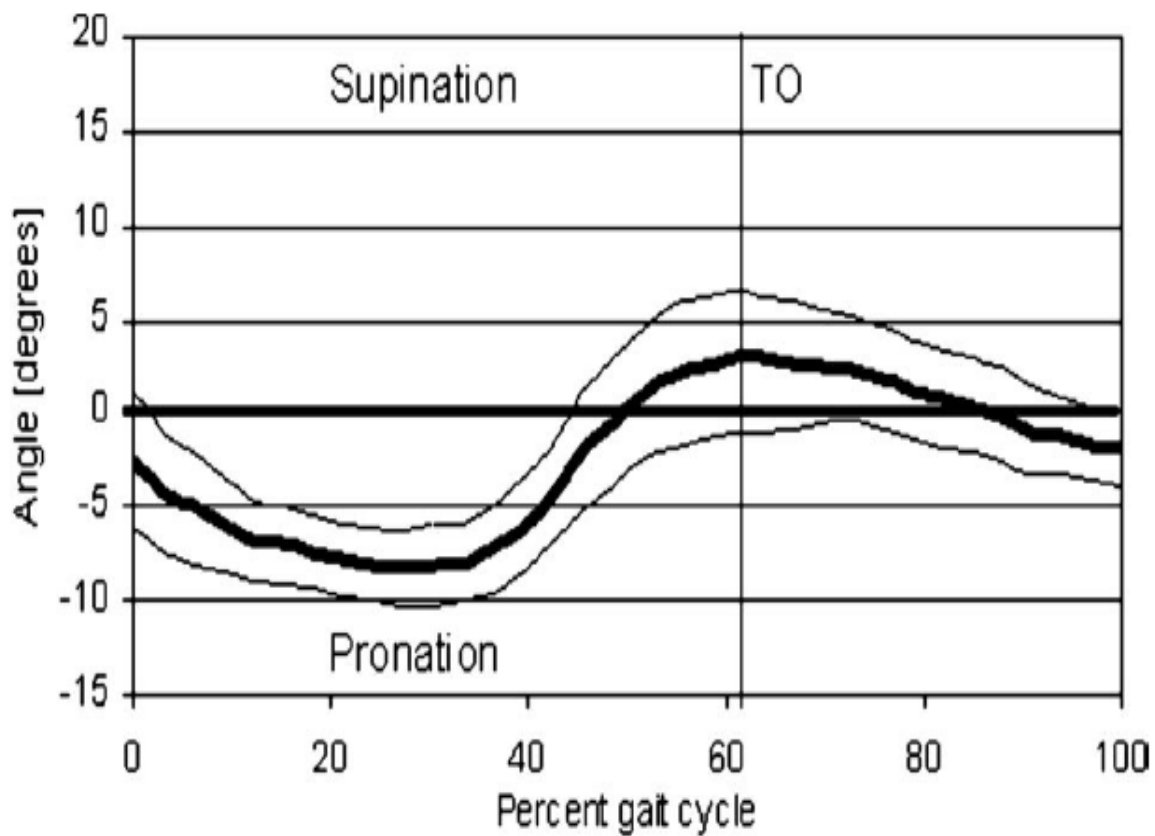
Fig. 3-21: The hindfoot segment supination/pronation with respect to the midfoot in measured in Jenkyn and Anas study (2009). The normalized to zero hindfoot segment supination/pronation with respect to the midfoot averaged over all 12 subjects with one positive and one negative standard deviation in Jenkyn and Anas study (Jenkyn and Anas, 2009).

3.3.4 Hindfoot internal/external rotation with respect to the midfoot

The averaged hindfoot segment motion in the transverse plane with respect to the midfoot over twelve subjects in Jenkyn and Anas study is shown in figure 3-20. The range of motion for hindfoot internal/external rotation in Jenkyn and Anas study was 8.2 degrees which was 3.9 degrees greater than the hindfoot range of motion in the transverse plane in our study. Figure 3-20 indicates that the hindfoot began at an internally rotated position at heel-strike with 1.7±1.5 degrees while hindfoot began at a neutral position in our study. The hindfoot then reached 6.2±2 degrees of internal rotation at flat-foot which was 4.8 degrees greater than the hindfoot internal rotation at foot-flat in our study. The hindfoot underwent slight external rotation from mid-stance until it reached -1.4±1.8 degrees at toe-off which was matching with the degrees of the hindfoot external rotation at toe-off in our study. In general, the standard deviation for the hindfoot internal/external rotation in Jenkyn and Anas study was smaller than the standard deviation in our study: 2.7 degrees, 1.3 degrees, and 1.2 degrees smaller at heel-strike, foot-flat, and toe-off respectively. The trend of the hindfoot internal/external rotation curve in our study is in good agreement with the trend of the graph in Jenkyn and Anas study (p < 0.03).
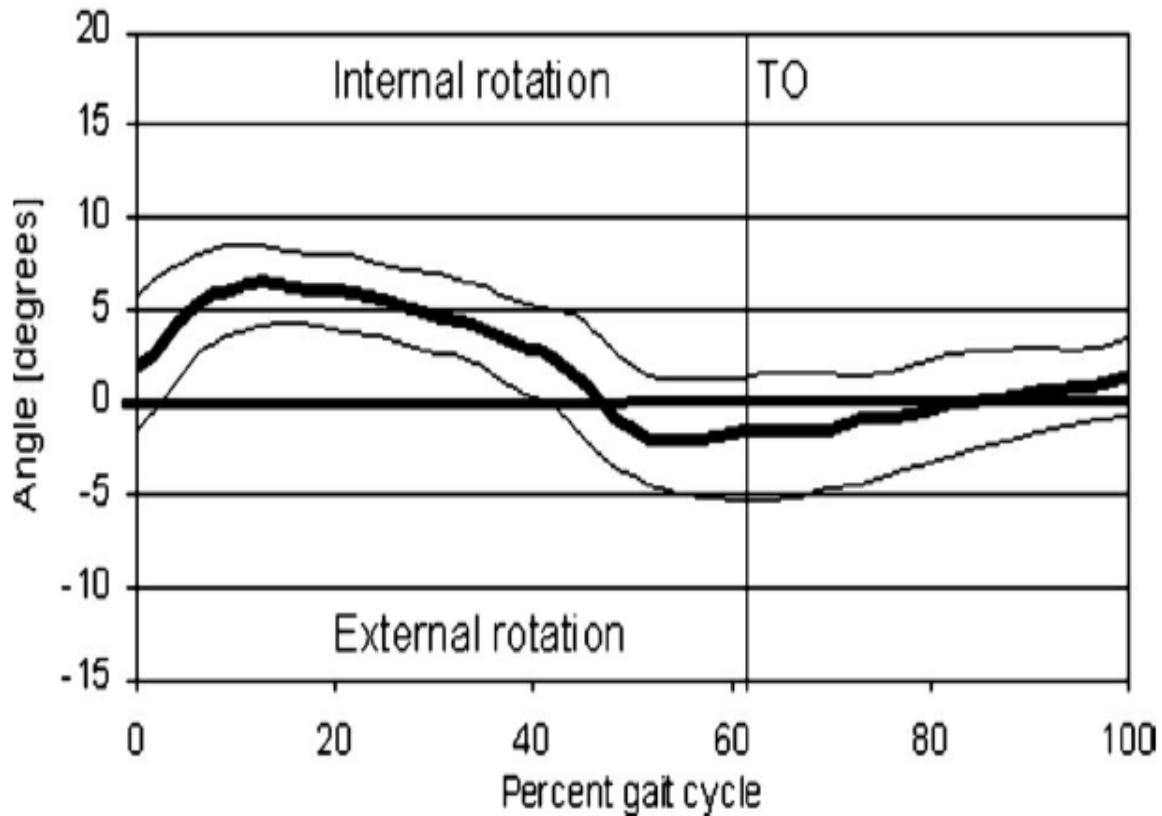
Fig. 3-22: The hindfoot internal/external rotation with respect to the midfoot measured in Jenkyn and Anas study (2009). Averaged over all twelve subjects hindfoot segment motion in the transverse plane with respect to the midfoot with one positive and one negative standard deviation in Jenkyn and Anas study (Jenkyn and Anas, 2009).

3.3.5 Forefoot supination/pronation with respect to the midfoot

Figure 3-21 indicates the average over all twelve subjects forefoot segment motion in the frontal plane with respect to the midfoot in Jenkyn and Anas study. It can be noticed from the figure that the range of motion for forefoot supination/pronation was 11.8 degrees that was 8.5 degrees greater than the forefoot range of motion in our study. At heel-strike, the forefoot was in a supinated position (6.0±1.0 degrees) in Jenkyn and Anas study. Then, the forefoot pronated to reach a minimum supination position at foot-flat (2.8±1.0 degrees) In Jenkyn and Anas study, while the forefoot was in a pronated position (-0.9±1.5 degrees) at foot-flat in our study. In the end, the

forefoot reached its maximum supination (15±1.3 degrees) at toe-off in Jenkyn and Anas study, however, the maximum forefoot supination occurred with 2.3±2.8 degrees in our study. The trends of the forefoot motion figures in the two studies are in good agreement ($p < 0.03$). The most perceptible difference in the figures was that the forefoot did not exceed to a pronated position in Jenkyn and Anas study, and yet the forefoot underwent slight pronation until it reached 1.0±1.8 degrees of pronation at mid-stance in our study.

In general, the standard deviation in Jenkyn and Anas study for the forefoot motion was smaller than the standard deviation in our study. The differences between standard deviation in the studies were 0.4 degrees at heel-strike, 0.8 degrees at foot-flat, and 1.5 degrees at toe-off.
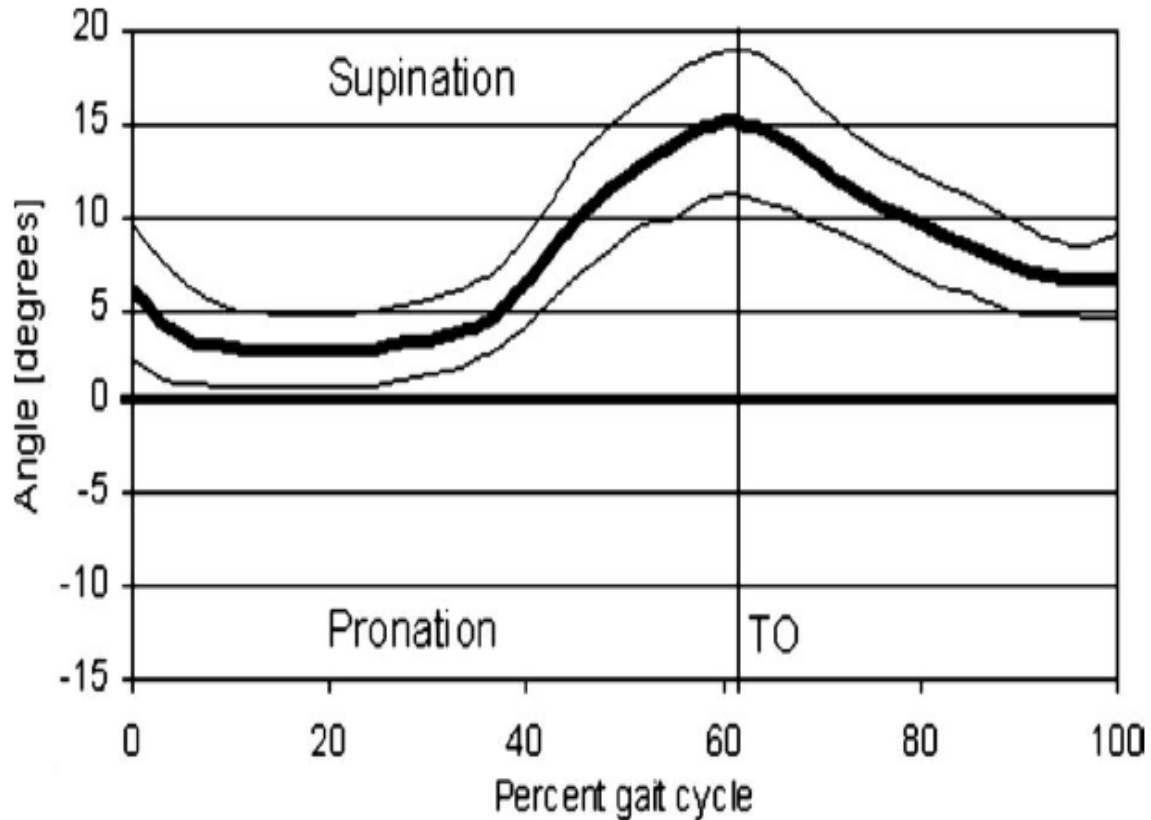
Fig. 3-23: The forefoot segment motion with respect to the midfoot in Jenkyn and Anas study (2009). The averaged over all 12 subjects forefoot segment supination/pronation with respect to the midfoot with one positive and one negative standard deviation in Jenkyn and Anas study (Jenkyn and Anas, 2009).

3.3.6   Rise and fall of the medial longitudinal arch

The averaged over all subjects rise and fall of the medial longitudinal arch is shown in figure 3-22. The figure shows the normalized to 1 height to length ratio of the MLA with respect to the gait cycle percentage. The range of the rise and fall of the MLA in Jenkyn and Anas study was 0.38 which was 1.1 greater than the range of the rise and fall of the MLA in our study. Comparing our study with the study of Jenkyn and Anas, the arch in both studies dropped starting from heel-strike until mid-stance, and from mid-stance up to the toe-off, the arch raised ($p < 0.03$). At the mid-stance, the height to length ratio of the MLA in both studies had the same amount (0.9). The ratio

75

then raised from mid-stance until it reached its maximum amount at toe-off (1.3±0.06) in Jenkyn

and Anas study which was closed to the amount of the MLA height to length ratio at toe-off in our

study (1.2±0.1).

The standard deviation at mid-stance in Jenkyn and Anas study was 0.95 greater than the standard

deviation in our study, however, it was nearly the same as the standard deviation in our study at

toe-off (the difference at toe-off was 0.04).
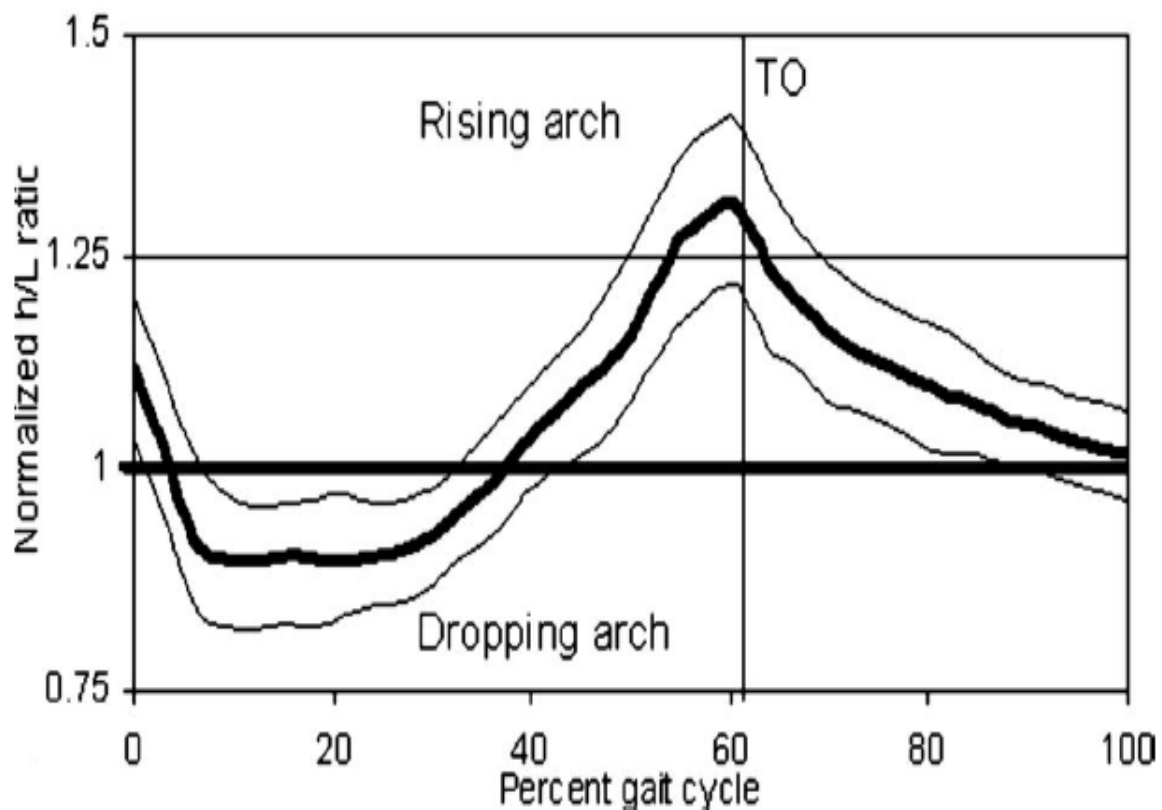
Fig. 3-24: The rise and fall of the medial longitudinal arch measured in Jenkyn and Anas study (2009). The
normalized to 1 averaged over all 12 subjects height to length ratio of the medial longitudinal arch with one positive
and one negative standard deviation in Jenkyn and Anas study (Jenkyn and Anas, 2009).

3.3.7   Summary

In summary, the joint angles measured using Vicon ProCalc were in a great agreement with the results of the Jenkyn and Anas (2008) study and their pattern and the range of motion were matching. This supports the conclusion that using Vicon ProCalc for measuring inter-segmental joint motions is accurate and valid. In the next section, the results of the joint angles measured using Oxford foot model will be reported and compared with the joint motions measured using Vicon ProCalc.

3.4 Comparison with the Oxford foot model

3.4.1 Joint motions measured using Oxford foot model

The testing session was repeated using the Oxford foot model for all eleven subjects, however, the post-processing and tracking model were only done successfully for ten subjects due to the missed hip marker for one of the subjects. Lower extremity was tracked using Oxford foot model in addition to the lower leg, hindfoot, forefoot, and the hallux of the right foot. The motion of five joint structures were reported using OFM: Ankle joint dorsi/plantarflexion, hindfoot motion with respect to the tibia, forefoot segment supination/pronation (forefoot motion with respect to the hindfoot), hallux dorsiflexion, and the rise and fall of the medial longitudinal arch. In this section, the joint motions measured using Oxford foot model are presented and compared with the results presented in previous sections.

3.4.2 Ankle JCS dorsi/plantarflexion

Figure 3-25 shows normalized to zero ankle joint dorsi/plantarflexion plotted individually for all ten subjects in a walking gait cycle. Figure 3-26 shows the averaged ankle joint motion over ten subjects with one positive and one negative standard deviation. It can be observed from the figures that the ankle began at a plantarflexed position (-7.8±5.2 degrees) at heel-strike and underwent gradual dorsiflexion until it reached -3.6±5.1 degrees at foot-flat and a neutral position (0.8±3.1 degrees) at mid-stance. The ankle reached its maximum dorsiflexion at 40% of the gait cycle and underwent gradual plantarflexion through which the ankle reached 4.2±8.2 degrees of plantarflexion at toe-off. From 65% of the gait cycle, the ankle again moved into dorsiflexion until 80% of the gait cycle and changed the movement to the plantarflexion from 80% of the cycle until it reached to the next gait cycle. The range of ankle joint motion measured using OFM was 16.1 degrees with 7.9 degrees of dorsiflexion as the maximum and 8.2 degrees of plantarflexion as the

minimum amount (table 3-4). The curve plotted based on the OFM results for the ankle joint motion is similar to the curve plotted for the ankle joint motion derived from Vicon ProCalc (p < 0.03). In general, the standard deviation for ankle joint motion obtained from OFM was greater than the standard deviation of the ankle dorsi/plantarflexion derived by the MSFM presented in section 3.1.1.
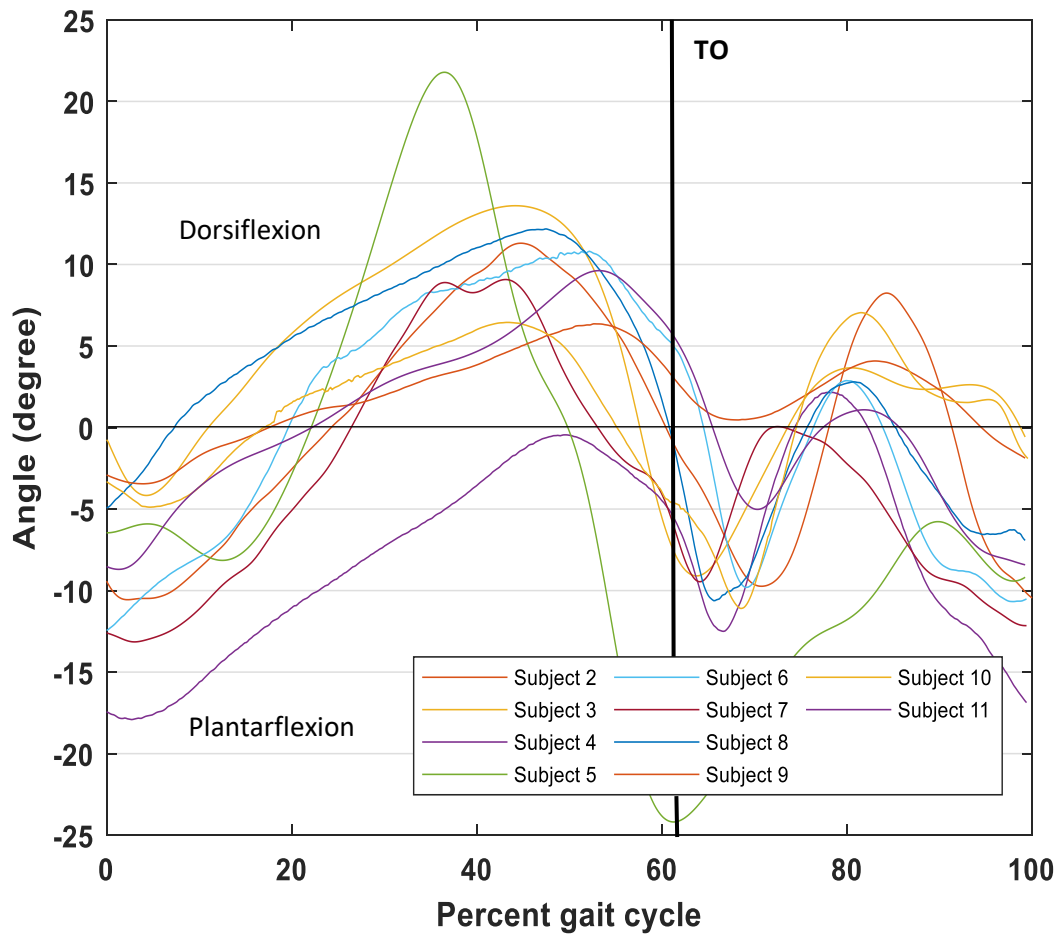
Fig. 3-25: The ankle joint motion measured Using the OFM for all subjects. The normalized to zero ankle joint motion plotted for all ten subjects in a complete gait cycle using the Oxford foot model.
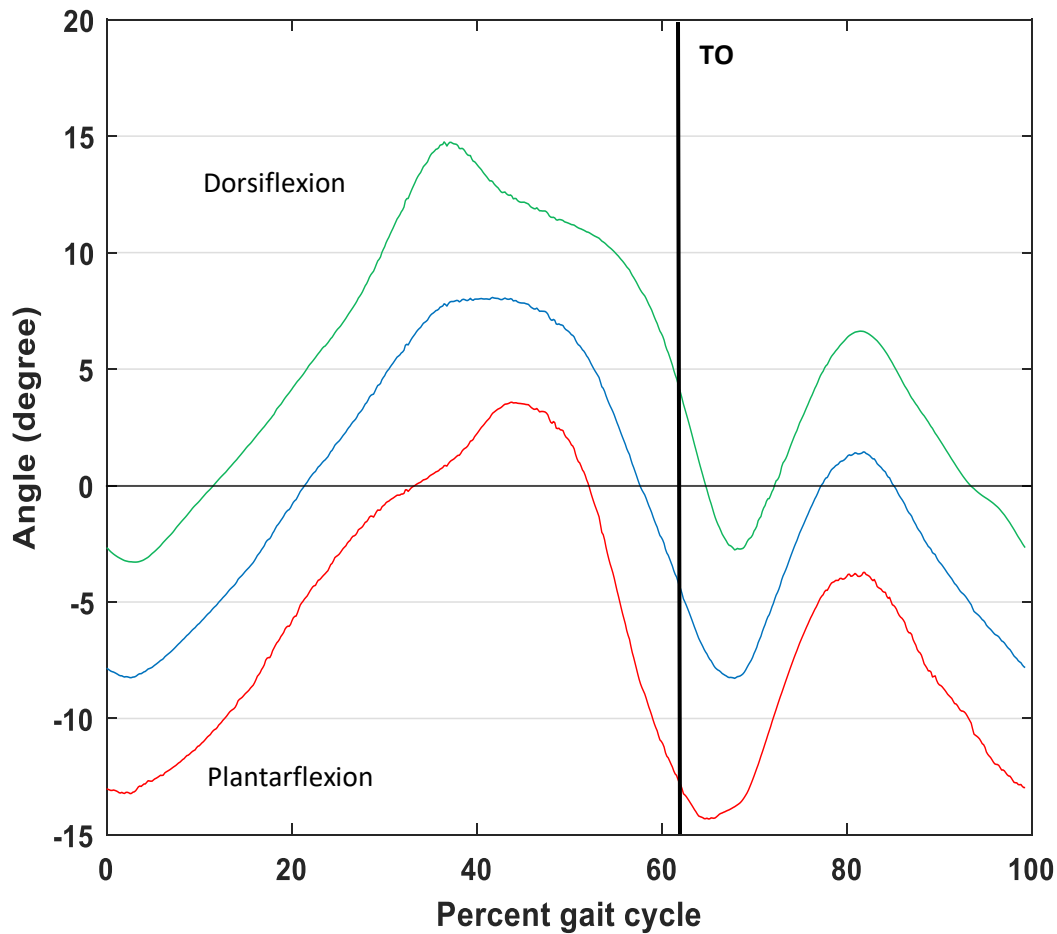
Fig. 3-26: The mean ankle joint motion over all subject measured using the OFM. The normalized to zero averaged overall ten subjects (blue) ankle joint dorsi/plantarflexion measured by the Oxford foot model with one positive (green) and one negative (red) standard deviation.

3.4.3 Hindfoot segment motion with respect to the tibia

The hindfoot segment motion in the frontal plane with respect to the tibia was measured using the Oxford foot model and shown in figures 3-27 and 3-28. Since the Oxford foot model does not consider the midfoot as an individual segment, it does not measure the subtalar joint motion (midfoot segment motion with respect to the talus) as an output angle. Hence, we compared the subtalar joint motion of the MSFM to its most related output angle of the Oxford foot model which

was the hindfoot segment motion with respect to the tibia. Figure 3-27 shows the hindfoot segment motion with respect to the tibia for all ten subjects and figure 3-28 indicates the averaged overall ten subjects motion with one positive and one negative standard deviation. The hindfoot started the gait cycle at an everted position (-1.7±3.9 degrees) and moved to a greater eversion until it reached -4.0±3.9 degrees of eversion at foot-flat. From foot-flat until toe-off, the hindfoot underwent a gradual inversion and it reached 5.5±6.3 degrees of inversion at toe-off. The range of hindfoot motion with respect to the tibia was 9.7 degrees with a minimum and maximum amount of -4.0 and 5.7 degrees respectively (table 3-4). The curve plotted using the results derived from the Oxford foot model was similar to the subtalar joint motion curve plotted by Vicon ProCalc ($p < 0.03$).
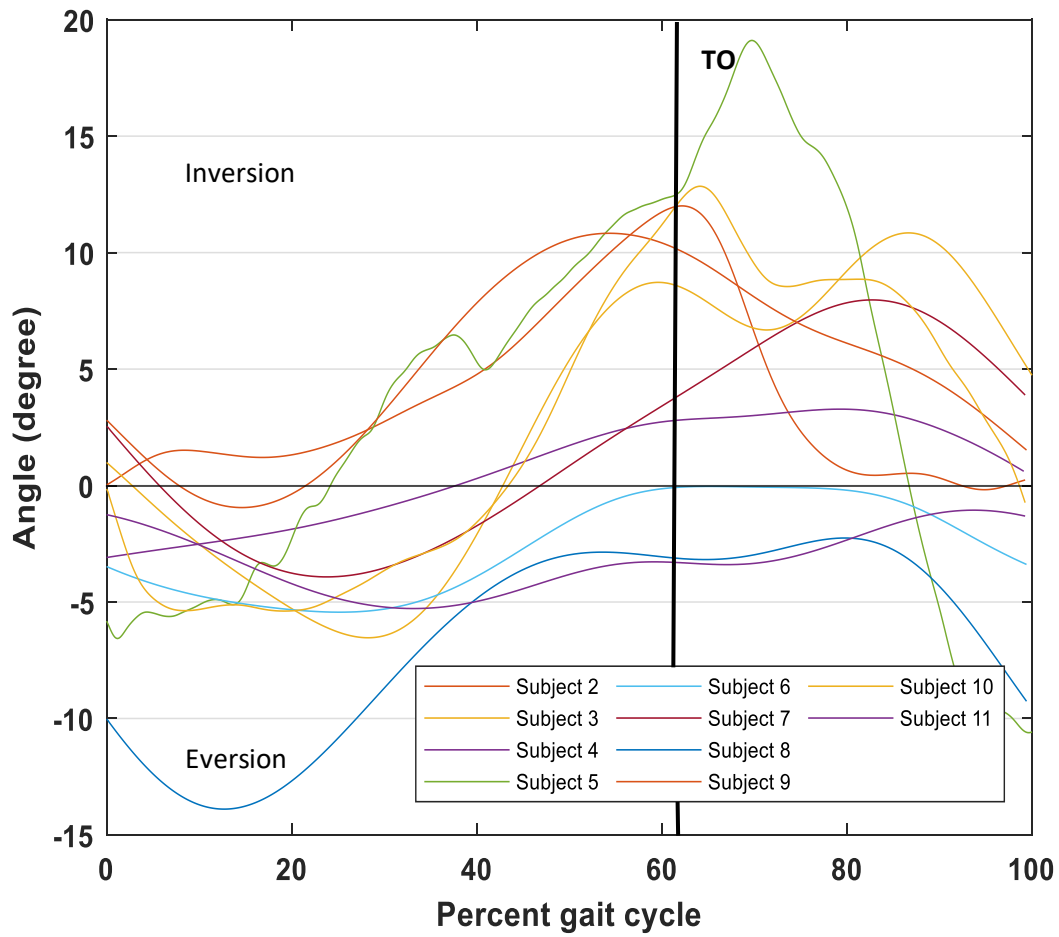
Fig. 3-27: The motion of the hindfoot with respect to the tibia measured using the OFM for all individual subjects. The normalized to zero hindfoot motion in frontal plane with respect to the tibia plotted for all ten subjects in a walking gait cycle using the Oxford foot model.
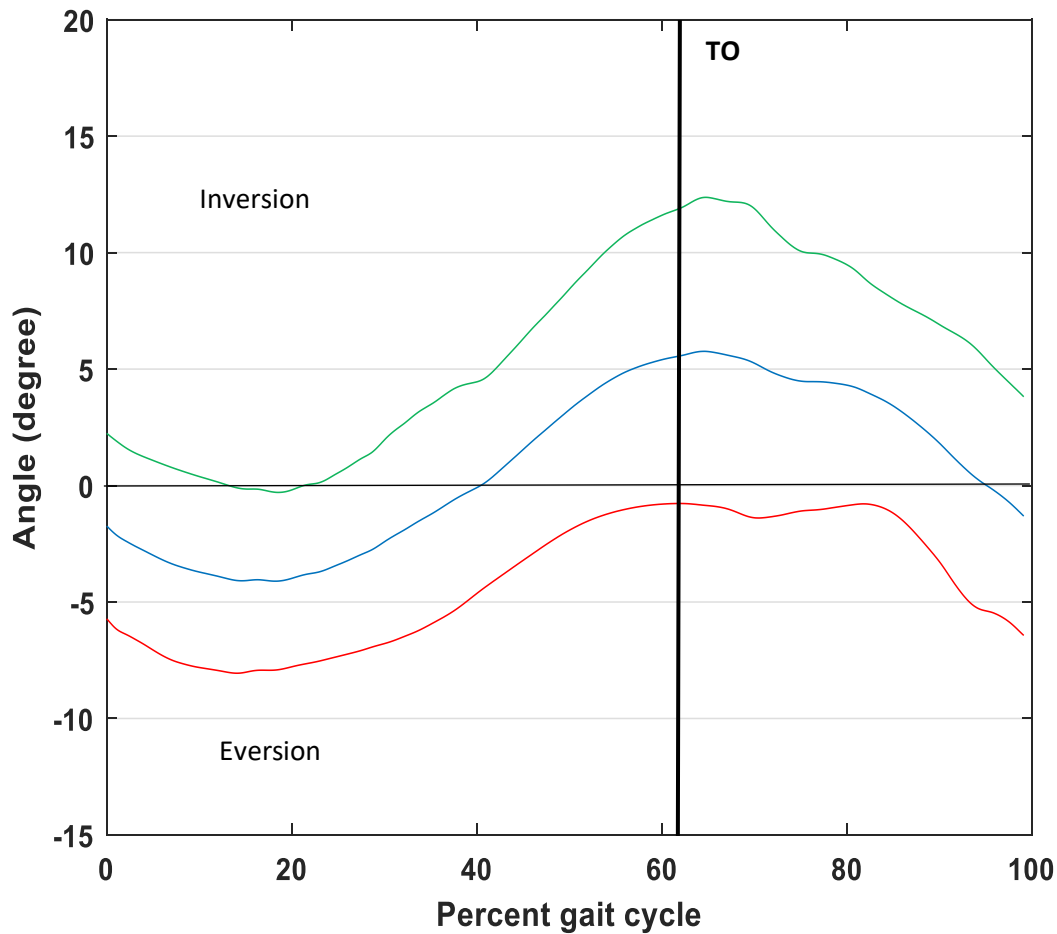
Fig. 3-28: The mean hindfoot motion with respect to the tibia over all subjects measured using the OFM. The normalized to zero averaged overall ten subjects (blue) hindfoot motion with respect to the tibia with one positive (green) and one negative (red) standard deviation measured using the Oxford foot model.

3.4.4 Forefoot segment motion with respect to the hindfoot

Figures 3-29 and 3-30 show the forefoot segment motion with respect to the hindfoot in the frontal plane measured by the Oxford foot model. The curves plotted for all individual subjects are shown in figure 3-29 and the averaged overall subjects motion with positive and negative standard deviation are shown in figure 3-30. The midfoot is not an individual segment for the Oxford foot mode, as a result, the forefoot motion with respect to the midfoot measured by the Vicon ProCalc

was compared with the forefoot motion with respect to the hindfoot calculated by the OFM. The range of forefoot motion with respect to the hindfoot was 5.3 degrees with the minimum and maximum amount of -1.0 and 4.3 degrees (table 3-4) which was greater than the range of forefoot motion with respect to the midfoot. Figure 3-30 represents that the forefoot began at a neutral position (0.18±4.1 degrees) at heel-strike and moved to a pronated position (-0.9±5.6 degrees) at mid-stance. The forefoot then moved into supination and reached the maximum supination (4.3±6 degrees) at toe-off. The pattern of the forefoot motion with respect to hindfoot measured by the OFM was similar to the curve plotted for the forefoot motion with respect to the midfoot measured by the Vicon ProCalc ($p < 0.03$). The standard deviation for the forefoot motion with respect to the hindfoot was generally greater than the standard deviation calculated for the forefoot motion with respect to the midfoot.
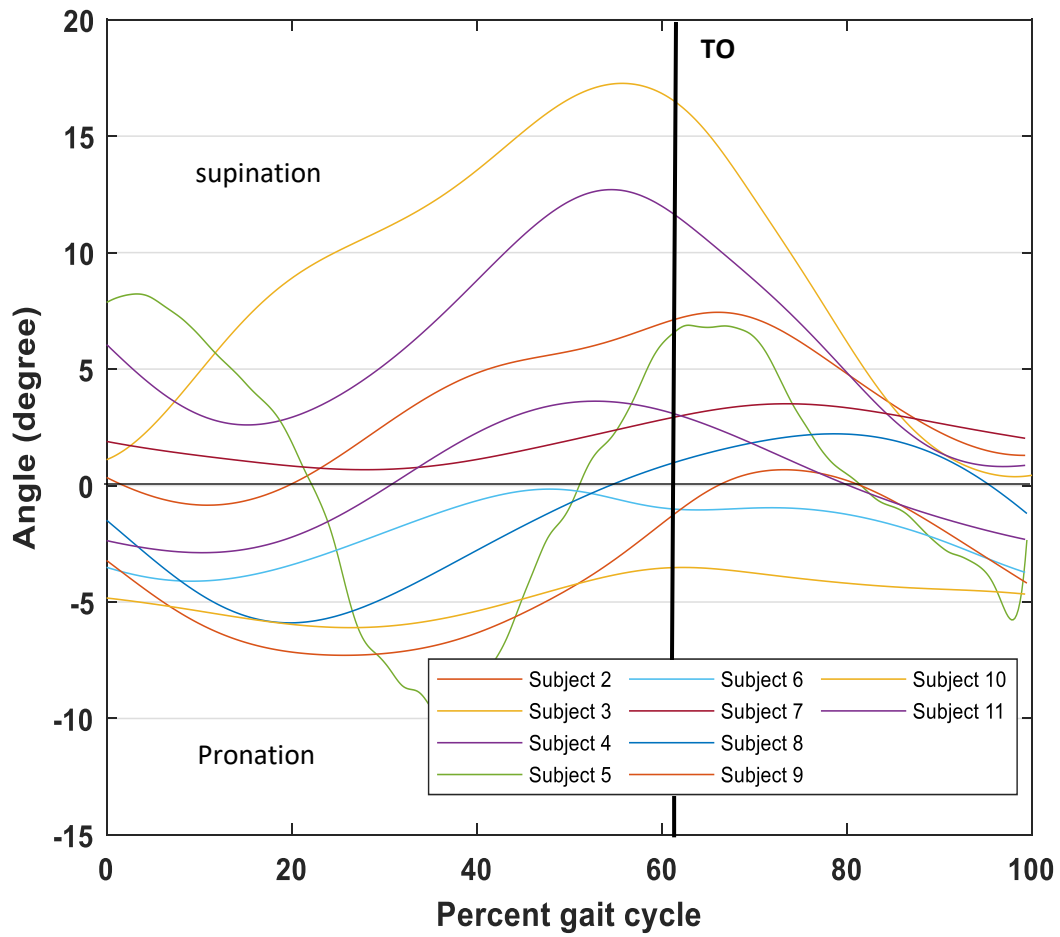
Fig. 3-29: The motion of the forefoot with respect to the hindfoot measured using the OFM for all individual subjects. The normalized to zero forefoot supination/pronation with respect to the hindfoot plotted for all ten subjects using the Oxford foot model.
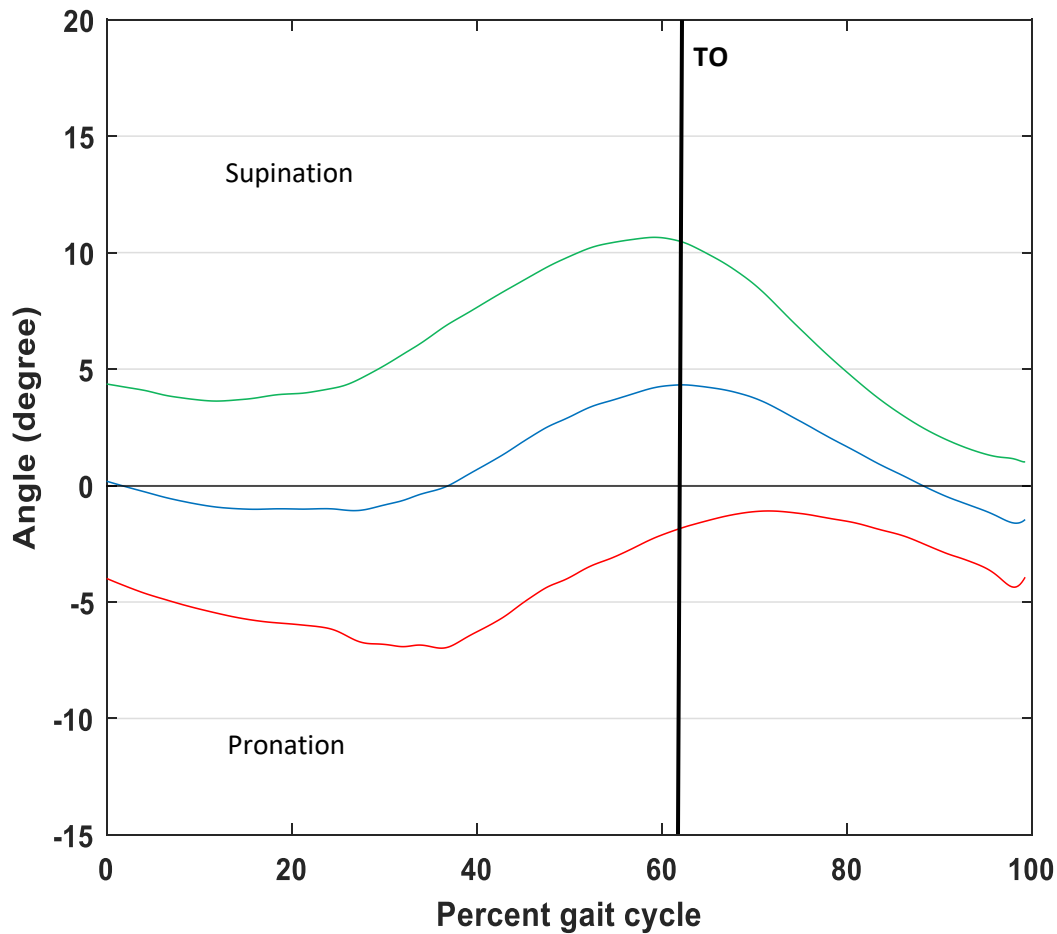
Fig. 3-30: The mean forefoot motion with respect to the hindfoot over all subjects using the OFM. The normalized to zero averaged overall subjects (blue) forefoot supination with respect to the hindfoot with one positive (green) and one negative (red) standard deviation measured using the Oxford foot model.

3.4.5   Hallux dorsiflexion

The first metatarsophalangeal joint (hallux) motion in the sagittal plane measured by the Oxford foot model is shown in figures 3-31 and 3-32. The hallux started the cycle at a plantarflexed position (-3.2±8.6 degrees) at heel-strike and moved to a greater plantarflexion (-3.9±7.0 degrees) at foot-flat. The hallux then moved into a dorsi-flexion and it reached close to the maximum degrees of dorsi-flexion (14±12.7 degrees) at toe-off. The range of motion measured by the Oxford

foot model was 18.9 degrees (table 3-4). The pattern of the averaged hallux motion plotted by the

Oxford foot model was similar to the curve of hallux motion presented in section 3.1.6 (p < 0.03).

The standard deviation calculated for the hallux motion in Oxford foot model was greater than the

standard deviation of hallux motion in MSFM measured by the Vicon ProCalc.
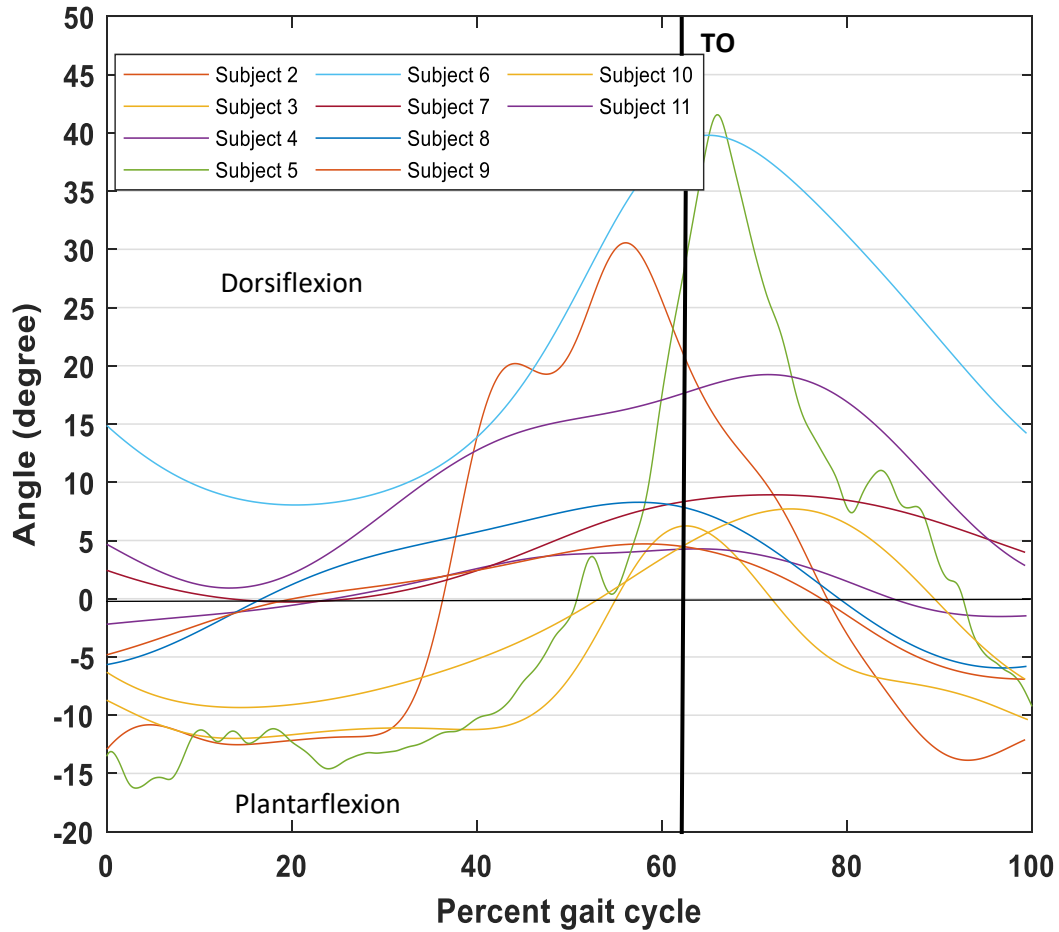
Fig. 3-31: The hallux joint motion measured using the OFM for all individual subjects. The normalized to zero hallux dorsiflexion measured by the Oxford foot model for all ten subjects.
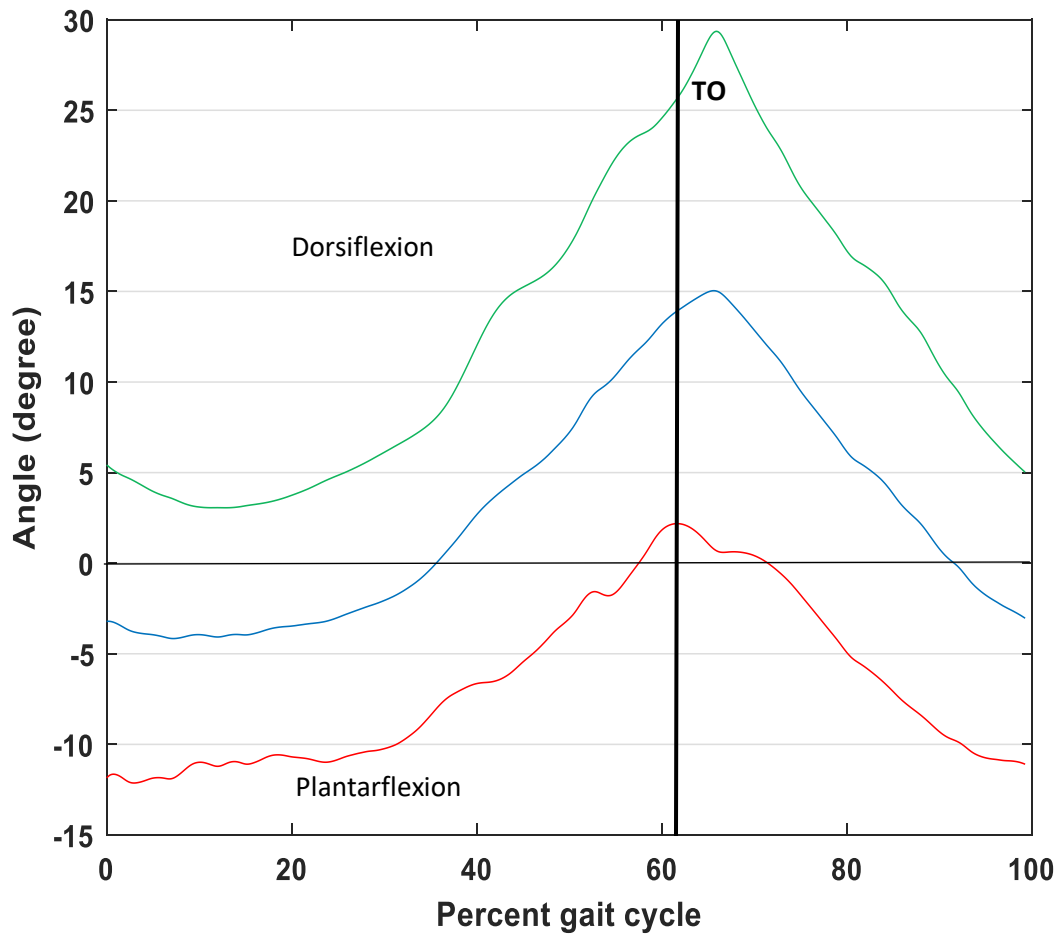
Fig. 3-32: The mean hallux dorsiflexion over all subject measured using the OFM. The averaged overall ten subjects (blue) hallux motion with one positive (green) and one negative (red) standard deviation in a walking gait cycle measured using the Oxford foot model.

3.4.6   Rise and fall of the medial longitudinal arch

The rise and fall of the medial longitudinal arch measured by the Oxford foot model is shown in figures 3-33 and 3-34. The y-axes of the graphs show the normalized height to length ratio of the medial longitudinal arch and the x-axes represents the percent of the gait cycle. The initial height to length ratio of the arch was 1.10 ± 0.28 and it raised slightly until it reached 1.16 ± 0.64 at mid-stance. From mid-stance until toe-off, the arch raised again and it reached its maximum ratio

(1.60±0.36) at toe-off. The range of the height to length ratio measured by the Oxford foot model was 0.54 (table 3-4).
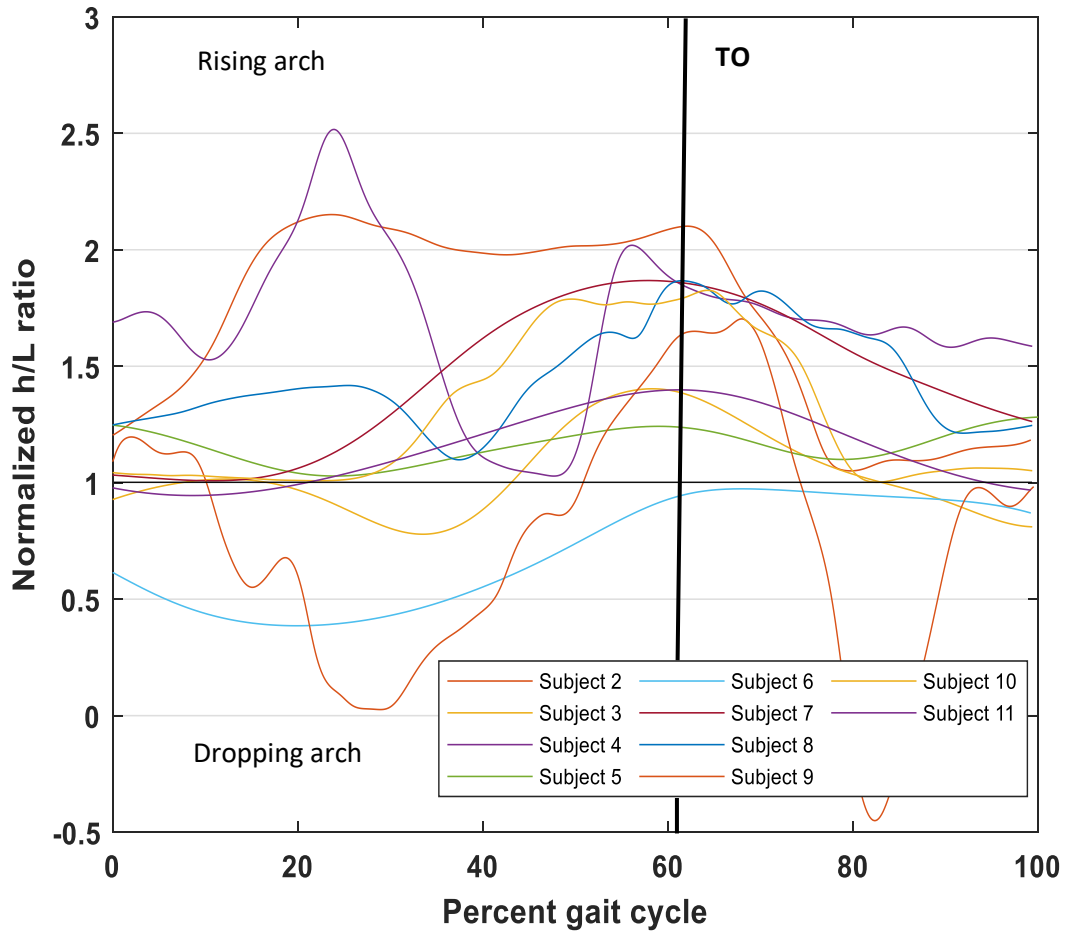
Fig. 3-33: The rise and fall of the MLA for all subjects measured using the OFM. The normalized to one height to length ratio of the medial longitudinal arch plotted for all ten subjects using the Oxford foot model.
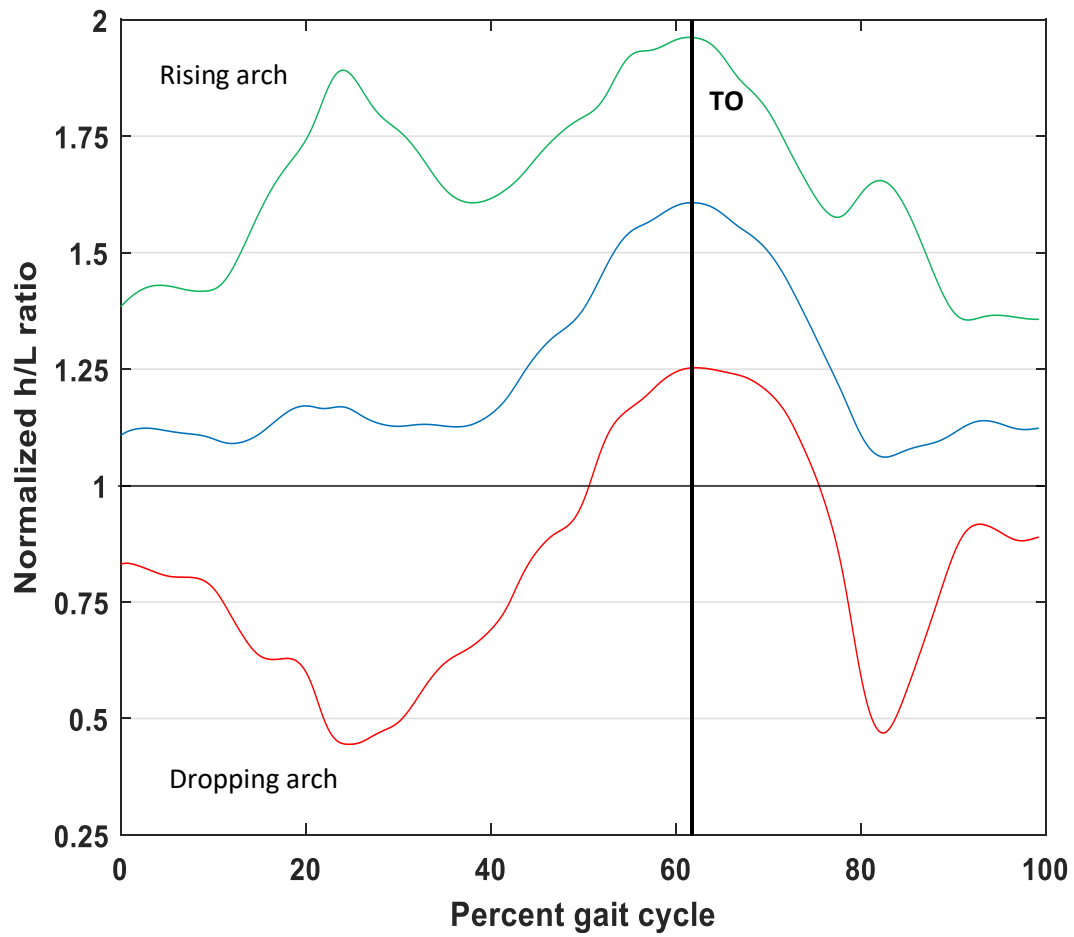
Fig. 3-34: The mean rise and fall of the MLA over all subjects measured using the OFM. The normalized to one averaged overall ten subjects (blue) height to length ratio of the MLA with one positive (green) and one negative (red) standard deviation measured using the Oxford foot model.

Joint motion	Range of motion	Maximum	Minimum
Ankle dorsi/plantarflexion	16.1°	7.9°	-8.2°
Hindfoot segment motion with respect to the tibia	9.7°	5.7°	-4.0°
Forefoot segment motion with respect to the hindfoot	5.3°	4.3°	-1.0°
Hallux dorsiflexion	18.9°	-3.9°	15.0°
Rise and fall of the medial longitudinal arch	0.54	1.6	1.06

Table 3-4: The maximum amount, minimum amount, and the range of motion for the Oxford foot model output angles and the rise and fall of the medial longitudinal arch. The range of motion and the maximum and minimum amount of the motion for all joint motions, except for the rise and fall of the medial longitudinal arch, are in degree. The height to length ration of the MLA is unitless.

3.4.7 Statistics

The coefficient of multiple correlation was measured for all output motions of Oxford foot model using Excel. Table 3-5 shows the CMC values for the five intersegmental joint motions and the mean standard deviation measured by OFM. The hallux motion had the greatest CMC value (0.68), whereas the rise and fall of the medial longitudinal arch had the smallest CMC value (0.36) among all motions.

Joint motion	CMC	SD (mean)
Ankle dorsi/plantarflexion	0.67	5.58
Hindfoot segment motion with respect to the tibia	0.59	4.94
Forefoot segment motion with respect to the hindfoot	0.50	4.97
Hallux dorsiflexion	0.68	9.69
Rise and fall of the medial longitudinal arch	0.36	0.41

Table 3-5: The coefficient of multiple correlation (CMC) and the mean standard deviation calculated for the OFM output joint motions. The CMC assessed the repeatability of joint motion curves between subjects and the mean standard deviation was calculated over the gait cycle for all joint motions.

3.5 Categorizing the arch type using Oxford foot model

The medial longitudinal arch type is categorized in table 3-6 for each subject based on the mean and standard deviation calculated for the minimum and maximum amount of normalized h/L ratio for the medial longitudinal arch measured using Oxford foot model. The normalized h/L ratio of the medial longitudinal arch for each subject is shown in figure 3-35 and the range of medial longitudinal arch motion for each subject and the averaged over all subjects range of motion are shown in figure 3-36. It can be concluded from the result of the table 3-6 that Comparing to the AHI measurement categorization, the arch type of the 50% of the subjects agreed with each other.
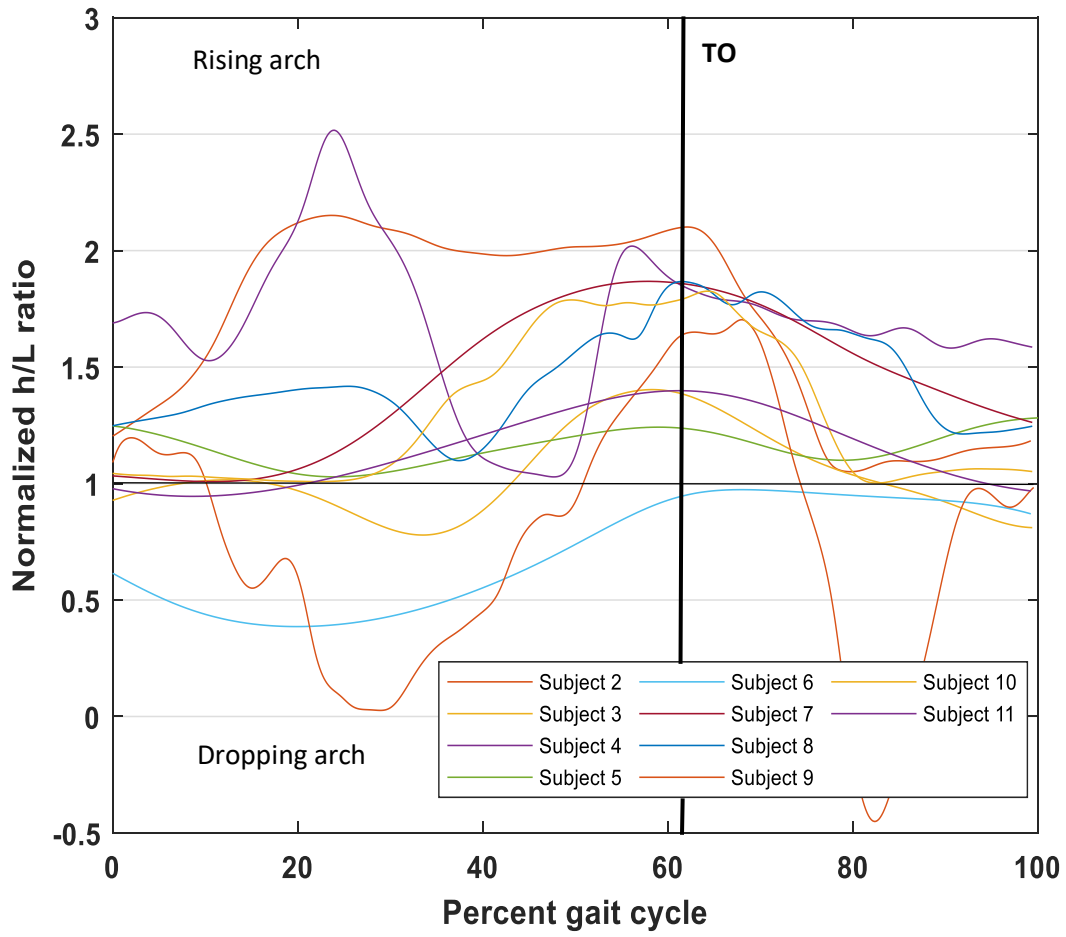
Fig. 3-35: The rise and fall of the MLA measured using the OFM for all subjects. The normalized to one h/L ratio measured using the Oxford foot model for each subject during a walking gait cycle.
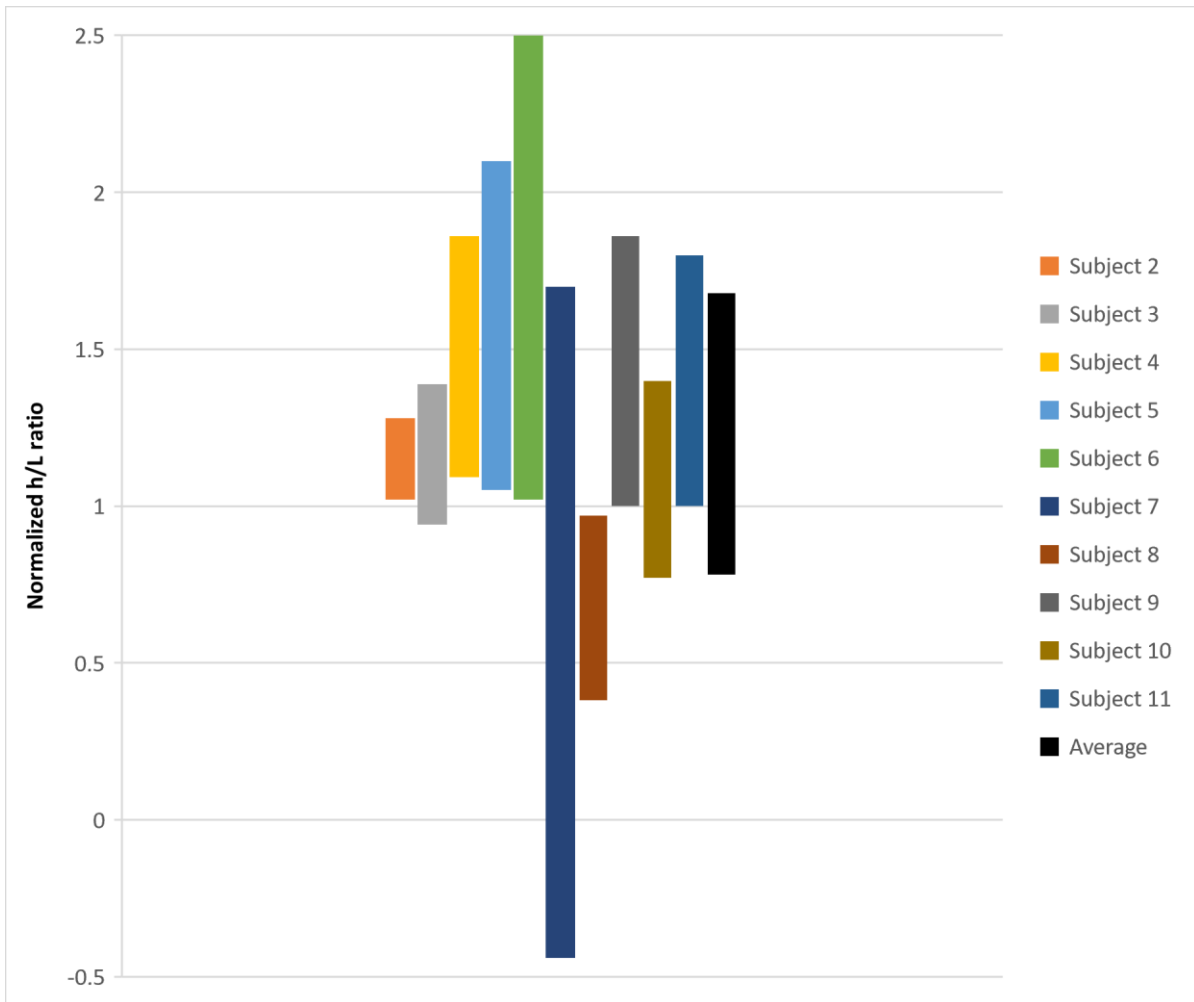
Fig. 3-36: The range of h/L ratio of the MLA measured using the OFM for all subjects. The range of normalized h/L ratio of medial longitudinal arch calculated using the Oxford foot model for each subject during a gait cycle and the averaged over all subjects range of the h/L ratio.

Subject	Maximum h/L ratio	Minimum h/L ratio	Arch type	Arch type based on the AHI measurement
Subject 2	1.28	0.95	Neutral	Neutral
Subject 3	1.39	0.94	Pes-Cavus	Neutral
Subject 4	1.86	0.63	Pes-Planus	Neutral
Subject 5	2.1	0.84	Neutral	Pes-Cavus
Subject 6	2.5	0.92	Neutral	Pes-Cavus
Subject 7	1.70	0.84	Neutral	Neutral
Subject 8	0.97	0.38	Pes-Cavus	Neutral
Subject 9	1.86	0.89	Neutral	Neutral
Subject 10	1.40	0.91	Neutral	Neutral
Subject 11	1.80	0.99	Neutral	Neutral
Mean	1.68	0.78	-	-
SD	0.41	0.45	-	-
Mean max+ SD	2.09	-	-	-
Mean min- SD	-	0.32	-	-

Table 3-6: Categorization of the arch type of the foot for all subjects using the Oxford foot model. The maximum and minimum h/L ratio of the medial longitudinal arch measured using the Oxford foot model for each subject, the mean and standard deviation of maximum amounts and minimum amounts, and the arch type categorized based on the mean and SD calculated for the h/L ratio and the AHI measurement.

3.6 Comparison

In this section, the joint motions measured using Vicon ProCalc will be compared with the results gathered from the Oxford foot model. The gait speed, cadence, and stride length for the tests

performed using the MSFM developed by Jenkyn and Nicole and the Oxford foot model are reported in table 3-7. Participants chose to walk on the treadmill with the speed that they were comfortable with and they selected the same speed for both test protocols. Hence, the cadence and stride length for each participant in the first test were similar to the cadence and stride length measured for the second test. The first test was performed using MSFM developed by Jenkyn and Nicole and the second test was performed using the Oxford foot model.

	Speed (Km/hr)	First test		Second test	
		Cadence Steps/min	Stride Length (m)	Cadence Steps/min	Stride Length (m)
Subject 1	3.0	35.82	1.42	37.5	1.35
Subject 2	2.8	38.70	1.24	37.5	1.28
Subject 3	2.4	25.00	1.60	24.00	1.67
Subject 4	2.4	21.05	1.91	20.00	2.01
Subject 5	2.0	33.89	1.02	32.43	1.07
Subject 6	2.4	29.26	1.37	27.90	1.44
Subject 7	2.4	26.90	1.49	29.26	1.37
Subject 8	2.0	29.33	1.18	31.57	1.10
Subject 9	2.5	30.76	1.39	31.57	1.35
Subject 10	2.7	32.43	1.40	33.33	1.36
Average	2.4	30.31	1.40	30.50	1.40

Table 3-7: The speed, cadence and stride length during the data collection. The walking speed, cadence, and stride length for each participant during data collection with the MSFM developed by Jenkyn and Nicole and the Oxford foot model.

In the following sections, the results derived from the Oxford foot model will be compared with the joint angles measured using Vicon ProCalc.

3.6.1 Hallux Dorsiflexion

Figure 3-37 represents the comparison between the motion of the first metatarsophalangeal joint measured by the Vicon ProCalc and the Oxford foot model. The figure indicates that the pattern of the curves plotted by these two methods are matching and they went through the same pattern. One of the differences between the motions was their range of motion that was 3.1 degrees greater in the motion measured by the Oxford foot model in comparison to the hallux dorsiflexion measured by the Vicon ProCalc. Also, the hallux motion measured using Oxford foot model began at a plantarflexed position and after going through a dorsiflexion, ended the cycle at a position where it started at, however, the curve measured using Vicon ProCalc only had dorsiflexed position during the entire gait cycle.
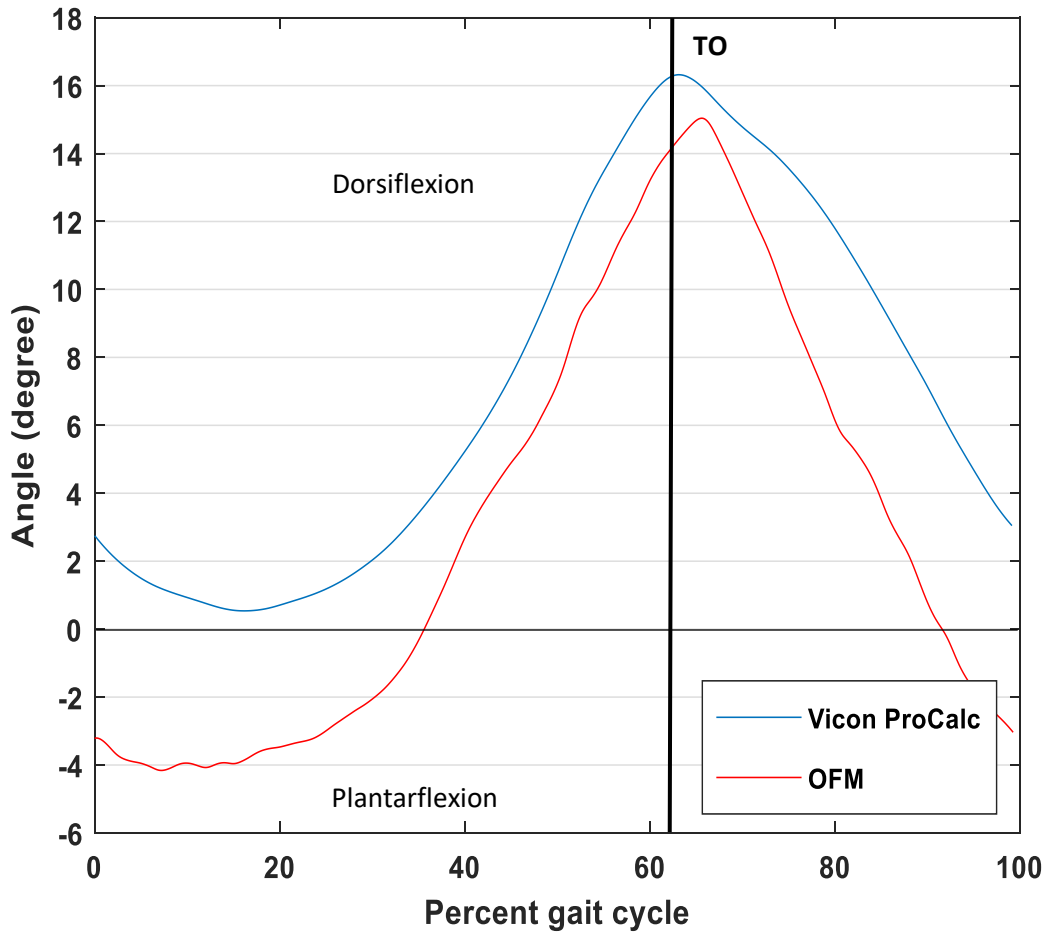
Figure 3-37: The comparison between the hallux dorsiflexion measured using the OFM and Vicon ProCalc. The averaged overall ten subjects hallux dorsiflexion measured using the Vicon ProCalc and Oxford foot model.

3.6.2 Forefoot segment supination/pronation

Figure 3-38 shows the forefoot segment motion with respect to the midfoot measured using Vicon ProCalc and the motion of the forefoot with respect to the hindfoot measured using Oxford foot model. The pattern of the motions and their initial point are matching, however, their maximum degree of supination at the toe-off differs from each other. The motion measured using Oxford foot model reached 4.3 degrees at toe-off while the degree of supination for the curve measured using Vicon ProCalc was 2.31 degrees.
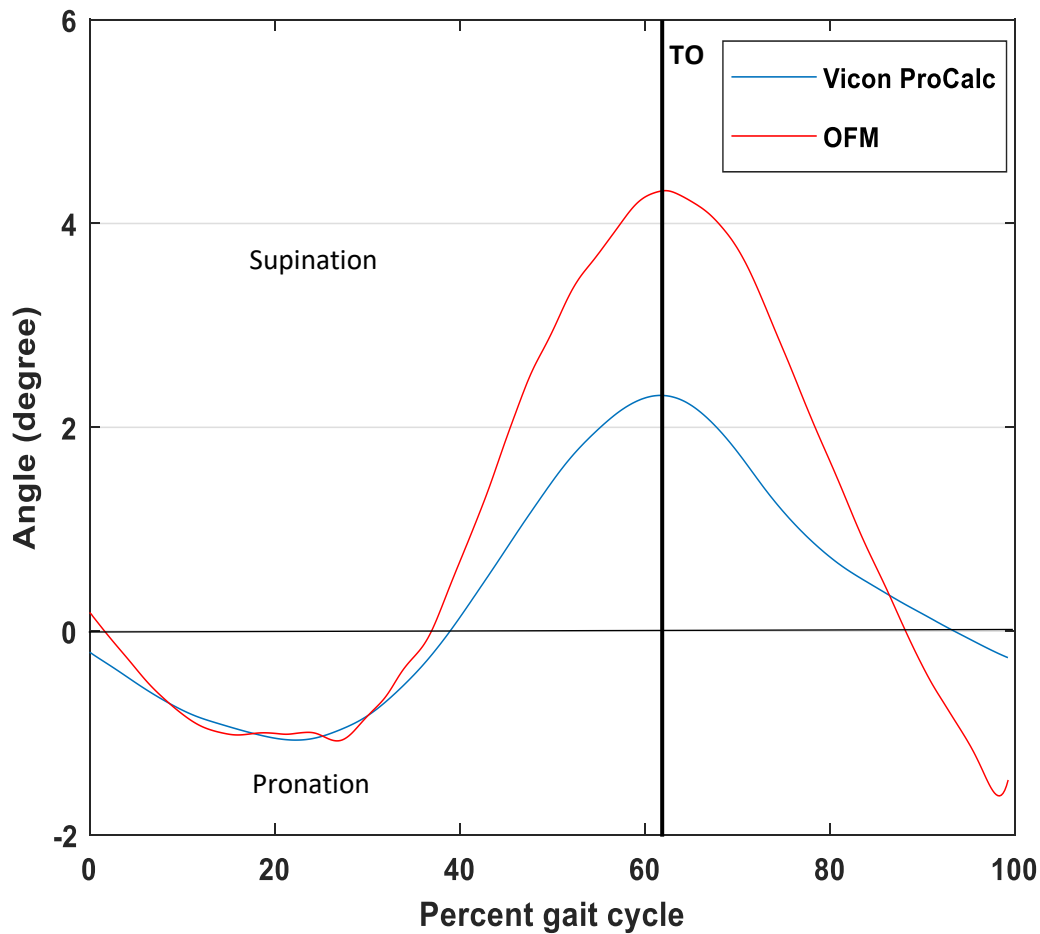
Figure 3-38: The comparison between the forefoot motion with respect to the midfoot and the forefoot motion with respect to the hindfoot measured using the Vicon ProCalc and OFM respectively. The averaged overall ten subjects forefoot segment motion with respect to the midfoot measured using Vicon ProCalc and forefoot segment motion with respect to the hindfoot measured using Oxford foot model.

3.6.3 Subtalar joint motion and the motion of the hindfoot with respect to the tibia

Figure 3-39 compares the subtalar joint motion measured by the Vicon ProCalc and the motion of the hindfoot with respect to the tibia measured by the Oxford foot model, since the Oxford foot model does not measure the motion of the midfoot with respect to the talus. As can be seen in the figure, the subtalar joint began the gait cycle at an inverted position (1.4 degrees) while the hindfoot initiated with an everted position (-1.7 degrees) with respect to the tibia. Both curves then

went through an eversion until foot-flat and reversed to inversion until they reached the maximum

degree at toe-off. The pattern of the motions measured by the Oxford foot model and the Vicon

ProCalc were similar to each other; even so, the range of hindfoot segment motion with respect to

the tibia was 1.4 degrees greater than the range of midfoot motion with respect to the talus

measured by the Vicon ProCalc.
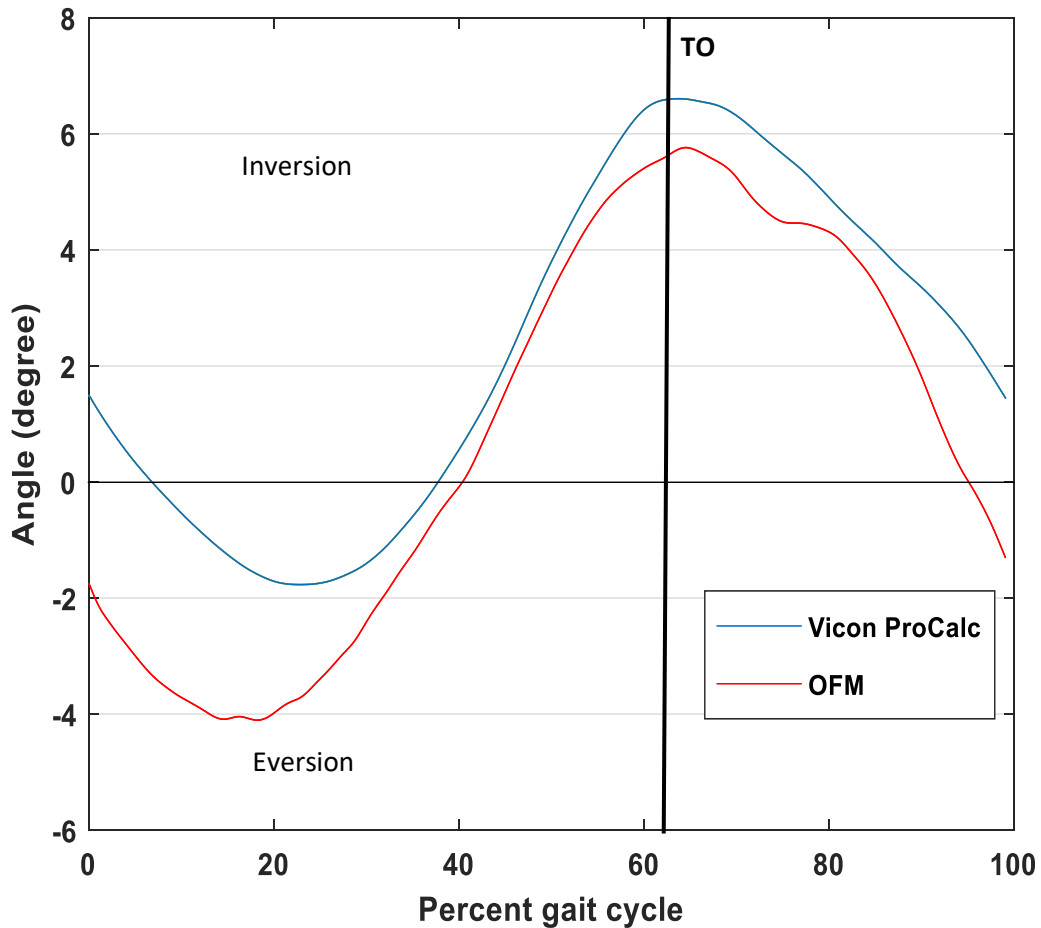
Figure 3-39: The comparison between the subtalar joint motion and motion of the hindfoot with respect to the midfoot measured using the Vicon ProCalc and OFM respectively. The averaged over all ten subjects subtalar joint motion measured using Vicon ProCalc and hindfoot segment motion with respect to the tibia measured using Oxford foot model.

3.6.4 Ankle JCS dorsi/plantarflexion

Figure 3-40 shows the averaged overall 10 subjects ankle joint motion measured using Vicon ProCalc and Oxford foot model. Both curves began at a plantarflexed position and went through a dorsiflexion until they reached the maximum dorsiflexion that happened at 50% and 40% of the gait cycle for the motion measured by Vicon ProCalc and Oxford foot model respectively. The curves then dropped until 68% of the gait cycle and again went through a dorsiflexion until they reached their second peak at 86% of the gait cycle. Overall, the pattern of the curves were very similar to each other, however, the range of ankle joint motion measured using Oxford foot model was 1 degree greater than the range of ankle joint motion measured using Vicon ProCalc.
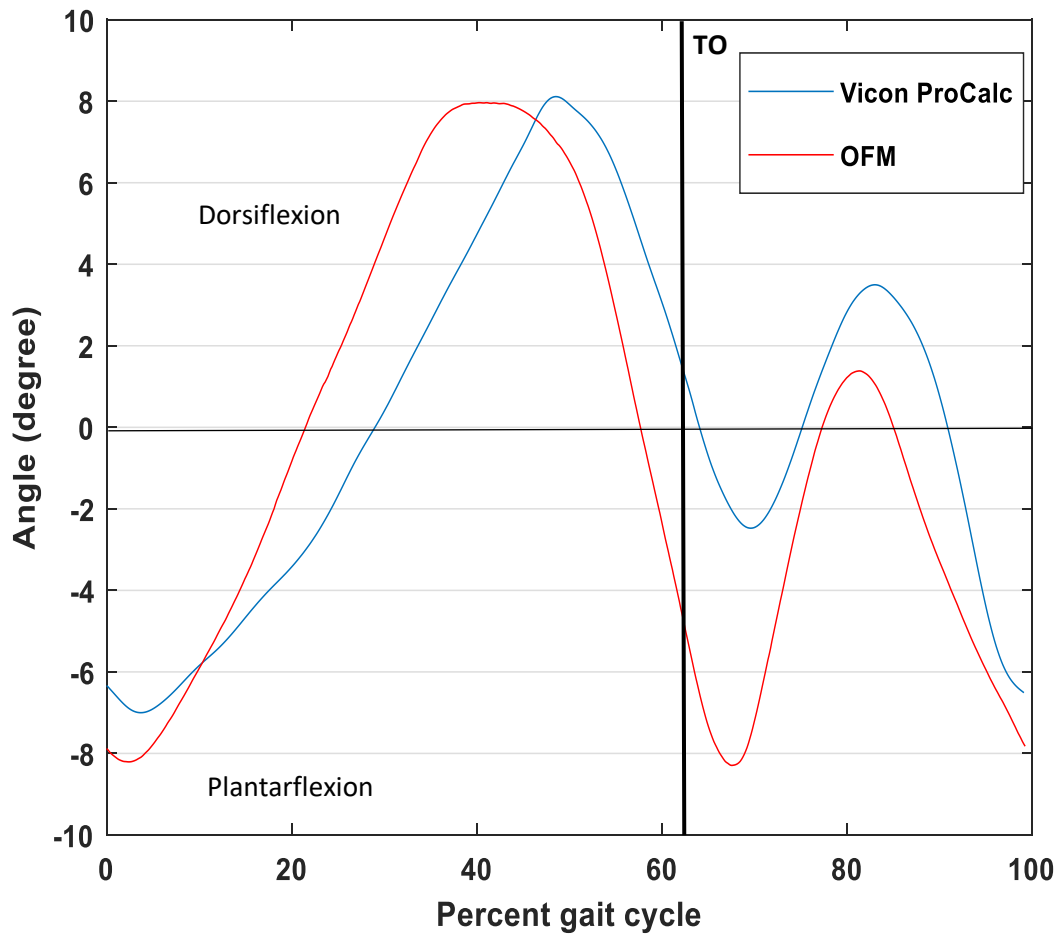
Figure 3-40: The comparison between the ankle joint motion measured using the OFM and Vicon ProCalc.
The averaged over all ten subjects ankle joint motion measured using Vion ProCalc and Oxford foot model.

3.6.5 Rise and fall of the medial longitudinal arch

The rise and fall of the medial longitudinal arch measured using Vicon ProCalc and Oxford foot model are shown in figure 3-41. From the mid-stance until the toe-off, the pattern of the curve plotted by the Oxford foot model for the medial longitudinal arch motion agrees with the curve measured by the Vicon ProCalc, however, they do not agree to each other in the first 23% of the gait cycle (p < 0.03). Also, the range of motion for the rise and fall of the MLA measured using Oxford foot model was 0.27 greater than the range of motion measured using Vicon ProCalc. The

103

differences between the curves plotted using the two methods can mainly explain by the position of the markers that these methods used to measure the motion of the medial longitudinal arch. The Oxford foot model measures the height of the arch as the distance between the marker on the dorsal surface of the base of the first metatarsal (P1M), and the same point projected on the plantar surface of the forefoot. It also measures the length of the foot by measuring the distance between HEEL and the TOE markers (Stebbins et al., 2006). On the other hand, the MSFM developed by Jenkyn and Nicole measures the height of the MLA by calculating the distance between navicular tuberosity marker and its projection on the floor and measures the length of the foot by calculating the distance between medial tuberosity marker (CAMT) and the first metatarsal head marker (MIH). The difference between the position of the landmarks that each model chooses to measure the height and the length of the foot can cause differences in the pattern of the curves measuring the rise and fall of the medial longitudinal arch. The motion of the MLA will be more discussed in chapter 4.
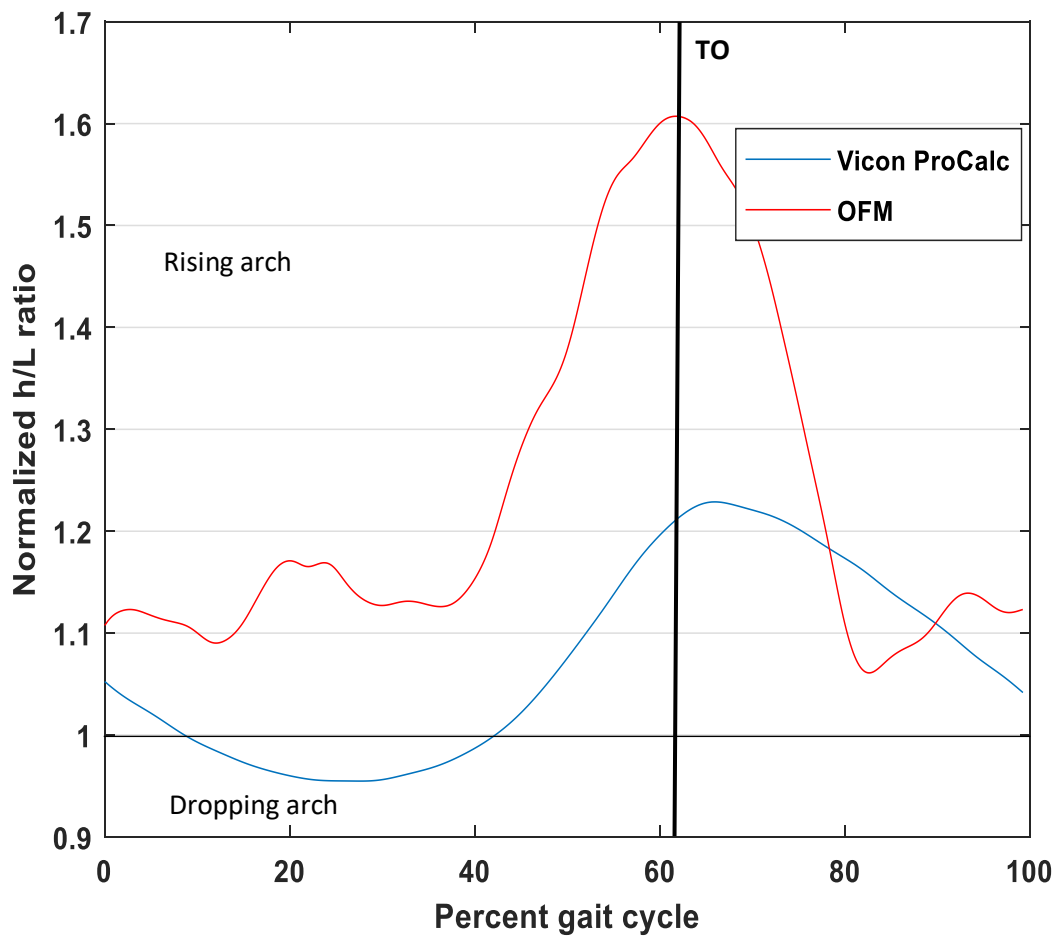
Figure 3-41: The comparison between the medial longitudinal arch motion measured using the OFM and Vicon ProCalc. The averaged overall ten subjects rise and fall of the medial longitudinal arch measured using Vicon ProCalc and Oxford foot model.

3.6.6 Statistics

The coefficient of multiple correlation between the mean of the joint motions measured using Oxford foot model and Vicon ProCalc was calculated and are reported for each motion in table 3-8.

Joint motion	CMC
Hallux dorsiflexion	0.98
Forefoot motion wrt midfoot – Forefoot motion wrt hindfoot	0.97
Subtalar inversion/eversion – HF motion wrt tibia	0.97
Ankle joint dorsi/plantarflexion	0.78
The rise and fall of the medial longitudinal arch	0.66

Table 3-8: The coefficient of multiple correlations (CMC) between the OFM and Vicon ProCalc results. The coefficient of multiple correlations calculated between the mean of each joint motion measured using Vicon ProCalc and Oxford foot model.

3.6.7   Summary

In summary, the results of the joint motions measured using the Oxford foot model and Vicon ProCalc, except for the rise and fall of the medial longitudinal arch, were matching and there was a great agreement between the pattern of the motions and the CMCs. This leads to the conclusion that using Vicon ProCalc for measuring intersegmental joint motions is valid and the results are accurate. The only joint motion measured using the Oxford foot model that did not greatly agree with the corresponding motion measured using Vicon ProCalc was the rise and fall of the medial longitudinal arch. As it was mentioned, this can be explained by different methods that these models use to calculate the height and the length of the foot. The joint motions measured using the Oxford foot model and Vicon ProCalc will be more discussed in chapter 4.

4. CHAPTER 4-DISCUSSION AND CONCLUSIONS

4.1 Summary

The objective of this study was to measure inter-segmental joint motions using the multi-segment foot model developed by Jenkyn and Nicole (2007) and a clinical setting which was Vicon ProCalc application in this study. The model divides the foot into five segments: the hindfoot (calcaneus), midfoot (tarsals: cuneiforms I–III, navicular, and cuboid), medial forefoot (metatarsals I and II), lateral forefoot (metatarsals III–V), and hallux (first metatarsophalangeal joint). The superiority of this model over other multi-segment foot models was that this model considers the midfoot as an individual segment allowing the measurement of the hindfoot and forefoot segments motion with respect to the midfoot, in addition to the ankle and subtalar joint coordinate systems motion. Moreover, this model divides the forefoot into medial and lateral forefoot segments so that the relative motion of the forefoot segments can be measured. Finally, this model uses triad cluster markers and fewer holes can be placed on the shoe by this way for collecting data with shoes on. On the other hand, using Vicon ProCalc is more clinically user-friendly and motions, events, and parameters can be easily calculated in this application. Once a model is implemented in the Vicon ProCalc, there is no need to change the calculations for individual subjects. The motions of eight joint structures were reported using Vicon ProCalc: Ankle JCS dorsi/plantarflexion, subtalar JCS inversion/eversion, hindfoot segment internal/external rotation with respect to the midfoot, hindfoot segment supination/pronation with respect to the midfoot, forefoot segment supination/pronation with respect to the midfoot, hallux dorsi/plantarflexion, the rise and fall of the medial longitudinal arch, and the relative motion of the forefoot segments.

4.2   Discussion

The results were validated with the previous study on the MSFM we used, and the results obtained from the Oxford foot model. The pattern of all motions calculated in this study agreed with the hypothesis. It was hypothesized in chapter 1 that in the first 15% of the gait cycle, the foot segments internally rotate and go into a plantarflexion. As a result of the internal rotation of the foot segments, they move into an eversion in the first 15% of the gait cycle. This can be seen in the hindfoot segment internal/external rotation, Hallux dorsiflexion, the relative motion of the forefoot segments, and the motion of the subtalar joint measured in this study. Only the motion of the ankle joint measured in this study did not support the hypothesis at the first 15% of the gait cycle and the ankle went into a dorsiflexion from 5% of the gait cycle until 40%. Also, it was hypothesized that the foot segments pronate from heel-strike until the mid-stance as a result of the inversion of the segments and this hypothesis was supported by the motion of the hindfoot and forefoot with respect to the midfoot in this study. Furthermore, it was hypothesized that the foot segments reverse to external rotation, inversion, dorsiflexion, and the supination from heel-strike until toe-off and reach the maximum degree of motion at the toe-off (62% of the gait cycle) due to the maximized muscle activation in lower leg at toe-off (Huang & Ferris, 2012) . This hypothesis was supported by all motions measured in this study as well. The coefficients of multiple correlations calculated for the motions measured by all three methods vary from method to method. The common motion that had small CMCs in all three methods was the rise and fall of the medial longitudinal arch. The CMC for this motion was 0.52, 0.36, and 0.48 calculated by Vicon ProCalc, Oxford foot model, and the study of Jenkyn and Anas respectively. The CMCs calculated for the height to length ratio measured by the Vicon ProCalc and the study of Jenkyn and Anas had a smaller difference. This can be due to the techniques that these methods used to measure the height

of the MLA and the length of the foot. The model developed by Jenkyn and Nicole (2007) measures the height of the foot by calculating the distance between the navicular tuberosity marker (MNT) and its projection on the floor and measures the length of the foot by calculating the distance between the medial tuberosity marker (CAMT) and the first metatarsal head marker (MIH). However, the Oxford foot model defines the height of the foot by measuring the distance between the marker on the base of the first metatarsal (P1MT) and its projection on the floor and it defines the length of the foot by calculating the distance between the HEEL and the TOE markers. The differences between the methods that these two models used to measure the height to length ratio of the MLA caused dissimilarity in the trends of figures and the repeatability between subjects. In the results gathered from the Oxford foot model for MLA, the pattern is still decreasing at the first 15% of the gait cycle and there is a peak at the 62% of the gait cycle (toe-off), however, there are some extra ups and downs in the pattern which makes small differences between the result of the methods used the MSFM developed by Jenkyn and Nicole and the Oxford foot model. The rise and fall of the medial longitudinal arch showed great variability in all three methods between subjects in comparison to other joint motions and it represents a great difference in the behavior of this joint in a gait cycle between subjects. This was not unanticipated since participants were selected from three groups of the high arch, flat foot, and normal arch and the arch of the participants in each group had unalike behavior during normal walking. Furthermore, in spite of other joint motions measuring the height to length ratio of the MLA depends on two parameters, the height and the length of the arch, and thus it increases the probability of more discrepancy between subjects. In general, the result of the medial longitudinal arch motion measured by the Vicon ProClac was comparable with the result of the Jenkyn and Anas study and represents the validity of using Vicon ProClac which is a clinical user-friendly software for

measuring the rise and fall of the MLA. Similar trends have been found in the literature for medial longitudinal arch motion. Bencke and his colleagues (Bencke et al., 2012) studied on the medial longitudinal arch deformation during gait. From foot-flat until mid-stance, a decreasing pattern can be observed in the results of the MLA motion during a walking gait cycle in this study. In addition, an increasing pattern can be seen from mid-stance until toe-off where the arch reached to the maximum height. Stebbins et al. (2005) showed a similar trend for the medial longitudinal arch in a gait study of children. Evaluating the medial longitudinal arch motion is clinically important. Lower arches (flat foot) can cause a change in the distribution of vertical ground reaction force (VGRF) of the plantar and bring greater muscle tensions. This is why people with flat foot experience pain when they walk for a long time (Fan et al., 2011). In addition, higher arches result in weaker ankle muscle and stiffer and less flexible feet. Stiffness of the foot reduces its ability to absorb the VGRF generated during walking and may cause injury (Zhao et al., 2017). The MSFM developed by Jenkyn and Nicole and the Vicon ProCalc application used in this study quantified the rise and fall of the medial longitudinal arch with valid results and more importantly, can be used in a clinical setting by clinicians and provide them with functional information of the patients' arch and foot joints. Furthermore, in comparison to the Oxford foot model results, the estimation of the arch type of the foot using Vicon ProCalc fitted better with the arch height index measurement that was performed at the beginning of the data collection for each participant.

The ankle JCS motion measured by the Vicon ProCalc and the result of the ankle JCS motion in the Jenkyn and Anas study were reported in chapter 3. Also, the ankle joint dorsi/plantarflexion measured by the Oxford foot model was reported in chapter 3. The trends of all three figures were similar to each other and the ranges of motion were so close. The only difference that can be noticed between curves was that the maximum degree of the plantarflexion for the motions

measured by the Vicon ProCalc and Oxford foot model occurred at 5% of the gait cycle while for the ankle motion measured by the study of the Jenkyn and Anas, the maximum degree of plantarflexion occurred at the mid-stance. Likewise, the toe-off event intersected with the part of the graph which was closer to the pick of the curve in the study of the Jenkyn and Anas, while the toe-off line crossed part of the curve which was closer to the neutral position in motions calculated by Vicon ProCalc and OFM. This is partly because of the different methods used for defining events for each study. In the study of Jenkyn and Anas, a visual assessment used to define events for each cycle, whereas events defined using Vicon ProCalc and Vicon Nexus for the motions calculated in this study. In addition, subjects who participated in this study were different from the subjects participated in Jenkyn and Anas study. Other studies also measured the ankle joint motion during gait. Brockett and Chapman (2016) showed the ankle joint motion in the sagittal, transverse, and frontal plane during walking (Brockett & Chapman, 2016). The motion of the ankle joint in the sagittal plane (dorsi/plantarflexion) in the study of Brockett and Chapman (2016) represented a similar pattern quantified for the ankle joint dorsi/plantarflexion in this study. Brockett and Chapman then explicated the pattern of the ankle motion in the transverse plane by the dorsi/plantarflexion moments of the ankle during gait. In this study, results for the ankle moment exhibited a dorsiflexion moment between 5% and 40% of the gait cycle. Brockett and Chapman explained this dorsiflexion moment as dorsiflexor muscles (tibialis anterior, the extensor hallucis longus (EHL), and the extensor digitorum longus) contract to control the internal rotation of the foot segments and prevent the foot from slapping the ground. From 40% of the gait cycle, the ankle moment reverses to plantarflexion to allow forward progression of the shank over the foot. The ankle moment measured by Brockett and Chapman can clearly explain the ankle joint motion pattern measured in our study as well.

The subtalar joint inversion/eversion is the motion of the midfoot segment with respect to the talus and plays an important role in defining the foot abnormalities in patients. Akiyama and his colleagues (Akiyama et al., 2015) indicated that the range of subtalar joint motion is greater in patients with medial tibial stress syndrome (MTSS) during the stance phase of a gait cycle. However, a midfoot segment is required to measure the motion of the subtalar joint. Many of the studies in literature as well as the Oxford foot model do not define the midfoot as an individual segment. Therefore, the subtalar joint motion measured by the MSFM developed by Jenkyn and Nicole was compared to its most related motion measured by the OFM which was the motion of the hindfoot with respect to the tibia. The subtalar joint motion measured by the Vicon ProCalc had the highest CMC between subjects (0.81) among other joint motions which shows that it had great repeatability between subjects. The repeatability of the subtalar joint motion measured in the study of Jenkyn and Anas and the relative motion of the hindfoot and the tibia measured by the OFM was 0.51 and 0.59 respectively. The pattern of the subtalar joint motion measured by the Vicon ProCalc and the study of Jenkyn and Anas were similar to each other and the pattern of the hindfoot segment motion with respect to the tibia measured by OFM was in a great agreement with them. In all three patterns, the curve was decreasing from heel-strike until mid-stance and reversed to increase from mid-stance until toe-off. The curve then reached its maximum inversion where lower-leg muscles reach their maximum activation level during gait. The range of motion was 8.3 and 9.7 angles for the subtalar joint motion measured by the Vicon ProCalc and 9.7 angles for the relative motion of the hindfoot and tibia segments measured by the OFM that were in a great agreement with each other. Overall, the results show that Vicon ProCalc can quantify subtalar joint motion with valid results and good repeatability between subjects and in a more clinical user-

friendly method than MATLAB. Oxford foot model cannot measure the exact subtalar joint motion due to the lack of separated midfoot segment in the model. However, the measured motion of the hindfoot segment with respect to the tibia by OFM can validly estimate the subtalar joint motion of the foot.

The motion of the hindfoot with respect to the midfoot was measured in two planes: Transverse plane and frontal plane. The pattern of the hindfoot motion in the transverse plane measured by the Vicon ProCalc was comparable with the hindfoot internal/external rotation measured in the study of Jenkyn and Anas. In both studies, the hindfoot went into an internal rotation from heel-strike until mid-stance as hypothesized and moved into external rotation from mid-stance until toe-off. The CMC between subjects was 0.61 and 0.41 for the hindfoot internal/external measure by Vicon ProCalc and for the motion measured in Jenkyn and Anas study respectively that shows the repeatability between subjects is greater for the motion measured by Vicon ProCalc. However, the range of hindfoot motion in the transverse plane measured by the Vicon ProCalc was 4.0 degrees smaller than the range of motion measured in the study of Jenkyn and Anas. There are a limited number of studies in the literature that considered the midfoot as an individual segment. Leardini and his colleagues (2007) showed the range of hindfoot motion in the sagittal, frontal, and transverse planes was 3, 8, and 4 degrees respectively. Other studies found a range of motion for the hindfoot segment 6 and 11 degrees (Hunt et al., 2001; Kidder et al., 1996). The controversy between studies for the hindfoot segment range of motion with respect to the midfoot can be partly because of the dissimilarity of in the definition of the local planes of the hindfoot as well as the unique foot characteristics of the subjects. This also can explain the difference between the range of hindfoot motions in the frontal plane in this study and the study of Jenkyn and Anas. The range

of motion of the hindfoot in the frontal plane with respect to the midfoot was 5.9 and 11.4 measured by the Vicon ProCalc and study of Jenkyn and Anas respectively.

The forefoot segment motion in the frontal plane with respect to the midfoot was also measured using Vicon ProCalc and compared with the forefoot supination/pronation in the study of Jenkyn and Anas. The motion of the forefoot measured in this study and the study of Jenkyn and Anas was a combined motion of the medial and lateral forefoot with respect to the midfoot. Since the Oxford foot model does not consider the midfoot as an individual segment, the motion of the forefoot segment with respect to the hindfoot was measured using the Oxford foot model as well. The pattern of the forefoot motion in all three studies was similar to each other. All three studies showed a pronation pattern for the forefoot from heel-strike until mid-stance, and a reversed motion from mid-stance until toe-off as hypothesized. The range of forefoot motion with respect to the midfoot was 3.3 and 11.8 measured by the Vicon ProCalc and the study of Jenkyn and Anas respectively that shows a great difference between the range of motions. Other studies have also measured the motion of the hindfoot in literature. Carson et al. (2001) measured the forefoot supination using the Oxford foot model during the stance phase of the gait cycle with respect to the hindfoot. This study also showed a pronation pattern of the forefoot in the first 23% of the gait and a supination pattern from mid-stance until toe-off. The range of motion measured by OFM in this study and in the study of Carson et al. was 5.3 and 6.5 angles respectively that represents a good agreement between the range of motions in these two studies.

The next motion measured in this study was the dorsiflexion of the hallux (first metatarsophalangeal joint) that plays an important role in biomechanics of the lower extremity. The MTP joint osteoarthritis (MTP OA), also referred to as hallux rigidus, is one of the abnormalities of this joint that causes pain and limitations in daily activities (Gilheany et al., 2008).

114

It has also been discovered that the low arch foot structure has been linked with the growth of the hallux rigidus (Mahiquez et al., 2006). Hence, developing methods in a clinical setting to measure the motion of the hallux in the sagittal plane is of great importance. Hallux dorsiflexion was measured in our study using Vicon ProCalc and Oxford foot model. Results of both methods show a slight plantarflexion pattern of the hallux from the beginning of the gait cycle until mid-stance, and a greater dorsiflexion pattern from mid-stance until toe-off, where it reached the maximum degree of dorsiflexion. The range of hallux motion in the sagittal plane was 15.8 and 18.9 degrees measured by the Vicon ProCalc and the Oxford foot model respectively. The difference between the range of motions measured by these two methods was small with respect to the total range of motion and it can be due to the different procedures that these two methods use to measure the hallux dorsiflexion. Other studies have also measured the motion of the hallux in the sagittal plane. Kuni et al. (2014) reported the hallux range of motion in the sagittal plane in a level walking as 34 degrees. Canseco et al. (2008) also measured the hallux dorsiflexion and represented 30 degrees range of motion for the normal subjects with no hallux rigidus and 10 degrees range of motion for subjects with hallux rigidus. The difference between the range of motions reported by several studies is directly related to the subjects' hallux type. Hallux rigidus decreases the range of motion of the hallux and as it is linked to the arch type of the foot, it can be perceived from studies that subjects with low arch foot structure have smaller hallux range of motion. Moreover, walking speed can affect the hallux range of motion based on the results of several studies. Keller et al. (1996) have found that increasing walking speed has a direct impact on the vertical ground reaction force (VGRF) and causes to increase the VGRF. On the other hand, Chang et al. (2014) studied on the foot kinematics and ground reaction force of the individuals with plantar fasciitis (PF) which is believed to be a result of the prolonged excessive loading (Chang et al., 2014). The results of

this study showed a smaller ground reaction force and a greater hallux range of motion for the subjects with PF and an inverse relationship between the ground reaction force and the hallux range of motion can be observed. Overall, it can be perceived from these studies that increasing speed can have impacts on the first metatarsophalangeal joint range of motion and this can explain the difference between the range of hallux motion represented by studies on individuals walked with self-selected speed.

The last motion measured in this study was the relative motion of the medial and lateral forefoot segments. A limited number of studies have divided the forefoot into medial and lateral segments (Kidder et al., 1996; Bok et al., 2016) and none of them have measured the motion of the medial forefoot with respect to the lateral forefoot. Hence, the relative motion of the forefoot segments measured in this study is difficult to compare. Only one study has measured the motion of the forefoot segments during walking gait in sagittal, frontal, and transverse planes (Cobb et al., 2016). The result of this study showed that the maximum degrees of dorsiflexion for the medial and lateral forefoot segments are 7.7 and 6.7 degrees respectively and figures represented that the maximum dorsiflexion happened at the toe-off. The result in our study agrees with the results reported by Cobb et al., since the degrees of dorsiflexion for the medial forefoot is greater than the dorsiflexion degrees for the lateral forefoot over the gait cycle and the difference was maximized at the toe-off where both segments reached to the maximum dorsiflexion degrees.

The mean standard deviation (SD) calculated for all motions measured by the Vicon ProCalc and Oxford foot model were reported in chapter 3. Among the motions measured by Vicon ProCalc, the ankle joint dorsi/plantarflexion and the hallux dorsiflexion had the largest mean standard deviation. The mean SD was 6.97 and 6.01 degrees for the ankle joint motion and the hallux dorsiflexion respectively. Likewise, the greatest SD calculated for the motions measured by OFM

was for the hallux dorsiflexion and ankle dorsi/plantarflexion with 9.69 and 5.58 degrees respectively. It can be observed from figures and mean standard deviations reported for all motions that there is a direct relationship between the range of motion and the standard deviation, that is to say, the growth of the range of motion can increase the standard deviation. Furthermore, it can be noticed from results that the standard deviation is varying during a gait cycle. The standard deviation was 3.4, 3.0, and 7.2 degrees at heel-strike, mid-stance, and toe-off respectively in the ankle joint motion measured by Vicon ProCalc. The same pattern can be seen for the standard deviation of hallux dorsiflexion measured by the Vicon ProCalc. The variation in standard deviation during gait can be explained by the study of Stephenson et al. (2010) on effect of arm movements on the muscle activation during walking gait cycle. The results of the quadriceps femoris and tibial anterior muscle activation during gait cycle in this study showed increased levels in muscle activation at the heel-strike and toe-off. Growth in muscle activation can cause an increase in soft tissue movement and displacement of reflective markers on the skin, also called soft tissue artefact (Perry & Burnfield, 2010). Displacement of markers increases the variation in motion and the standard deviation consequently.

4.3   Strengths

This study measured the inter-segmental joint motions of the foot in a clinical setting using the multi-segment foot model developed by Jenkyn and Nicole (2007). This method was accurate and clinical user-friendly and can easily be used by clinicians. The most significant strength of this method over MATLAB is that only one-time set up is required for this method and once the model is implemented in the application, inter-segmental joint motions can be measured for a limitless number of subjects and there is no need to change the settings for individuals. Furthermore, any joint motion can be measured in Vicon ProCalc by defining variables for each segment and

measuring the variation of a segment's variable with respect to the other segment. In addition, the modification of a joint motion calculated in Vicon ProCalc can be observed 3-dimensional over the gait cycles of a trial. Vicon ProCalc can also define the events of a gait cycle accurately based on the repeatable parameters. This reduces the errors caused by visual assessment of events in a gait cycle. Using Vicon ProCalc enables to use of any customized multi-segment foot model and measure desired joint motions.

One of the advantages of the multi-segment foot model developed by Jenkyn and Nicole (2007) used in this study over the Oxford foot model is that this model considers the midfoot as an individual segment and the relative motion of the hindfoot and forefoot can be measured with respect to the midfoot. Also, by having midfoot as a separated segment, the motion of the subtalar joint can be measured which is of great clinical importance. Moreover, this model divides the forefoot into medial and lateral forefoot segments so that the relative motion of the forefoot segments can be measured as well. Due to the use of triad cluster markers, this model uses fewer reflective markers on the foot in comparison to the Oxford foot model and it reduces the errors caused by skin movement artefact. Additionally, fewer holes are required on the shoe for collecting data with shoes on by having fewer required markers. One of the strengths of the Vicon ProCal is that this application allows us to find the position of a marker with respect to the local coordinate system and recreate the marker in the trials that the marker is missed in. This feature is beneficial when the cameras are able to capture a marker in the static trial, but the marker cannot be seen by the cameras in the dynamic trials and vice versa.

4.4 Limitations and future research recommendations

This study had several limitations as well:

- The walking test was only performed on a treadmill, however, there might be some differences between the inter-segmental joint motion results of walking on a treadmill and normal walking on the ground. Song and Hidler (2008) studied the biomechanics of over ground vs. treadmill walking in healthy individuals and demonstrated different joint moments in the sagittal plane between over ground and on treadmill walking. Also, White et al., (1998) discovered the same pattern for the vertical ground reaction force (GRF) in walking over ground and on treadmill, but different magnitudes were found between the vertical GRF in the two forms of locomotion. Quantifying the inter-segmental joint motions by performing a normal walking test on the ground and using Vicon ProCalc would allow more accurate results to be observed.

- The walking test for this study was only performed barefoot and the accuracy of this method in measuring inter-segmental joint motions for walking test with shoes-on was not quantified. Validating this method with a data walking test protocol with shoes-on provides a better understanding of the accuracy of this method in assessing the biomechanics of lower extremity during daily activities such as walking.

- Another limitation of this study was the soft tissue movement during walking which causes movement of the markers on the skin and errors in evaluating the motions consequently. Researching on how to reduce the effects of skin movement artefact on the inter-segmental joint motion results is another recommendation for future research.

- This study was only carried out for adult subjects and the validity of this method in measuring inter-segmental joint motions of the foot in children or elderly subjects was not evaluated. Measuring joint motions within the foot for the subjects with a wide range of

ages using this method can better quantify its validity and accuracy in measuring inter-segmental joint motions.

- The Comparison of Using Vicon ProCalc application and MATLAB for measuring intersegmental joint motions was done between two different study groups and it limits the accuracy of the comparison. Comparing the results of using Vicon ProCalc and MATLAB for measuring joint motions of the foot with the same group of study would give us a better idea of the differences between using these two methods for measuring the intersegmental joint motions.

5. REFERENCES

1. Alonso-Vázquez A, Villarroya MA, Franco MA, Asín J, Calvo B. Kinematic assessment of paediatric forefoot varus. *Gait Posture*. 2009. doi:10.1016/j.gaitpost.2008.08.009

2. Baker R. Gait analysis methods in rehabilitation. *J Neuroeng Rehabil*. 2006. doi:10.1186/1743-0003-3-4

3. Cappozzo A, Cappello A, Croce UD, Pensalfini F. Surface-marker cluster design criteria for 3-d bone movement reconstruction. *IEEE Trans Biomed Eng*. 1997. doi:10.1109/10.649988

4. Carson MC, Harrington ME, Thompson N, O'Connor JJ, Theologis TN. Kinematic analysis of a multi-segment foot model for research and clinical applications: A repeatability analysis. *J Biomech*. 2001. doi:10.1016/S0021-9290(01)00101-4

5. Cavanagh PR, Morag E, Boulton AJM, Young MJ, Deffner KT, Pammer SE. The relationship of static foot structure to dynamic foot function. *J Biomech*. 1997. doi:10.1016/S0021-9290(96)00136-4

6. CHAN CW, RUDINS A. Foot Biomechanics During Walking and Running. *Mayo Clin Proc*. 1994;69(5):448-461. doi:10.1016/S0025-6196(12)61642-5

7. Crenshaw SJ, Richards JG. A method for analyzing joint symmetry and normalcy, with an application to analyzing gait. *Gait Posture*. 2006. doi:10.1016/j.gaitpost.2005.12.002

8. Della Croce U, Leardini A, Chiari L, Cappozzo A. Human movement analysis using stereophotogrammetry Part 4: Assessment of anatomical landmark misplacement and its effects on joint kinematics. *Gait Posture*. 2005. doi:10.1016/j.gaitpost.2004.05.003

9. Franco AH. Pes cavus and pes planus. Analyses and treatment. *Phys Ther*. 1987. doi:10.1093/ptj/67.5.688

10. Grood ES, Suntay WJ. A joint coordinate system for the clinical description of three-dimensional motions: Application to the knee. *J Biomech Eng*. 1983;105(2):136-144. doi:10.1115/1.3138397

11. Hösl M, Böhm H, Multerer C, Döderlein L. Does excessive flatfoot deformity affect function? A comparison between symptomatic and asymptomatic flatfeet using the Oxford Foot Model. *Gait Posture*. 2014. doi:10.1016/j.gaitpost.2013.05.017

12. Hunt AE, M. Smith R, Torode M, Keenan AM. Inter-segment foot motion and ground reaction forces over the stance phase of walking. *Clin Biomech*. 2001. doi:10.1016/S0268-0033(01)00040-7

13. Jenkyn TR, Nicol AC. A multi-segment kinematic model of the foot with a novel definition of forefoot motion for use in clinical gait analysis during walking. *J Biomech*. 2007. doi:10.1016/j.jbiomech.2007.04.008

14. Jenkyn TR, Anas K, Nichol A. Foot segment kinematics during normal walking using a multisegment model of the foot and ankle complex. *J Biomech Eng*. 2009;131(3). doi:10.1115/1.2907750

15. Joseph Hamill KMK. *Biomechanical Basis of Human Movement*.; 2013. doi:10.1017/CBO9781107415324.004

16. Kadaba MP, Ramakrishnan HK, Wootten ME, Gainey J, Gorton G, Cochran GVB. Repeatability of kinematic, kinetic, and electromyographic data in normal adult gait. *J Orthop Res*. 1989. doi:10.1002/jor.1100070611

17. Kapandji I. The Physiology of the Joints. Volume 2. *Postgrad Med J*. 1975. doi:10.1002/bjs.1800570821

18. Kidder SM, Abuzzahab FS, Harris GF, Johnson JE. A system for the analysis of foot and ankle kinematics during gait. *IEEE Trans Rehabil Eng*. 1996. doi:10.1109/86.486054

19. Knudson D. *Fundamentals of Biomechanics*.; 2003. doi:10.1007/978-1-4757-5298-4

20. Kudo S, Hatanaka Y, Inuzuka T. Effects of a foot orthosis custom-made to reinforce the lateral longitudinal arch on three-dimensional foot kinematics. *Foot Ankle Online J*. 2018;11(1). doi:10.3827/faoj.2018.1101.0001

21. Leardini A, Benedetti MG, Catani F, Simoncini L, Giannini S. An anatomically based protocol for the description of foot segment kinematics during gait. *Clin Biomech*. 1999. doi:10.1016/S0268-0033(99)00008-X

22. Liu W, Siegler S, Hillstrom H, Whitney K. Three-dimensional, six-degrees-of-freedom kinematics of the human hindfoot during the stance phase of level walking. *Hum Mov Sci*. 1997. doi:10.1016/S0167-9457(96)00057-7

23. Mindler GT, Kranzl A, Lipkowski CAM, Ganger R, Radler C. Results of gait analysis including the oxford foot model in children with clubfoot treated with the ponseti method. *J Bone Jt Surg - Am Vol*. 2014. doi:10.2106/JBJS.M.01603

24. Moseley L, Smith R, Hunt A, Gant R. Three-dimensional kinematics of the rearfoot during the stance phase of walking in normal young adult males. *Clin Biomech*. 1996. doi:10.1016/0268-0033(95)00036-4

25. Motion V. Getting started with Vicon Shogun. 2018:1-26.

26. Nordin M, Frankel VH. *Basic Biomechanics of the Musculoskeletal System*.; 2012. doi:10.1136/bjsm.26.1.69-a

27. Rattanaprasert U, Smith R, Sullivan M, Gilleard W. Three-dimensional kinematics of the forefoot, rearfoot, and leg without the function of tibialis posterior in comparison with normals during stance phase of walking. *Clin Biomech*. 1999. doi:10.1016/S0268-0033(98)00034-5

28. Routh EJ, Routh EJ. THE ADVANCED PART OF A TREATISE ON THE DYNAMICS OF A SYSTEM OF RIGID BODIES. In: *The Advanced Part of a Treatise on the Dynamics of a System of Rigid Bodies*. ; 2015. doi:10.1017/cbo9781139237284.001

29.   Saraswat P, MacWilliams BA, Davis RB, D'Astous JL. Kinematics and kinetics of normal and planovalgus feet during walking. *Gait Posture*. 2014. doi:10.1016/j.gaitpost.2013.08.003

30.   Swartz MH. *Textbook of Physical Diagnosis.*; 2009. doi:10.1016/B978-1-4160-6203-5.00021-6

31.   Vicon. Vicon Nexus User Interface Guide. 2010.

32.   Vicon Motion Systems Limited. Oxford Foot Model 1.4. 2012;(June):1-16. www.vicon.com.

33.   Whittaker ET, McCrae SW. *A Treatise on the Analytical Dynamics of Particles and Rigid Bodies.*; 1988. doi:10.1017/cbo9780511608797

34.   Williams DS, McClay IS. Measurements Used to Characterize the Foot and the Medial Longitudinal Arch: Reliability and Validity. *Phys Ther*. 2000. doi:10.1093/ptj/80.9.864

35.   Winter DA. *Biomechanics and Motor Control of Human Movement: Fourth Edition.*; 2009. doi:10.1002/9780470549148

36.   Zuk M, Pezowicz C. Kinematic analysis of a six-degrees-of-freedom model based on ISB recommendation: A repeatability analysis and comparison with conventional gait model. *Appl Bionics Biomech*. 2015. doi:10.1155/2015/503713

37.   Shultz, S., Houglum, P. and Perrin, D., 2016. *Examination Of Musculoskeletal Injuries*. Champaign, IL: Human Kinetics.

38.   O'Donoghue, D., 1984. *Treatment Of Injuries To Athletes*. Philadelphia: W.B. Saunders.

39.   Salah, A. and Gevers, T., 2011. *Computer Analysis Of Human Behavior*. London: Springer.

40.   Hunter, S., Prentice, WE., 2001. *Rehabilitation of the ankle and foot*. In: Prentice, W.E. (Ed.), *Techniques in Musculoskeletal Rehabilitation.McGraw*-Hill, New York, pp. 603–642.

41. Stebbins J, Harrington M, Thompson N, Zavatsky A, Theologis T. Repeatability of a model for measuring multi-segment foot kinematics in children. Gait Posture. 2006. doi:10.1016/j.gaitpost.2005.03.002

42. Huang S, Ferris DP. Muscle activation patterns during walking from transtibial amputees recorded within the residual limb-prosthetic interface. J Neuroeng Rehabil. 2012. doi:10.1186/1743-0003-9-55

43. Bencke J, Christiansen D, Jensen K, Okholm A, Sonne-Holm S, Bandholm T. Measuring medial longitudinal arch deformation during gait. A reliability study. Gait Posture. 2012. doi:10.1016/j.gaitpost.2011.10.360

44. Fan Y, Fan Y, Li Z, Lv C, Luo D. Natural gaits of the non-pathological flat foot and high-arched foot. *PLoS One*. 2011. doi:10.1371/journal.pone.0017749

45. Zhao X, Tsujimoto T, Kim B, Tanaka K. Association of arch height with ankle muscle strength and physical performance in adult men. *Biol Sport*. 2017. doi:10.5114/biolsport.2017.64585

46. Brockett CL, Chapman GJ. Biomechanics of the ankle. *Orthop Trauma*. 2016. doi:10.1016/j.mporth.2016.04.015

47. Gilheany MF, Landorf KB, Robinson P. Hallux valgus and hallux rigidus: A comparison of impact on health-related quality of life in patients presenting to foot surgeons in Australia. *J Foot Ankle Res*. 2008. doi:10.1186/1757-1146-1-14

48. Mahiquez MY, Wilder F V., Stephens HM. Positive hindfoot valgus and osteoarthritis of the first metatarsophalangeal joint. *Foot Ankle Int*. 2006. doi:10.1177/107110070602701210

49. Kuni B, Wolf SI, Zeifang F, Thomsen M. Foot kinematics in walking on a level surface and on stairs in patients with hallux rigidus before and after cheilectomy. *J Foot Ankle Res*. 2014. doi:10.1186/1757-1146-7-13

50. Canseco K, Long J, Marks R, Khazzam M, Harris G. Quantitative characterization of gait kinematics in patients with hallux rigidus using the Milwaukee Foot Model. *J Orthop Res*. 2008. doi:10.1002/jor.20506

51. Keller TS, Weisberger AM, Ray JL, Hasan SS, Shiavi RG, Spengler DM. Relationship between vertical ground reaction force and speed during walking, slow jogging, and running. *Clin Biomech*. 1996. doi:10.1016/0268-0033(95)00068-2

52. Chang R, Rodrigues PA, Van Emmerik REA, Hamill J. Multi-segment foot kinematics and ground reaction forces during gait of individuals with plantar fasciitis. *J Biomech*. 2014. doi:10.1016/j.jbiomech.2014.06.003

53. Bok SK, Lee H, Kim BO, Ahn S, Song Y, Park I. The effect of different foot orthosis inverted angles on plantar pressure in children with flexible flatfeet. *PLoS One*. 2016. doi:10.1371/journal.pone.0159831

54. Cobb SC, Joshi MN, Pomeroy RL. Reliability of a seven-segment foot model with medial and lateral midfoot and forefoot segments during walking gait. *J Appl Biomech*. 2016;32(6):608-613. doi:10.1123/jab.2015-0262

55. Stephenson JL, Serres SJ De, Lamontagne A. Gait & Posture The effect of arm movements on the lower limb during gait after a stroke. 2010;31:109-115. doi:10.1016/j.gaitpost.2009.09.008

56. Perry J, Burnfield J. GAIT Normal and Pathological Function. J Sports Sci Med. 2010. doi:10.1001

57. Song JL, Hidler J. Biomechanics of overground vs. treadmill walking in healthy individuals. *J Appl Physiol*. 2008. doi:10.1152/japplphysiol.01380.2006

58. White SC, Yack HJ, Tucker CA, Lin HY. Comparison of vertical ground reaction forces during overground and treadmill walking. In: *Medicine and Science in Sports and Exercise*. ; 1998. doi:10.1097/00005768-199810000-00011

6. APPENDIX

6.1 Calculating the average of motion for one participant in MATLAB

```
numData_Average1= xlsread('T:\Pilot Data\MSFM-OFM\MSFM
OFM\Alex\session 1\Alex Cal 02.csv');
AAnkDor= numData_Average1;
aAnkDor=mean(AAnkDor(5:end,3));
numData_Average2= xlsread('T:\Pilot Data\MSFM-OFM\MSFM-
OFM\Alex\session 1\Alex Cal 03.csv');
BAnkDor= numData_Average2;
bAnkDor=mean(BAnkDor(5:end,3));
numData_Average3= xlsread('T:\Pilot Data\MSFM-OFM\MSFM-
OFM\Alex\session 1\Alex Cal 04.csv');
CAnkDor=numData_Average3;
cAnkDor=mean(CAnkDor(5:end,3));

AnkleDorsiSt=(aAnkDor+bAnkDor+cAnkDor)/3;
numData_Dorsi1= xlsread('T:\Pilot Data\MSFM-OFM\MSFM-OFM\Alex\session
1\Alex Cal 19.csv');
G = numData_Dorsi1;
AnkleDorsiDyn1 = G(5:end,3);
AnkleDorsiflexion1 = AnkleDorsiDyn1-AnkleDorsiSt;
H = AnkleDorsiflexion1;
Sum1=0;
for i=1536:310:4636
hi= H(i:i+310,:);
Sum1=Sum1+hi;
end
Average1=Sum1/10;
delta= 100/310;
j= (0:delta:100);
plot(j,Average1,'color','red');
```

6.2 Calculating the averaged over all eleven subjects motion with one positive and one negative standard deviation

```
numData_Average1= xlsread('T:\Pilot Data\MSFM-OFM\MSFM-OFM\All
Results\OFM Results\Ankle Dorsi\AnkleDosri.xlsx');
A1=numData_Average1;

a1=imresize(A1(2:312,1), [670 1]);
a2=imresize(A1(2:362,3), [670 1]);
a3=imresize(A1(2:337,5), [670 1]);
a4=imresize(A1(2:432,7), [670 1]);
a5=imresize(A1(2:412,9), [670 1]);
a6=imresize(A1(2:671,11), [670 1]);
a7=imresize(A1(2:382,13), [670 1]);
a8=imresize(A1(2:352,15), [670 1]);
a9=imresize(A1(2:322,17), [670 1]);
a10=imresize(A1(2:532,19), [670 1]);



A=[a1,a2,a3,a4,a5,a6,a7,a8,a9,a10];
AVG=(a1+a2+a3+a4+a5+a6+a7+a8+a9+a10)/10;
delta1=100/669;
j= 0:delta1:100;



S= std(A,[],2);

S_Positive=AVG+S;
S_Negative=AVG-S;
plot(j,S);

plot(j,AVG); hold on
plot(j,S_Positive); hold on
plot(j,S_Negative);
```

6.3 T-test output data for Vicon ProCalc results and the results of Jenkyn and Anas study (2008)

6.3.1 Medial longitudinal arch motion

T Test: Paired Two Sample for Means

Mean	1.090397
Variance	0.012736
Observations	96
Pearson Correlation	0.317138
Hypothesized Mean Difference	0.03
df	95
t Stat	-2.56155
P(T<=t) one-tail	0.005997
t Critical one-tail	1.661052
P(T<=t) two-tail	0.011994
t Critical two-tail	1.985251

6.3.2 Ankle JCS motion

T Test: Paired Two Sample for Means

Mean	0.369252
Variance	19.08148
Observations	96
Pearson Correlation	0.6349
Hypothesized Mean Difference	0.03
df	95
t Stat	5.024026
P(T<=t) one-tail	1.19E-06
t Critical one-tail	1.661052
P(T<=t) two-tail	2.37E-06
t Critical two-tail	1.985251

6.3.3 Subtalar JCS motion

T Test: Paired Two Sample for Means

Mean	2.323919
Variance	8.792565
Observations	96
Pearson Correlation	0.872334
Hypothesized Mean Difference	0.03
df	95
t Stat	17.71713
P(T<=t) one-tail	3.61E-32
t Critical one-tail	1.661052
P(T<=t) two-tail	7.21E-32
t Critical two-tail	1.985251

6.3.4 Hindfoot supination/pronation with respect to the midfoot

T Test: Paired Two Sample for Means

Mean	-0.54062
Variance	4.69316
Observations	96
Pearson Correlation	0.778749
Hypothesized Mean Difference	0.03
df	95
t Stat	4.8874
P(T<=t) one-tail	2.07E-06
t Critical one-tail	1.661052
P(T<=t) two-tail	4.14E-06
t Critical two-tail	1.985251

6.3.5 Hindfoot internal/external rotation with respect to the midfoot

T Test: Paired Two Sample for Means

Mean	0.276446
Variance	2.832702
Observations	96
Pearson Correlation	0.841734
Hypothesized Mean Difference	0.03
df	95
t Stat	-16.4864
P(T<=t) one-tail	6.39E-30
t Critical one-tail	1.661052
P(T<=t) two-tail	1.28E-29
t Critical two-tail	1.985251

6.3.6 Forefoot supination/pronation with respect to the midfoot

T Test: Paired Two Sample for Means

Mean	0.386189
Variance	1.26384
Observations	96
Pearson Correlation	0.691792
Hypothesized Mean Difference	0.03
df	95
t Stat	-20.9157
P(T<=t) one-tail	1.25E-37
t Critical one-tail	1.661052
P(T<=t) two-tail	2.49E-37
t Critical two-tail	1.985251

6.4 T-test output data for Vicon ProCalc and Oxford foot model results

6.4.1 Ankle JCS motion

T Test: Paired Two Sample for Means

Mean	-0.43478
Variance	28.22169
Observations	96
Pearson Correlation	0.788011
Hypothesized Mean Difference	0.03
df	95
t Stat	-2.49469
P(T<=t) one-tail	0.007167
t Critical one-tail	1.661052
P(T<=t) two-tail	0.014333
t Critical two-tail	1.985251

6.4.2 Subtalar JCS motion and hindfoot segment motion with respect to the tibia

T Test: Paired Two Sample for Means

Mean	0.897479
Variance	12.49227
Observations	96
Pearson Correlation	0.972101
Hypothesized Mean Difference	0.03
df	95
t Stat	-14.9692
P(T<=t) one-tail	4.93E-27
t Critical one-tail	1.661052
P(T<=t) two-tail	9.86E-27
t Critical two-tail	1.985251

6.4.3 Forefoot segment supination/pronation

T Test: Paired Two Sample for Means

Mean	1.029409
Variance	3.829479
Observations	96
Pearson Correlation	0.974298
Hypothesized Mean Difference	0.03
df	95
t Stat	6.690453
P(T<=t) one-tail	7.67E-10
t Critical one-tail	1.661052
P(T<=t) two-tail	1.53E-09
t Critical two-tail	1.985251

6.4.4 Hallux dorsiflexion

T Test: Paired Two Sample for Means

Mean	3.296675
Variance	40.56947
Observations	96
Pearson Correlation	0.980226
Hypothesized Mean Difference	0.03
df	95
t Stat	-27.1764
P(T<=t) one-tail	6.83E-47
t Critical one-tail	1.661052
P(T<=t) two-tail	1.37E-46
t Critical two-tail	1.985251

6.4.5 Medial longitudinal arch motion

T Test: Paired Two Sample for Means

Mean	1.246164
Variance	0.031726
Observations	96
Pearson Correlation	0.662849
Hypothesized Mean Difference	0.03
df	95
t Stat	10.41526
P(T<=t) one-tail	1.07E-17
t Critical one-tail	1.661052
P(T<=t) two-tail	2.15E-17
t Critical two-tail	1.985251

Curriculum Vitae

Name:	Tahereh Amiri
Post-secondary Education and Degrees:	Sharif University of Technology Tehran, Iran 2012-2017 B.Sc. The University of Western Ontario London, Ontario, Canada 2018-2020 M.Sc.
Honours and Awards:	Ranked in top 0.15% of 260,000+ participants in nationwide Mathematics/Physics University Entrance Exam, Tehran, Iran 2012
Related Work Experience	Teaching Assistant The University of Western Ontario (Fall 2018) Introduction to Biomaterials Engineering- CBE 4421A Teaching Assistant The University of Western Ontario (Winter 2019) Advanced Biomaterials Engineering- CBE 9250B Teaching Assistant The University of Western Ontario (Winter 2020) Biomechanics of Musculoskeletal system- MME 4469B